ASSESSMENT OF MAXIMUM GAS PRODUCTION RATE OF AN UNTEMPERED SYSTEM UNDER RUNAWAY CONDITIONS

A Thesis

by

NEPU SAHA

Submitted to the Office of Graduate and Professional Studies of
Texas A&M University
in partial fulfillment of the requirements for the degree of

MASTER OF SCIENCE

Chair of Committee,	Luc Véchot
Co-Chair of Committee,	M. Sam Mannan
Committee Member,	Mahmood Amani
Head of Department,	M. Nazmul Karim

December 2016

Major Subject: Chemical Engineering

ABSTRACT

Runaway reactions are characterized by the exponential increase of the temperature and pressure of a chemical system that could potentially lead to the explosion of the reactor or storage vessel of concern. The consequences of a runaway reaction may be very severe in terms of life, economic and environmental losses.

Emergency relief systems (ERS) are the ultimate mitigation method to prevent vessel explosion following the runaway reaction. In the case of the runaway of gas producing chemical systems, ERS sizing requires the assessment of the maximum gas production rates. Significant work was performed in the 1980's by the Design Institute for Emergency Relief Systems to develop vent sizing methods for runaway reaction cases. While vent sizing methods developed for vapor systems provided relatively good results, those developed for gas generating systems (hybrid or gassy) tend to be oversized and still need to be improved. A very significant part of this work includes the improvement of the current methods for the measurements of the maximum gas production rate for such systems.

The objective of this thesis work is to experimentally study the decomposition of a gas generating system under runaway condition using adiabatic calorimetry and assess the maximum gas production rate corresponding to the runaway. A critical analysis of the current methodologies to interpret experimental data to compute the maximum gas production rate was done. The decomposition of Cumene Hydroperoxide in Cumene was chosen for the study.

The results of the research show that the measurement of the specific gas production rate for a given peroxide concentration highly depends on the experimental conditions of the tests using adiabatic calorimetry. They also demonstrated that the correction of the experimental data to take into account the influence of thermal mass of the test cell was critical in the evaluation of the gas production rate. Finally, the simulation of a similar reactive mixture using a computer model showed that the assessment of the gas production rate using temperature and pressure data as well as an equation of state may be misleading.

ACKNOWLEDGEMENTS

I would like to express my deep and sincere gratitude to my advisor, Dr. Luc Vechot for his selfless support in various ways in my graduate study. His guidance and encouraging have provided a good basis for this thesis. His wide knowledge and logical way of thinking have been of great help for me.

A special thanks and appreciation go to my co-chair, Dr. Sam Mannan and my committee member, Dr. Mahmood Amani for their efforts, time and advice.

I gratefully thank my officemates, whom I spend most of my time with. In the past two years, we shared the same stressful but happy time, which makes us families. Their care, support and encouragement give me confidence and make me warm even in the toughest day.

Also, many thanks go to all the member of MKOPSC for their help to make this research project reach this final stage.

Last but not least, I am deeply grateful to my parents, who gave me life and dedicate all their love to me. They have always put education as the first priority in my life and raised me to set high goals for myself. Their selfless love supports me to study abroad and fight against any challenge in front me.

NOMENCLATURE

Parameters

m	Mass of reactant	kg
T	Temperature	°C
P	Pressure	Bar
ΔHr	Heat of reaction	J/kg
h_{fg}	Latent heat of vaporization	
k_0	Pre-exponential factor	1/s
E	Activation energy	J/mole
L	Characteristic length	M
h	Heat transfer coefficient	$W/K/m^2$
R	Gas constant	J/mole/K
n	Number of moles	moles
A_s	Surface area	m^2
A	Area of ERS	m^2
V	Volume	m^3
Bi	Biot Number	-
δ	Frank-Kamenetskii parameter	-
Q	Gas production rate	m^3/s
G	Mass flux through ERS	$kg/m^2/s$

Cp	Specific heat capacity	J/kg/K
φ	Thermal inertia	-
ρ	Density	kg/m^3
v	Specific volume of gas	m^3/kg
t	Time	s
$\dot{n}_g$	Specific gas production	Moles of gas /kg of liquid
χ	Conversion of the reaction	%
M_w	Molecular weight	g/mole

Subscripts

a	Ambient
c	Cell
on	Onset
max	Maximum
R	Reactor
s	Sample
g	Gas
l	Liquid
p	Pad gas
v	Vapor
0	Initial

f	Final
crit	Critical
adj	φ corrected

TABLE OF CONTENTS

LIST OF FIGURES

Page

LIST OF TABLES

Page

1 INTRODUCTION

An exothermic chemical reaction over which control of the temperature has been lost is known as runaway reaction [1]. A runaway reaction is characterized by an exponential increase of the temperature and pressure on the reactor vessel or storage tank in which the reaction takes place, which can lead to the explosion of the vessel. The consequences of a runaway reaction can therefore be very severe in terms of life, economic and environmental losses. According to U.S. Chemical Safety and Hazard Investigation Board (CSB), out of 167 incidents which involved reactive chemical during the period of 1980 to 2001 in U.S., 35 percent of the incidents were caused by runaway reactions [2].

Emergency Relief Systems (ERS, e.g. bursting disc and relief valves) are the most commonly used risk reduction measures used to protect the reactor or vessel from the consequences of a runaway reaction. The main advantages associated to their applications are that they are independent of the main control system, and they may still provide adequate protection if all other systems fail [3]. The proper sizing of the ERS to protect a vessel in the case of a runaway reaction requires the understanding of the reaction kinetics and thermodynamics, and fluid dynamics of the reactive system. Such phenomena are quite complex and yet to be fully understood.

Significant work was performed in the 1980's by the Design Institute for Emergency Relief Systems (DIERS) to develop vent sizing methods for runaway reaction cases. Very well established methods were developed for vapor systems, which are

chemical systems for which the pressurization of the vessel is due to the increase of vapor pressure of the vessel contents. This is not the case of *gas generating systems* (hybrid or gassy) for which the pressurization of the vessel is due to the increase of vapor pressure and the production of permanent gasses. Some organic peroxide (R-O-O-R′) when decomposing under runaway conditions belong to the category of *gas generating systems*. Indeed, the O-O bond organic peroxide can easily break and producing free radicals of the form R-O. Because of this property, organic peroxides are used worldwide as initiators, activators, and catalysts in rubber and plastics industries. However, this functional group makes organic peroxides both useful and prone to self-decomposition and runaway reaction. Many peroxides when decomposing give off permanent gasses like CH_4, CO_2 and O_2.

The existing vent sizing existing methods for gas generating systems tend to be oversizing and are not well reputed [4]. At present, there is significant work still to be done in designing ERS for such systems. A very significant part of this work, and probably the first step, includes the improvement of the current methods for the measurements of the maximum gas production rate corresponding to the decomposition of a gas generating system under runaway conditions to subsequently improve the design of ERS.

The objective of this thesis work is to experimentally study the decomposition of a gas generating system under runaway condition using adiabatic calorimetry and assess the maximum gas production rate corresponding to the runaway. A critical analysis of the current methodologies to interpret experimental data to compute the maximum gas

production rate was done. Cumene Hydroperoxide (CHP) in Cumene was chosen as the chemical system for the study.

2 LITERATURE REVIEW

A chemical reaction enters a thermal runaway when the rate of heat produced by an exothermic reaction exceeds the heat removal rate. This results in an exponential increase of the temperature of the reactive mixture along with the pressure of the reactor vessel due to the vapor pressure of the liquid components and/or the production of permanent gasses from the chemical reaction. The pressure increase in the vessel can lead to the explosion of the vessel if the vessel design pressure is exceeded. This can happen if the vessel is not equipped with a venting device to relieve the excess pressure [5], [6] such as an emergency relief system (ERS) or if the ERS is too small to relieve the pressure generated during the maximum rate of the runaway.

This part provides a review of:

- Selected major incidents in the process industry that involved runaway reaction;
- The theory is describing the phenomena of thermal runaway;
- The classification of reactive systems according to the Design Institute for Emergency Relief Systems (DIERS) and the associated vent sizing methodology;
- The experimental characterization of runaway reaction using adiabatic calorimetry in the particular case of gas generating systems.

A summary of the gaps in the literature will be done to highlight the areas of improvements for the improvement of the ERS sizing methodology for gas generating systems.

2.1 SELECTED MAJOR INCIDENTS INVOLVING RUNAWAY REACTIONS

There have been many accidents in the process industry involving thermal runaway reactions. The following provide a brief description of the Bhopal (India, 1984), Seveso (Italy, 1976) and T2 Laboratories (USA, 2007).

2.1.1 Bhopal, India, 1984

The horrific accident at Bhopal, India that took place at the Union Carbide India Limited (UCIL) plant on December 3, 1984 [7]–[10] was a result of the thermal runaway of the reaction between Methyl Isocyanate (MIC) and water [11]. MIC, a highly toxic substance with a relatively low boiling point (39°C), was used in the manufacture of Carbaryl, a pesticide. MIC was produced and stored on site in three 57 m^3 underground refrigerated storage tanks.

On the day of the accident, around 1 ton of water used during the washing operation of the pipelines connected to the storage tank vent line entered in a storage tank containing 41 tons of impure MIC through a faulty valve. The resulting runaway reaction led to the temperature increase of the reactive mixture. Along with the temperature, the pressure increased in the storage tank due to the production of CO_2 and MIC vapor pressure. This in turn led to a large release of MIC vapor through the vessel pressure relief valve at around 1:00 am. A combination of failure so the safety system led to the escalation of the event:

- The 30 ton refrigeration unit, that normally served as a safety component to cool the MIC storage tank, had been drained of its coolant for use in another part of the plant, rendering impossible to cooling of the storage tank.

- The scrubber system downstream the pressure relief valve that was turned off and put in a stand-by mode.
- The flare system downstream the pressure relief valve was taken out of service for maintenance.

The release of dense and highly toxic MIC gas dispersed offsite leading to the death of more than 3000 people over night and thousands of people seriously injured.

2.1.2 Seveso, Italy, 1976

The chemical plant owned by ICMESA Chemical Company in Seveso, Italy, was the site of a well-known incident case involving a runaway reaction. The plant produced hexachlorophene and a highly toxic byproduct, 2,3,7,8-Tetachlorodibenzo para Dioxin (TCDD) [12]. On July 9, 1976, the total batch process was stopped and was scheduled to be continued on the following day. The steam valve to the heating coil of the reactor was closed, and the stirring of the content in the reactor was stopped 15 minutes later. These conditions led to the thermal instability of the reaction mixture in the reactor resulting in the production of a large amount of hydrogen gas in the reactor, thus a pressure increase. At 12:37 am on July 10, 1976, the bursting disc opened and approximately 2 kg of toxic TCDD was released, contaminating around 10 square miles around the site.

Following the event thousands of animals either died from exposure to TCDD or were slaughtered to prevent TCDD from entering the food chain. Nearby population was evacuated. The population exposed to TCDD was found to have developed chloracne. Even if no fatality were associated with this accident, it was a turning point in the history

of the regulation of major hazard site in the European Union (EU). The current EU directive for industrial safety regulations is known as the Seveso III Directive.

2.1.3 T2 Laboratories, USA, 2007

T2 Laboratory was a gasoline additive manufacturer in Jacksonville, Florida, USA[13]. On December 19, 2007, while preparing a batch of Methylcyclopentadienyl Manganese Tricarbonyl (MCMT), the cooling system of the reactor, which lacked redundancy, failed, leading to a runaway of the reactive mixture. The pressure increase led to the opening of the bursting disc. As the bursting disc was undersized, the pressure kept increasing in the vessel leading to the explosion of the reactor vessel. The explosion caused the death of four employees and triggered a chemical fire that destroyed the entire facility [14].

2.2 THEORY OF THERMAL RUNAWAYS

Thermal runaway refers to a situation where the heat generation rate of an exothermic reaction exceeds heat removal rate of the reactor of storage vessel. The following described the two main theories, based on the thermal balance of vessel, to describe the conditions at which thermal runaways occur.

They can be used to design and reactor/storage vessel and decide on operating conditions to prevent the phenomena of a runaway.

2.2.1 Semenov's theory of thermal ignition

Semenov [15] developed a model for thermal explosions, in which he assumed the following:

- The temperature (T) of a reacting system, is constant and uniform across the whole volume of the system. This corresponds to low viscosity liquid mixtures or vessel with an efficient agitation system.
- The temperature of the reactor's external walls is the same as the liquid temperature and the vessel surrounding is at ambient temperature T_a (*Figure 1*).

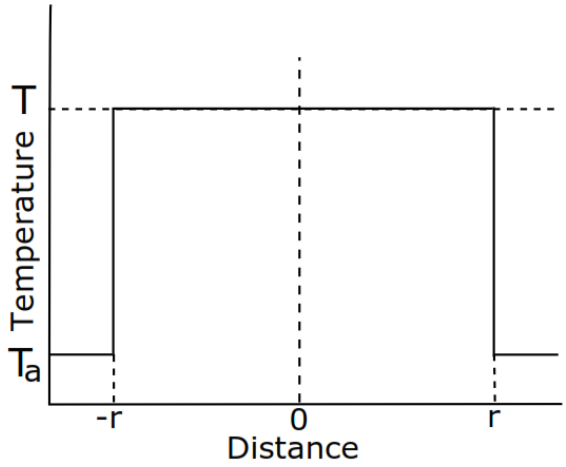

Figure 1: Temperature profile in the reacting system, as assumed by the Semenov theory

- The heat production rate, Q_+, of a zero-order reaction is given by:

$$Q_+ = \mathrm{m}\Delta H_r k_0 \exp(\frac{E}{RT}) \quad (1)$$

Where,

m = reactive liquid mass, kg

ΔH_r = heat of reaction, J/kg

k_0 = pre-exponential factor, 1/s

E = Activation energy, J/mole

R = Molar gas constant, J/mole/K

T = Temperature inside of reacting system, °C

- The heat loss rate, Q_- , is linear and is calculated from the Newton's law of cooling:

$$Q_- = hA_s(T - T_a) \quad (2)$$

Where,

h = Heat transfer coefficient, W/k/m^2

A_s = Surface area of reacting system, m^2

T_a = Temperature outside of reacting system, °C

Semenov graphically represented the heat fluxes (Q_+ and Q_-) and highlighted the three following cases (*Figure 2*):

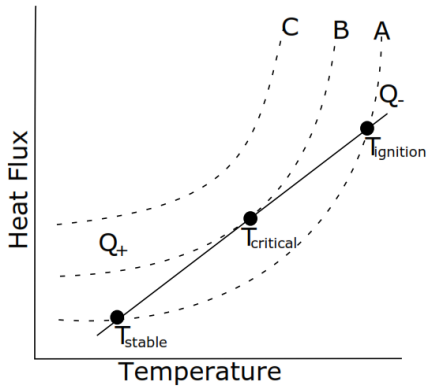

Figure 2: Plot of thermal fluxes against temperature

Case I: The heat production curve (Q_+, Curve A) intersects the heat loss line (Line Q_-) at two points (T_{stable} and $T_{ignition}$).

When the reactive mixture temperature less than T_{stable}, Q_+ is higher than Q_-, which leads to the increase of the temperature of the mixture. If the reactive mixture temperature

exceeds T_{stable}, then Q_- is higher than Q_+ which results in the cooling of the mixture back to T_{stable} (this explains the name T_{stable} as the systems return to thermal stability).

If the temperature of the reactive mixture is somehow raised to above $T_{ignition}$ (e.g. heating by some external source), Q_+ is higher than Q_-, which leads to the increase of the temperature of the mixture and the reactive system will runaway. $T_{ignition}$ is then a no return point.

Case II: The heat loss line (Line Q_-) is tangential to the heat production curve (Q_+, Curve B) at point $T_{critical}$.

In this case, $T_{critical}$ is an unstable temperature. If the temperature of the mixture is less than $T_{critical}$ then Q_+ is higher than Q_-, and the temperature of the system will be brought back to $T_{critical}$. Any disturbance in the system leading to a small temperature increase above $T_{critical}$ will lead to a runaway.

Case III: The heat production curve (Q_+, Curve C) is higher than the heat loss line (Line Q_-).

In this case, Q_+ is always higher than Q_-, meaning that the runaway reaction is inevitable. Semenov's theory is the origin of the quantitative study of thermal explosions, from which remarkable interpretation of many aspects of thermal theory has been achieved. However, this theory applies only to the system with uniform temperature distribution such as well-stirred liquids.

2.2.2 Frank-Kamenetskii's theory of thermal ignition

To overcome the limitation of the Semenov theory related to the uniformity of the temperature in the vessel. Frank-Kamenetskii [16] developed a theory of thermal

explosion that takes into account temperature gradient within the reactive mixture (*Figure 3)* where there could be a significant resistance to heat transfer (e.g. components with low thermal conductivity, viscous contents).

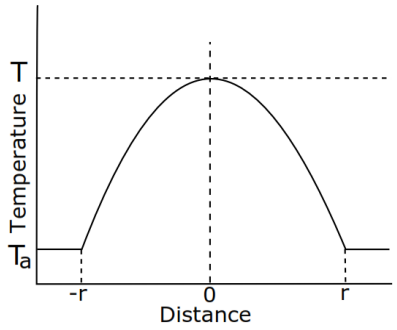

Figure 3: The temperature profile in a reacting system according to the Frank-Kamenetskii's theory

The theory only considers that the main mode of heat transfer within the mixture is conduction. The heat production and loss equations can be expressed similarly to the Semenov's theory. A new dimensionless parameter, the Biot Number (Bi), is introduced to describe the temperature gradient at the boundaries of the reactive mixture:

$$Bi = \frac{hL}{k} \qquad (3)$$

Where, L is the characteristic length of the body and k is the thermal conductivity of the solid material. In the case of chemical reaction hazard, bulk of liquid can be treated as a solid body (see *Figure 4*).

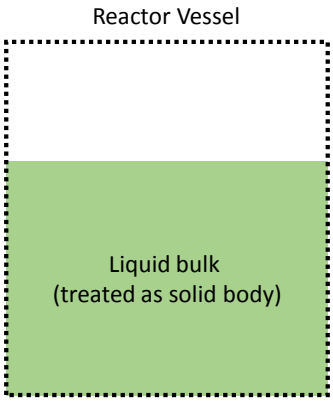

Figure 4: Understanding of solid body in chemical reaction hazard

A low Biot number results in liquid surface temperature (T_s) being significantly different to the ambient temperature (T_a) and a high Biot number results in T_s being close to T_a.

Frank-Kamenetskii defined a parameter (δ), which is a function geometry there exist critical values of the Frank-Kamenetskii parameter (δ_c) above which self-ignition will occur ($\delta > \delta_c$) and below which there is failure to ignite [17]

Frank-Kamenetskii's theory is more versatile than Semenov's theory and can predict bulk heating and hot-spots within reactive mixtures.

2.3 DIERS CLASSIFICATION OF REACTIVE SYSTEMS (VAPOR, GASSY AND HYBRID)

The above theories of thermal runaway were developed to design a reactor/storage vessel and decide on operating conditions to prevent the phenomena of a runaway. There is still need to act on the mitigation of the consequences of runaway reactions, in particular

the design of emergency relief systems (ERS) to prevent the explosion of a vessel following a runaway.

In the 1980's, the Design Institute for Emergency Relief Systems (DIERS), a consortium of 29 companies under the umbrella of the American Institute of Chemical Engineers (AICHE), made an outstanding effort to develop methods to design of ERS based on:

- Adiabatic calorimetry measurements to characterize the runaway reaction experimentally;
- Two-phase flow models describing the hydrodynamics of the flow in the vessel and through ERS (note: flow models are outside the scope of this thesis so no further description will be provided).

DIERS proposed to classify reactive systems into three major types (vapor, gassy and hybrid) according to the phenomena at the origin of the pressure production following the runaway and their associated thermal behavior (tempered or untempered), as follows:

- **Vapor systems:** when the pressure generation of a chemical system under runaway condition is entirely due to the vapor pressure of the liquid contents, the system is classified as a *vapor system*. The pressure rises as the temperature of the reactive mixture increases during the runaway. During the operation of a properly designed ERS, the latent heat of vaporization of the chemical mixture can be removed at a sufficient rate to maintain the temperature at a constant level at constant pressure (see *Figure 5*). Therefore, the control of the pressure by the ERS allows the control of the rate of reaction [3]. This system has a *tempered* behavior.

- **Gassy systems**: when the pressure generation in a system by the runaway reaction is entirely due to the production of permanent gas (e.g. CO_2, CH_4, O_2), the system is classified as a *gassy system*. Unlike vapor systems, gassy systems exhibit an *untempered* behavior meaning that the operation of an ERS cannot control the temperature of the reactive mixture and thus the reaction rate. The ERS simply acts to depressurize the vessel but does not stop the temperature of the reacting mixture from increasing exponentially. When the runaway reaches its maximum rate a second pressure peak can occur corresponding to maximum gas production rate [3] (see *Figure 5*)
- **Hybrid systems:** When the pressure generation in a system by the runaway reaction is due to both the production of a permanent gas and vapor, the system is classified as a *hybrid system*. Hybrid systems can be tempered or untempered, depending on the relative rates of vapor and gas production in the vessel. As a rule of thumb, when the vapor pressure constitutes only about 10% of the total pressure, the hybrid systems can usually be treated as gassy systems [3].

All the above systems are found in the chemical industry depending on the chemical mixtures subject to potential thermal runaways. For instance, many organic peroxides (infamous for their thermal instability [18], [19] and [20]) when entering a runaway reaction tend to decompose by producing permanent gasses and thus behave as hybrid or gassy systems [3], [21].

While DIERS has developed user-friendly vent sizing methods for all of these three types od systems, most of the efforts of the DIERS was towards the development

and experimental validation of vent sizing methods for vapor and tempered hybrid [22]. The vent sizing methods for gassy and untempered hybrid systems, on which this thesis os focused, still require major improvements as described below.

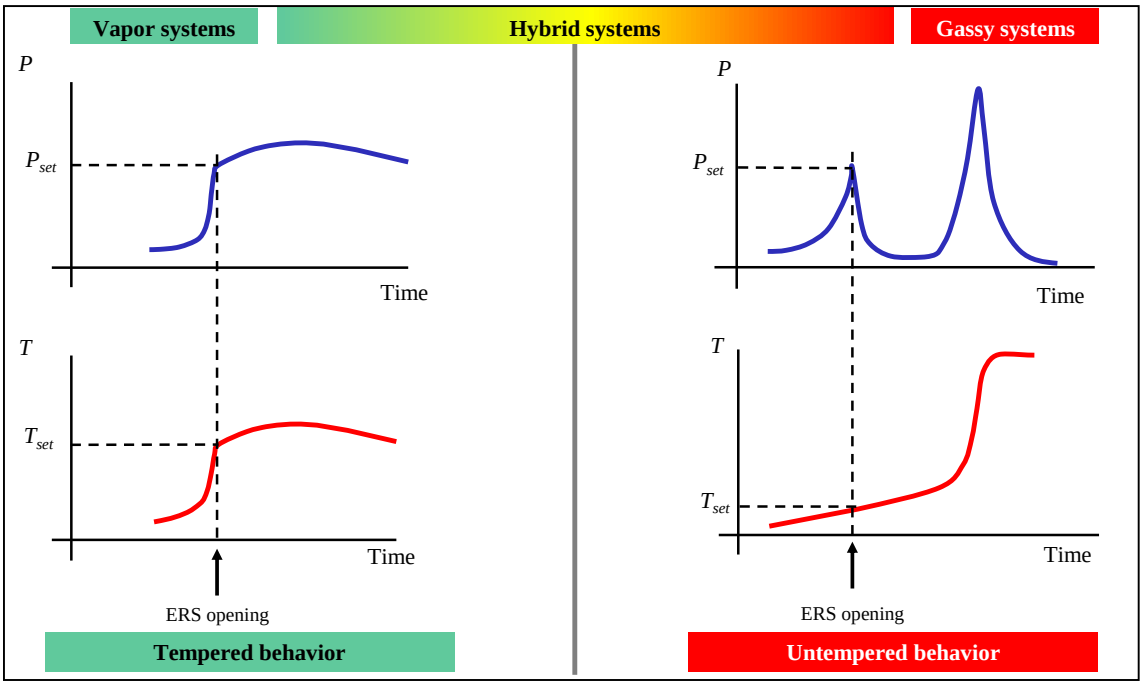

Figure 5: DIERS classification of reactive systems (vapor, gassy and hybrid). Behavior of tempered and untempered systems before and after the opening of an ERS at P_s (ERS opening pressure).

2.4 EXPERIMENTAL CHARACTERIZATION OF THERMAL RUNAWAYS

Large industrial reactor or storage vessels tend to behave adiabatically [23]. This is due to the relatively small ratio of the heat exchange surface area over the mass of the reactive mixture. This ratio tends to decrease when increasing the scale of a vessel. Therefore, the proper characterization of runaway reactions to design ERS for large

industrial reactor or storage vessels requires the use of laboratory equipment, *adiabatic calorimeters*, that can reproduce the "adiabatic" behavior of such industrial vessels. The data obtained from adiabatic calorimetry are used to size emergency relief systems that protect the reactor against explosion should a runaway reaction occur.

2.4.1 Adiabatic calorimeter

Adiabatic calorimeters are laboratory bench scale equipment that allows the experimental investigations of runaway reactions. In adiabatic calorimeters, adiabaticity (elimination of the heat losses) is achieved by placing a sample of the reactive mixture (10 – 100 ml) into a test cell (metal or glass) surrounded by an electrical heater that follows the temperature of the sample during the runaway (see *Figure 6*). The temperature difference between the sample and the surrounding being close to zero, the heat losses to the surroundings are eliminated and the test can be conducted under adiabatic conditions.

Figure 7 shows typical data obtained with adiabatic calorimeters. The following characteristics of the runaway reactions can be extracted:

- The onset temperature (T_{on}), i.e. the temperature at which self-heating is detected by the calorimeter in adiabatic conditions,
- The temperature and pressure evolution,
- The temperature and pressure rise rate and their maximum values,
- The time to reach a maximum rate of reaction and,
- the type of reactive system according to DIERS classification.

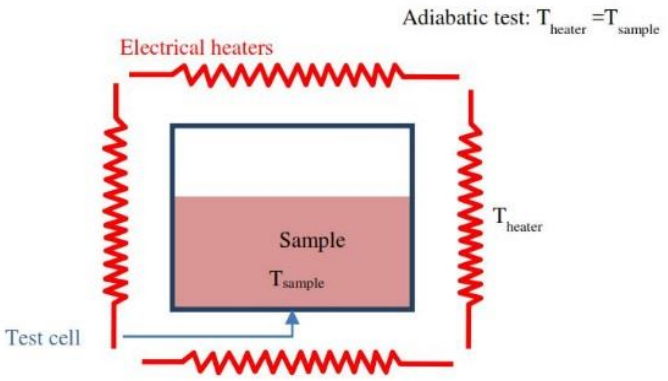

Figure 6: Schematic of an adiabatic calorimeter

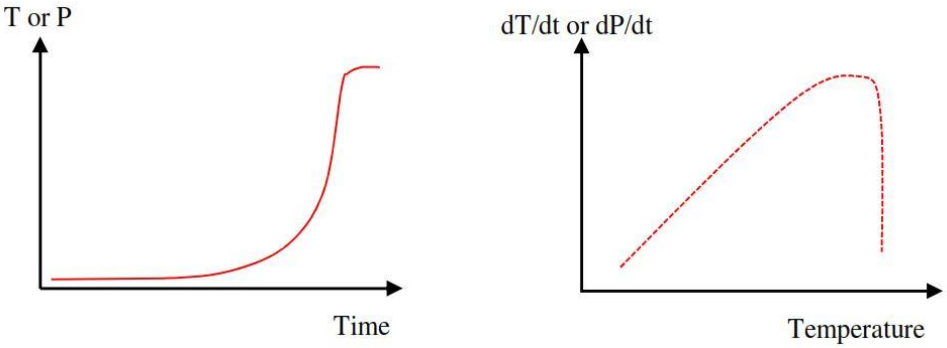

Figure 7: Schematic of adiabatic calorimeter results

2.4.2 φ factor and low φ adiabatic calorimeters

In an adiabatic test, the heat released by the reaction goes towards increasing the temperature of the sample and the sample holder. Thus, the thermal mass of the test cell itself can play an important role in the temperature and pressure profiles resulting from test. The thicker the wall of the test cell, the higher the thermal mass of the text cell, the more energy is used to heat up the wall (so less for the reactive mixture itself). The relative

significance of the thermal inertia of the test cell is quantified by the φ factor (phi factor) as follows:

$$\varphi = \frac{Thermal\ mass\ of\ sample\ plus\ test\ cell}{Thermal\ mass\ of\ sample} = \frac{m_s c_{p_s} + m_c c_{p_c}}{m_s c_{p_s}} \quad (4)$$

Where,

m_s = mass of the sample, kg

m_c = mass of test cell, kg

Cp_s = specific heat capacity of sample, J/kg/K

Cp_c = specific heat capacity of test cell, J/kg/K

Large scale vessel tends to have a negligible thermal mass compared to the thermal mass of the liquid they contain; thus, their φ is close to unity.

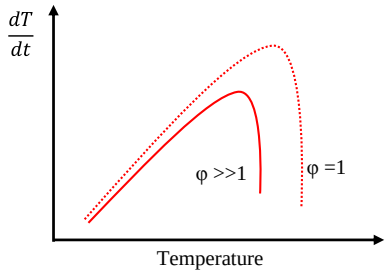

Figure 8: Influence of φ on the temperature rate profile

As shown in *Figure 8*, experimental data obtained with equipment with φ >>1 may lead to an underestimation of the temperature and temperature rise rate that will occur at large scale (φ close to 1). However, φ close to unity is very difficult to achieve at small scale. It is recommended to use equipment with low φ -factor within a range of 1.05-1.1 to best approach the industrial conditions. Low φ -factor equipment usually uses a thin-

walled cell that stands a relatively low pressure (less than 3 bars). To avoid the explosion of the cell during the experiment, the cell is placed within a containment vessel and a pressure compensation system using inert gas maintains the difference of pressure between the cell and the containment vessel to a low value (see *Figure 9*).

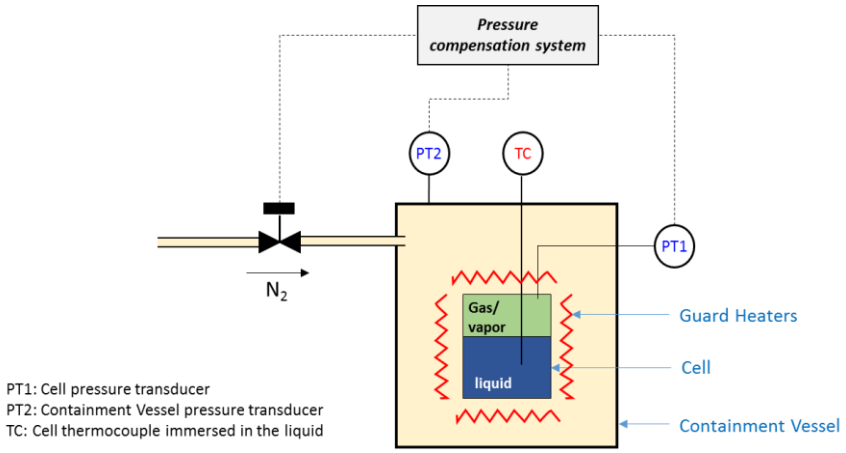

Figure 9: Schematic diagram of low phi adiabatic calorimeter (pressure compensation)

2.4.3 Correction of adiabatic data for φ factor

Ideally, experiments with equipment that show a φ factor = 1 are needed to reproduce correctly for large scale behavior of the runaway reaction. Unfortunately, such equipment does not exist and the temperature and pressure data obtained at laboratory scale (with φ>1) must be corrected. This correction is necessary to assess the temperature and pressure rise rate and therefore the specific gas production rate at large scale.

2.4.3.1 Fisher's method (1992)

The most widely used method for adiabatic data correction is proposed by Fisher in 1992 [24]. This method is very practical, relatively simple. It is built for a nth order single stage reaction.

The general energy balance equation for calorimetric experiment (φ>1) is given by:

$$\left(m_s c_{p_s} + m_c c_{p_c}\right)\left(\frac{dT}{dt}\right)_{\varphi>1} = m_s \Delta H_r \frac{d\chi}{dt} \quad (5)$$

Where,

ΔH_r is the heat of reaction

$\left(\frac{dT}{dt}\right)_{\varphi>1}$ is the temperature rise rate of the liquid measured experimentally with the adiabatic calorimeter.

$\frac{d\chi}{dt}$ is the rate of conversion of the reaction and can be expressed as:

$$\frac{d\chi}{dt} = k_o e^{(-E/RT)} f(\chi) \quad (6)$$

Where,

k_0 is the pre-exponential component

E is the activation energy

Rearranging Equation *(5)* using Equation *(4)* and *(6*) gives:

$$c_{p_s}\varphi\left(\frac{dT}{dt}\right)_{\varphi>1} = \Delta H_r k_o e^{(-E/RT)} f(\chi)_{\varphi>1} \quad (7)$$

The adjusted energy balance for $\varphi=1$ can be written as:

$$c_{p_s}\left(\frac{dT}{dt}\right)_{adj} = \Delta H_r k_o e^{(-E/RT_{adj})} f(\chi)_{adj} \quad (8)$$

To calculate the adjusted values of temperatures (T_{adj}) and temperature rise rates $\left(\left(\frac{dT}{dt}\right)_{adj}\right)$ from experimental data, one can divide Equation *(8)* by Equation *(7)*, which gives:

$$\left(\frac{dT}{dt}\right)_{adj} = \varphi.\left(\frac{dT}{dt}\right)_{\varphi>1} \frac{f(\chi)_{\varphi>1}}{f(\chi)_{adj}}\ exp\left[\frac{E}{R}\left(\frac{1}{T} - \frac{1}{T_{adj}}\right)\right] \qquad (9)$$

$\left(\frac{dT}{dt}\right)_{adj}$ is also referred to as the adiabatic Self Heat Rate (SHR)

The φ correction proposed by Fisher therefore requires the following steps:

- *Step 1: Estimation of the adjusted onset temperature ($T_{on,\ adj}$):*

Assuming that the consumption of reactant is negligible near the onset temperature (low conversion), then $\left(\frac{dT}{dt}\right)_{adj} = \left(\frac{dT}{dt}\right)_{\varphi>1}$, The adjusted onset temperature ($T_{on,adj}$) is given by:

$$\frac{1}{T_{on,adj}} = \frac{1}{T_{on}} + \frac{R}{E} ln\ \varphi \qquad (10)$$

Where, T_{on} is the onset temperature measured experimentally with the adiabatic calorimeter.

- *Step 2: Reconstruction of the adjusted temperature profile from the adjusted onset temperature:*

$$T_{adj}(t) = T_{on,adj} + \varphi.[T(t) - T_{on}] \qquad (11)$$

Where, *T(t)* is the experimental temperature.

- *Step 3: Reconstruction of the adjusted Self Heat Rate (SHR) curve:*

If one assumed that the same reaction conversion $\left(f(\chi)_{\varphi>1} = f(\chi)_{adj}\right)$ is reached along the experimental time scale the corrected temperature rise rate is given by:

$$\left(\frac{dT}{dt}\right)_{adj} = \varphi.\left(\frac{dT}{dt}\right)_{\varphi>1} exp\left[\frac{E}{R}\left(\frac{1}{T} - \frac{1}{T_{adj}}\right)\right] \quad (12)$$

In 2015, A. A Kossoy *et al.*[25] showed that the Fisher's method provides relatively good results in terms of adjusted onset temperature and SHR predictions $\left(\left(\frac{dT}{dt}\right)_{adj} = f\left(T_{adj}\right)\right)$ for:

- A single stage, N order, nonautocatalytic reactions (decomposition of 20% di-tert butyl peroxide in toluene)
- A multistage reaction involving two overlapping stages (polymerization of methyl methacrylate) which kinetics is reasonably evaluated using a N order model (which does not necessarily represent the correct autocatalytic behavior).

A.A. Kossoy *et al.*[25] also showed that the Fisher's correction method overestimated the SHR in the case of a single stage autocatalytic reaction (curing of a resin) but underestimated the SHR in the case of a multistage reaction with partly overlapping stages (Phenol – Formaldehyde reaction). In both these cases the kinetics of the reactions are reasonably simulated using N order models (that here again do not necessarily represent the correct chemical mechanisms).

A. A. Kossoy *et al.*[25] finally showed that in the case of more complex reaction (e.g. reactions with well-separated stages) the Fishers method fails for correct for φ factor.

When Fisher's method seems to work (e.g. N order reaction and overlapping multistage reaction), the Fisher's method has the following significant limitations [25]:

- The adjusted temperature profile calculated by Equation *(11)* is obtained using the experimental time scale. This equation ignores the fact that that the reaction will be faster at low φ factor. This means that the $T_{adj} = f(t)$ curve is not correct!
- **The method does not include any technique to correct for the pressure data, which is a very severe limitation in the case of gas generating system (gassy and hybrid).**

2.4.3.2 Enhanced Fisher method (2015)

As mentioned above, Fisher's method can correctly predict the onset temperature and adjusted SHR in selected cases. In 2015, A. A. Kossoy *et al.*[25] proposes a method to reconstruct the adjusted time scale by integrating the reciprocal adjusted SHR with respect to temperature [25].

$$t_{adj} = \int_{T_{on,adj}}^{T_{adj}} \frac{dT}{(dT/dt)_{adj}} \qquad (13)$$

This reconstruction provides good estimates of the adjusted time scale as it gives the adjusted time points corresponding to the experimental time scale. Therefore, the corresponding temperature and SHR can be calculated by using Equation *(12)*.

2.5 VENT SIZING METHODOLOGY FOR GASSY AND UNTEMPERED HYBRID SYSTEMS

As shown in *Figure 10* for an untempered system, the pressure relief following the opening of the ERS does not control the temperature of the reactive mixture. As a result, after the first pressure peak corresponding to the opening of the ERS at P_s, the reaction

keeps running away until it reaches the maximum rate of gas production which can result in a second pressure peak at P_{max}.

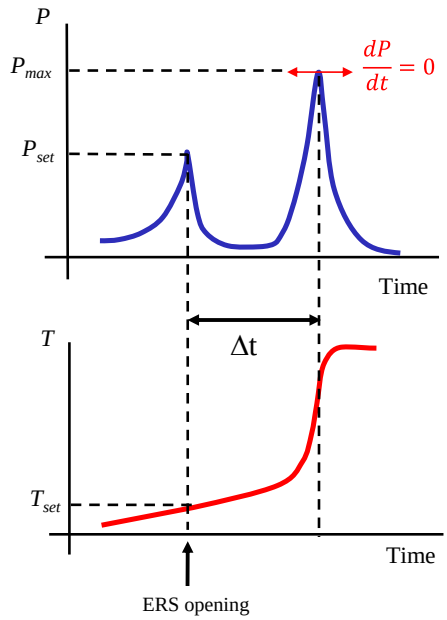

Figure 10*: DIERS vent sizing criteria for untempered systems*

The following describes and discusses the limitations of the current vent sizing methodologies for ERS sizing for gassy and untempered hybrid systems.

2.5.1 Derivation of the DIERS vent sizing equations

DIERS vent sizing methods for untempered systems therefore aim to calculate the ERS size which will result in a second pressure peak ($dP/dt = 0$) at a given P_{max} (which of the corresponds to the vessel maximum allowable working pressure, MAWP) when the runaway reaction reaches its maximum rate (maximum gas production rate) as illustrated

in *Figure 10*. This P_{max}, or second pressure peak, is also referred to as the turnaround. The condition *dP/dt = 0* at turnaround is achieved when the volumetric vented flow through the ERS equals the volumetric gas production rate in the vessel (Q_{gmax}) [3], [26]:

$$GAv_i = Q_{g\,max} \tag{14}$$

Where G (kg/m^2/s) the mass flux through the ERS (one phase of two-phase), A (m^2) the ERS venting area and v_i (m^3/kg), the specific volume of the vented material (one phase of two-phase) at the ERS entrance.

The nature of the vented flow (one-phase of two-phase) and the mass of reactive mixture remaining in the vessel at the second pressure peak **being unknown**, DIERS recommends the following conservative assumptions:

- All the reaction mixture remains in the reactor until the maximum gas production rate (i.e., there's no mass venting through the vent during Δt; see *Figure 10*); and
- Homogeneous two-phase flow occurs at the maximum gas production rate, with the specific volume of the vented material (v_i) the ERS entrance estimated by:

$$v_i = \frac{V_R}{m_R} \tag{15}$$

Where, m_R is the initial mass in the reactor and V_R is the reactor volume.

The vent sizing equation is therefore given by:

$$A = \frac{1}{G} Q_{g\,max} \frac{m_R}{V_R} \tag{16}$$

Where, $Q_{g\ max}$ is experimentally estimated using adiabatic calorimetry and G calculated using an applicable one-phase or two-phase flow models for non-flashing flow.

For hybrid systems, the existing vent sizing methods take into account the contribution of the vapor and gas production to the overall maximum gas/vapor production rate [3], [26]:

$$A = \frac{1}{G}\left(Q_{g\ max} + Q_{v\ max}\right)\frac{m_R}{V_R} \qquad (17)$$

Where $Q_{v\ \max}$ is the peak vapor production rate. $Q_{v\ \max}$ could be calculated from:

$$Q_{v\ max} = \frac{m_R C_p}{h_{fg}\rho_v}\left(\frac{dT}{dt}\right)_{max} \qquad (18)$$

Where,

h_{fg} is the latent heat of vaporization of the liquid mixture

ρ_v is the vapor density.

$\left(\frac{dT}{dt}\right)_{max}$ is the maximum adiabatic rate of temperature rise

An open cell calorimetric test tends to measure $Q_{g\ max}$, rather than the sum of Q_{gmax} and $Q_{v\ max}$, because the vapor produced will tend to condense in the relatively cold containment vessel. Even a closed cell test also underestimate $Q_{v\ max}$ because, the high pressure suppress the vaporization. However, DIERS suggested that the value of $Q_{g\ max}$ (obtained from calorimetric data) could be used to represent the sum of $Q_{g\ max}$ and $Q_{v\ max}$. This may be less reasonable if the amount of vapor produced is high.

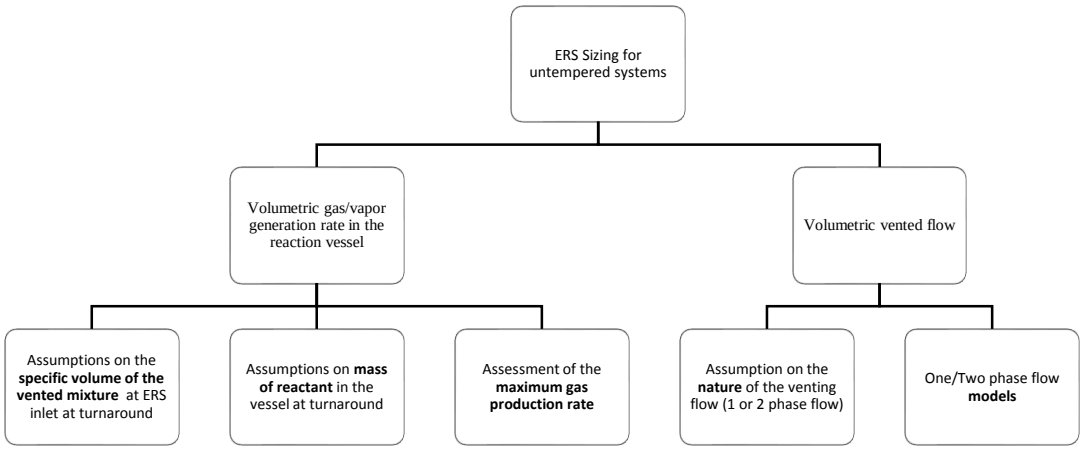

Figure 11: Factors affecting vent sizing for untempered systems

Figure 11 shows the factors affecting the vent sizing calculation for an untempered system. It is currently very difficult to predict the nature of the vented flow (one-phase of two-phase) and the value of the volumetric vented flow of a reactive mixture. This in turn renders difficult the prediction of the mass of reactive mixture left in the vessel at turnaround. These areas constitute research areas that still require a very significant effort from the research community. In this thesis, we will only be focusing on the assessment of the maximum gas production rate.

2.5.2 Measurement of the maximum gas production rate with low-φ calorimeters

2.5.2.1 Test cell configurations

Two test cell configurations can be used with low φ adiabatic calorimeters for the characterization of runaway reactions (see *Figure 12*). Both configurations will have issues associated with the φ factor as discussed above. The main difference lies in the

assessment of the gas production through the measurement of the pressure of the gas generated by the runaway.

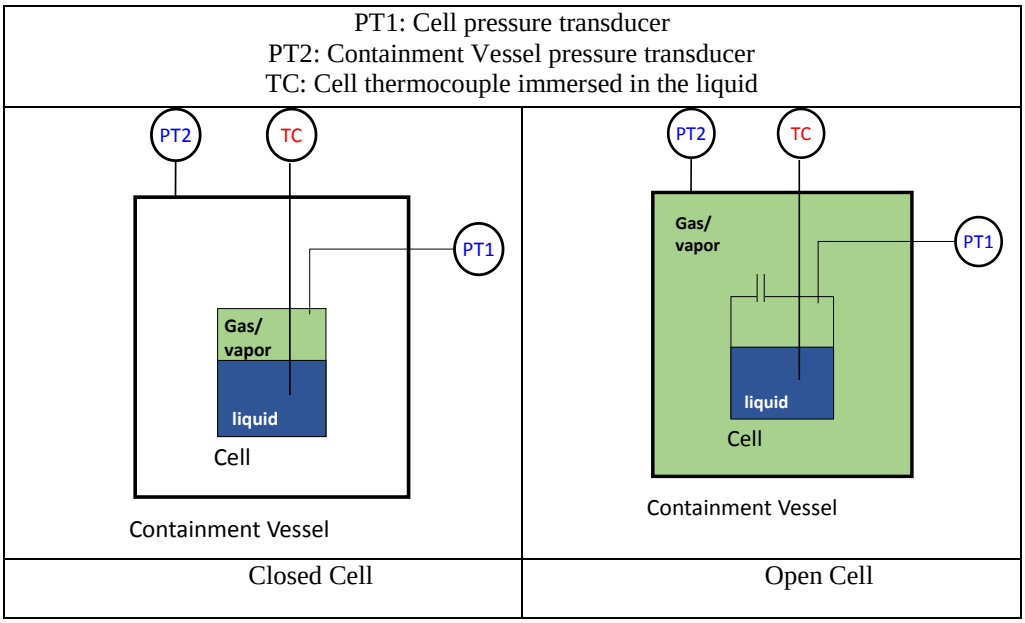

Figure 12: Schematic diagram of the closed cell and open cell configurations

Closed Cell Configuration:

For the closed cell configuration (*Figure 12* - left), the gas/vapor produced by the runaway is pressurizes the cell itself [3]. In this configuration, the temperature of the liquid sample and the gas/vapor phase are well defined. The volume available for the gas/vapor in the cell depends on the test cell fill level and is relatively small. In the case of vapor system, the volume available for the gas does not have any influence on the pressure as the vapor pressure is only a function of the temperature of the liquid. DIERS recommends the use of closed cell configuration for vapor systems [3].

For gas generating chemical systems, for which the pressure is not only due to vapor pressure but also permanent gasses, the small volume available for the gas generally leads to very significant pressures and pressure rise rate of the close cell. This pressure rise rate may lead to the explosion of the test cell in the containment vessel during the exponential pressure increase of the runaway and the failure of the test. Besides, the high pressure of the cell encourages gas dissolution phenomena, which means that the only pressure reading may not be a good indicator of the gas production rate.

Open Cell Configuration:

To overcome the limitations above for gas generating systems, DIERS recommends the use of the open cell configuration (*Figure 12* - right) in which the test cell is open to the containment vessel (e.g. with a hole in the upper side/lid of the test cell). The gas/vapor produced by the runaway reaction pressurizes the containment vessel (the vapor condenses on the cold wall of the containment vessel) which offers a much larger volume for the gas compared to the closed cell configuration. Consequently, lower pressures are reached, gas dissolution effects are reduced and potential explosion of the test cell is much less likely.

Because, for the open cell, a high back pressure is required to superimpose on the containment vessel to suppress boiling of the sample.

The advantages and disadvantages of the configurations are shown in *Table 1*.

Table 1: Advantages and disadvantages of different test configurations

Test configuration	Advantages	Disadvantages
Closed cell	- Sample and gas phase temperatures are well defined and known.	- Explosion of the cell (rapid increase of pressure in the cell). - Gas dissolution.
Open cell	- Limits of the gas dissolution effects (lower pressure in the containment vessel). - No bursting of the cell.	- Temperature of the gas not well defined. - Loss of reactant from the cell during the test.

2.5.2.2 Assessment of gas production rate from calorimetric data

According to DIERS, $Q_{g\ max}$ is proportional to the maximum specific gas production rate $(d\dot{n}_g/dt)_{max}$, moles of gas/kg of liquid/s measured in an adiabatic calorimeter [3].

$$Q_{g\,max} = \nu_g M_w m_R \left(\frac{d\dot{n}_g}{dt}\right)_{max} \quad (19)$$

Where,

M_w is the molecular weight of gas

ν_g is the specific volume of gas in the vessel

ν_g is calculated at maximum pressure rate in the calorimetry test. Considering the ideal gas law:

$$\nu_g = \frac{V}{m} = \frac{R}{M_w}\left(\frac{T_g}{P}\right)_{at\ \left(\frac{dP}{dt}\right)_{max}} \quad (20)$$

The maximum gas production rate resulting from a runaway reaction performed in an adiabatic calorimeter can be derived from ideal gas law:

$$PV_g = n_g R T_g \quad (21)$$

Where,

P is the pressure of gas measured by the calorimeter

V_g is the volume of gas that occupies in the calorimeter

R is the ideal gas constant

n_g is the number of moles of gas produced

T_g is the temperature of the produced gas

Differentiating Equation *(21)* with respect to time gives:

$$P\frac{dV_g}{dt} + V_g\frac{dP}{dt} = R\left[T_g\frac{dn_g}{dt} + n\frac{dT_g}{dt}\right] \quad (22)$$

The volume available to the gas volume can be assumed to be constant in a calorimeter so Equation *(22)* can be reduced to:

$$V_g\frac{dP}{dt} = R\left[T_g\frac{dn_g}{dt} + n_g\frac{dT_g}{dt}\right] \quad (23)$$

Equation (23) can be rearranged to assess the specific gas production rate (per mass of liquid sample):

$$\frac{d\dot{n_g}}{dt} = \frac{V}{m_s R T_g}\left(\frac{dP}{dt} - \frac{P}{T_g}\frac{dT_g}{dt}\right) \quad (24)$$

Where, m_s is the mass of liquid sample in the calorimeter.

When the maximum pressure change in the calorimeter is measured, *Equation (23)* is used to assess the maximum specific gas production rate:

$$\left(\frac{d\dot{n_g}}{dt}\right)_{max} = \frac{V_g}{m_s R}\frac{1}{T_{g\ at\left(\frac{dP}{dt}\right)_{max}}}\left[\left(\frac{dP}{dt}\right)_{max} - \left[\frac{P}{T_g}\left(\frac{dT_g}{dt}\right)\right]_{at\left(\frac{dP}{dt}\right)_{max}}\right] \quad (25)$$

The following assumptions are usually made for the different calorimeter configurations to calculate the maximum specific gas production rate:

- For closed cell test, T_g is the same as the liquid temperature;

- For open cell test, when not measured, the gas temperature is taken as the average between ambient and the liquid temperature. However, the validity of this assumption is disputed [3];
- The mass of liquid (m_s) used to calculate the specific gas production rate is assumed to the initial mass of the sample for the test. The validity of this assumption is disputed for open cell tests as significant reactant mass can be lost to the containment vessel during an experiment [3]. Indeed, it is only possible to measure the mass of the liquid sample at the beginning and at the end of the experiment. It is not possible to the exact mass of reactant still in the test cell when the gas production rate is maximum.

2.5.3 Limitation of the current vent sizing methods

Several authors have reported the vent sizing methods for gassy systems are significantly oversizing, meaning that the resulting vent sizes are very often unrealistic (sometimes as large as the vessel diameter), impractical and expensive [24],[27]. The approach developed by the DIERS on the design of ERS for untempered hybrid systems is also known to be rather simplistic and to lead to oversizing [28], [29].

In 2009, the UK Health and Safety Laboratory and the French INERIS organized a series of Round Robin tests on vent sizing for gassy systems [29]. The exercise required the assessment of the size of a bursting disc (vent area) that would allow the protection of a 340 litre reactor vessel filled at 70% (v/v) with a gassy system (40% w/w dicumyl peroxide in 2,2,4-trimethyl-1,3-pentanediol dissobutyrate) and subject to fire loading (5°C/min). The vent opening pressure was set a 4 bars and the Maximum Allowable

Working Pressure (MAWP) was 7 bars. The participating companies based vent sizing calculations on experimental data obtained from their respective adiabatic calorimeters using the peroxide and solvent (from the same production batch).

Table 2 presents the different test conditions and assumptions made by the participant in their assessment of the vent area. It can be seen that:

- Different types of adiabatic calorimeters were and test configurations were used (open and closed cell);
- Only closed cell data (2 participants) were corrected for φ factor for the temperature response and only in one case the pressure data were corrected for φ factor using a zero order correction of dP/dt;
- When not measured, different assumptions were made on the temperature of the gas to be used for the calculation for the open cell tests;
- Different assumptions were made as per the nature of the gas produced by the runaway, and;
- The assumption of the nature of the flow during venting (1-phase or 2-phase) differed between the participants (see 2.5.1).

Table 2: Round Robin tests: summary of the test conditions of the calorimetric experiments and assumptions. Adapted from L. Véchot et al. 2011 [29]

	Participant					
	A	B	C	D	E	F
Calorimeter	Phitec II	VSP2	ARSST	VSP2	Phitec II	VSP2
Test conditions	Close cell	Close cell	Open cell	Open cell	Open cell	Open cell
Correction of heat rate for φ factor	Yes	Yes	No	No	No	No
Correction of gas production rate for φ factor	No	Yes	No	No	No	No
Gas temperature in the calorimeter	$T_g = T_l$	$T_g = T_l$	$T_g = T_l$	Measured	Average of T_g and T_a	$T_g = T_a$
Nature of the gas	CH_4 +CO + CO_2	CH_4	CO_2	CH_4	CH_4	CH_4
Flow type	Gas	Gas	Gas	Two-phase	Two-phase	Two-phase
Model used for the calculation of vented flux	Gas venting	Gas venting	Gas venting	Tangren	Omega	Tangren

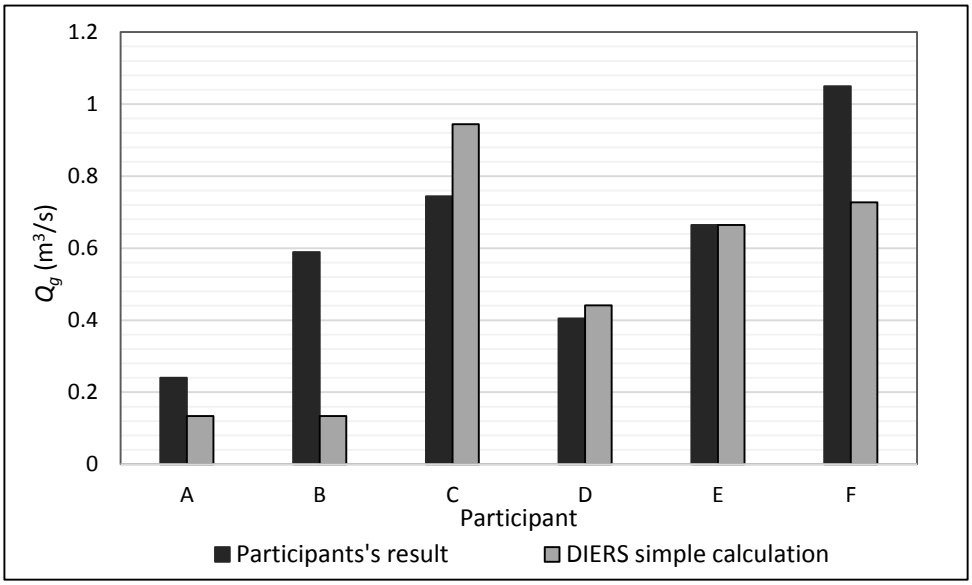

Figure 13: Comparison of volumetric gas production rate. Adapted from L. Véchot et al. 2011 [29]

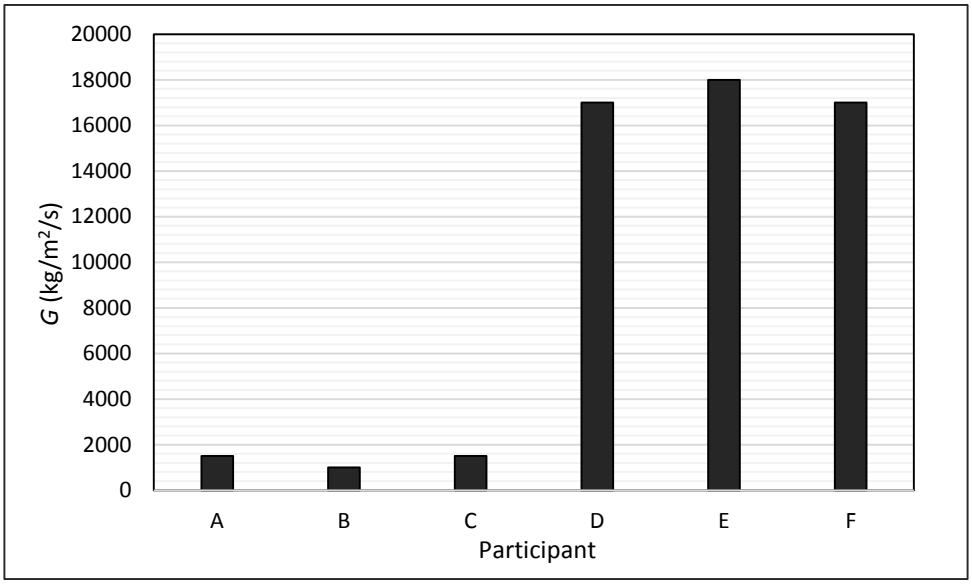

Figure 14: Calculation of the vented mass flux. Adapted from L. Véchot et al. 2011 [29]

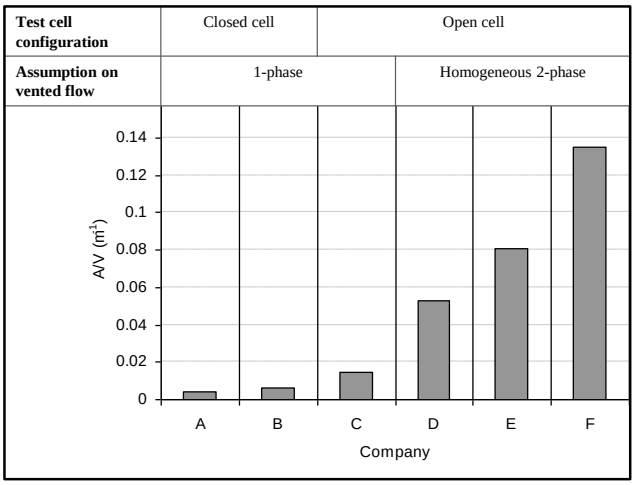

Figure 15: Calculated vent area/volume ratio. Adapted from L. Véchot et al. 2011 [29]

Figure 13 show that the volumetric gas production rate (Q_g) calculated by the participants – (Participant's results) could differ by a factor of 4. Q_g calculated with open cell data was not necessarily less than the ones calculated with closed cell data, and large variation in the assessed Q_g are apparent for a given test cell configuration. To better

understand the origin of the difference of results the calorimetric data generated by the participant were used to calculate Q_g by assuming the following (referred to as DIERS simple calculation on *Figure 13*):

- For closed cell test, the temperature of the gas is same as the temperature of the liquid;
- For closed cell tests, when not measured, the temperature of the gas is assumed to be the average of ambient temperature and liquid temperature;
- The assumption on the nature of the gas is the same as the participant.

The difference found between the Participant's result and simple DIERS calculation showed that:

- While similar experimental result were obtained by participant A and B, the correction of the pressure response by participant B resulted in an estimated Q_g 3 times higher than B.
- Experimental result differs from the calorimeters for similar experiments in open cells.
- The assumption on the temperature of the gas for open cell configuration can play a significant role in the assessment of Q_g.

Figure 14 shows the difference in vented mass flux (G) at the second pressure peak calculated by the participants by assuming the one-phase or two-phase relief models. As expected, G was significantly lower for the single phase venting compared two-phase venting. The difference between two approaches is more than one order of magnitude. It is very important to note that no solid justification of the justification of the assumption

on the nature of the flow for the calculation of G at the second pressure peak was given by the participants.

The differences above resulted in very significant differences in the vent area calculated by the participants as illustrated in *Figure 15*. Consequently, participants D, E and F concluded that the reaction could not be carried out safely in the vessel whereas participants A, B and C concluded that this was possible.

The Round Robin exercise highlighted the issues associated with the application of the DIERS methodology. Despite the fact that the prediction of the nature of the vented flow (1 or 2 phase) played a very significant roles in the differences in the calculated vent areas, the exercise showed that experimental conditions of the calorimetric tests can have a significant influence on the gas production rate at a large scale. The major sources of differences are:

- The choice of configuration (close or open);
- The correction of adiabatic data for φ factor;
- The assumption of gas temperature(when not measured).

The results showed that there is still no consensus on the best approach to measure $Q_{g\ max}$ from calorimetric data [29].

2.5.4 Latest development in vent sizing methodology for gassy systems – reconstruction of pressure curve from adiabatic data (Kossoy's method)

Within the context of the improvement of Fisher's method, A.A. Kossoy *et al.* [25] proposed a method for the first time to correct the pressure for the φ factor and thus obtain an adjusted pressure rise rate and specific gas production rate. His approach consists in

expressing the total pressure as a sum of the initial pressure of air or inert gas in the calorimeter (also called pad gas pressure, P_p), the vapor pressure of the mixture contents (P_v) and the pressure of the permanent gasses generated (P_g):

$$P = P_p + P_v + P_g \tag{26}$$

Calculation of pad gas pressure (P_p):

In a typical case, the initial pad gas pressure ($P_{p,in}$) is known at the initial temperature (T_{in}). The pad gas pressure can be expressed as:

$$P_p(t) = P_{p,in} \times \frac{T(t)}{T_{in}} \tag{27}$$

Calculation of vapor pressure (P_v):

The vapor pressure is a function of temperature and composition of the vapor phase. Since the exact composition of the reactive liquid is often unknown, it is very difficult of predict the P_v. For simplicity, it is assumed that only one volatile component in the mixture exists in the vapor phase. The P_v can be calculated from the Antoine Equation as expressed below:

$$P_v(t) = 10^{\left(A - \frac{B}{T(t)+C}\right)} \tag{28}$$

Where, *A, B, C* are Antoine constant.

Calculation of gas pressure (P_g):

The term P_g is directly related to the chemical reaction. P_g can be expressed as:

$$P_g(t) = P(t) - P_p(t) - P_v(t) \tag{29}$$

Whenever the value $P_g(t)$ is estimated, the specific gas production in experimental time scale, $\dot{n}_g(t)$ can be calculated from the following equation;

$$\dot{n}_g(t) = \frac{P_g(t)V}{m_s RT} \tag{30}$$

As the pressure components and gas g production have been estimated in experimental time scale, the adjusted pressure components can be calculated in following steps:

$$P_{p,adj}(t_{adj}) = P_{p,in} \times \frac{T_{adj}(t_{adj})}{T_{in}} \quad (31)$$

$$P_{v,adj}(t_{adj}) = 10^{\left(A - \frac{B}{T_{adj}(t_{adj})+C}\right)} \quad (32)$$

$$P_{g,adj}(t_{adj}) = \frac{\dot{n}_{g,adj}(t_{adj}) m_s R T_{adj}(t_{adj})}{V} \quad (33)$$

$$P_{adj}(t_{adj}) = P_{p,adj}(t_{adj}) + P_{v,adj}(t_{adj}) + P_{g,adj}(t_{adj}) \quad (34)$$

Finally, the *Equation (25)* can be rewritten for adjusted maximum specific gas production rate as below [25]:

$$\left(\frac{d\dot{n}_g}{dt}\right)_{max,adj} = \frac{V}{m_s R T_{adj}} \left[\left(\frac{dP}{dt}\right)_{max,adj} - \left[\frac{P}{T}\left(\frac{dT}{dt}\right)\right]_{at\left(\frac{dP}{dt}\right)_{max,adj}}\right] \quad (35)$$

The above approach is novel and promising but currently has the following limitations:

- The available volume of the gas (V) is assumed to be constant. However, V should be known in time and taken into account. It is difficult to know V in each time because it depends on many factors such as the thermal expansion of the cell, change of sample volume due to change in its composition, due to the generation of gaseous product, etc.
- The **solubility of the gaseous product in the reactive mixture is not considered.** This may have a significant impact because it depends on mixture composition, pressure, and temperature.

- In Equation *(33)*, the gas pressure and specific gas production both are unknown. It is not possible to calculate the gas pressure without knowing the specific gas production rate. As a result, to calculate the gas pressure, A. A Kossoy *et al.* assumed that the specific gas production is same in both experimental and adjusted time scale i.e., $\dot{n}_g\ (t) = \dot{n}_{g,adj}\ (t_{adj})$.

  This approach needs to be investigated further.

2.6 SUMMARY OF THE GAPS AND AREA OF INVESTIGATIONS

As discussed in the previous paragraphs the main areas of uncertainties associated to the calculation of the suitable vent area to protect a reactor vessel for an untempered system are associated with the difficulty to predict:

- the nature of the vented flow (one-phase of two-phase);
- the calculation of the vented mass flow in the particular case of a venting of reactive two-phase mixture;
- the mass of reactive mixture in the vessel at turnaround and;
- **the assessment of maximum gas production rate for the reactive mixture from calorimetric data**, on which this research work will focus.

The knowledge gaps associated with the assessment of the maximum gas production rate for gas generating systems can be summarized as follows *Figure 16)*.

There's no consensus in the industry as per the best choice of the experimental conditions to be used with the adiabatic calorimeter for the experimental determination of the gas production rate for an untempered system (open cell versus closed cell configurations, see *Figure 12*).

When experiments are performed with the closed cell configuration, the temperature of the gas and the φ factor are pretty well defined which represents an advantage in the calculation of the specific gas production rate. On the other hand, closed cell tests be associated with potential issues of explosion of the test cells with low-φ calorimeters. Besides this technical limitation, close cell tests often lead to the underestimation of the gas production rate because of **gas dissolution effects**.

For open cell tests, the gas dissolution effect may be reduced but significant uncertainties remain associated with the temperature of the gas phase (when the gas temperature is not measured) to be used for the calculation of the gas production rate. In addition, during an experiment a significant amount of the reactant can be lost to the containment vessel. Indeed, it is only possible to measure the mass of the liquid sample at the beginning and at the end of the experiment. It is not possible to the exact mass of reactant still in the test cell when the gas production rate is maximum. This adds a significant uncertainty on the calculated value of the specific gas production rate.

φ factor correction:

The classical Fisher's method for the correction of the adiabatic data only takes into account the effect of thermal inertia (φ factor) for temperature but does not allow the correction of the pressure data. Consequently, the current practice tends to neglect the φ correction for the calculated specific gas production rate. The recent Enhanced Fisher method proposed by A.A. Kossoy *et al.*[25] provided a relatively good solution (for selected types of reactions) for the correction of the temperature and time dimension. His method also for the first time a correction strategy for pressure data. However, this

correction still neglects the **gas dissolution effects**, which can be significant with closed cell data. In addition, the correction method for the pressure still needs to be experimentally validated.

Experimental validation:

The scarcity of the large scale venting experiments for untempered systems make difficult to validate the vent sizing method in general and of the prediction methods for the gas production rate from calorimetric data in particular.

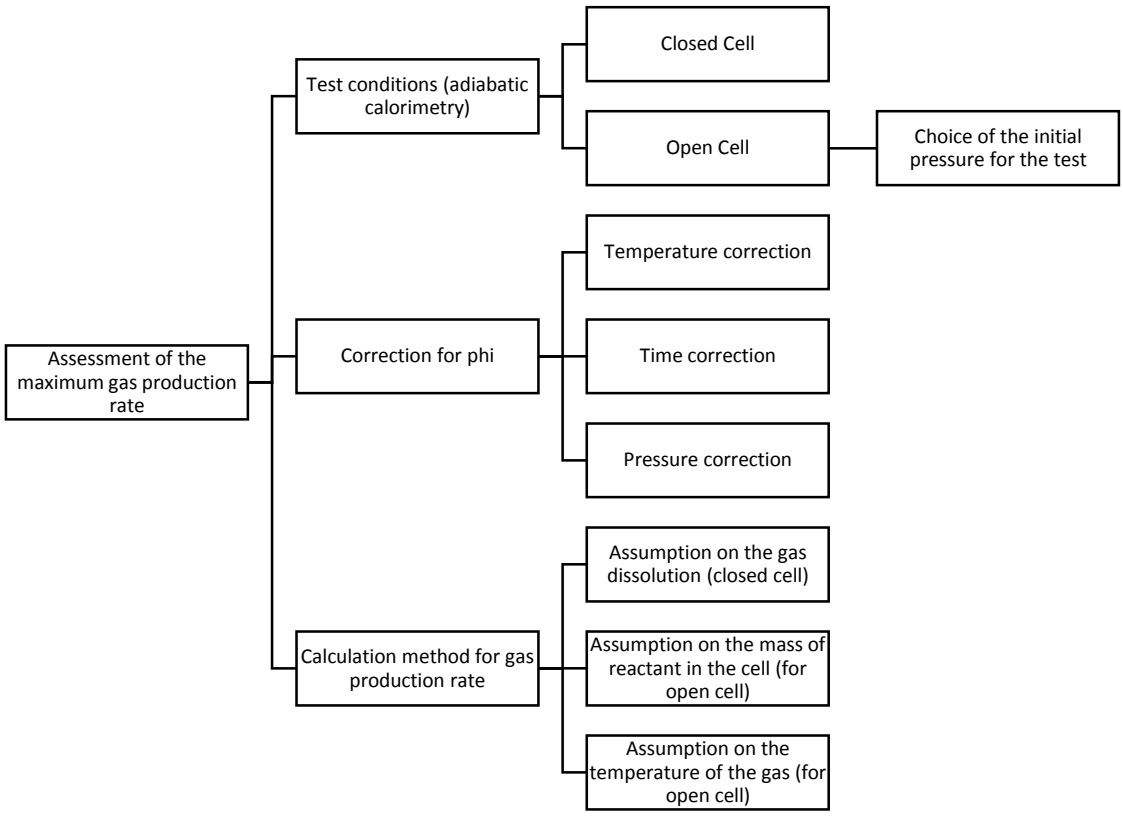

Figure 16: Factors affecting the assessment of the maximum gas production rate from adiabatic calorimetry data

3 MOTIVATION AND SCOPE OF WORK

An exothermic chemical reaction over which control of the temperature is lost is known as a runaway reaction. Runaway reactions are characterized by the exponential increase of the temperature and pressure in the reactor or storage vessel that can eventually lead to the explosion of the vessel. The consequences of the runaway reactions can be severe in terms of loss of life, economic and environmental losses. Emergency relief systems (ERS) are used as the last layer of the defense to prevent the explosion of the vessel following the runaway reaction [23]. In the 1980's the DIERS developed ERS sizing methodologies for reactive systems or runaway reaction cases based on adiabatic calorimetry techniques. While significant efforts were devoted to ERS sizing for vapor systems (for which the pressure increase in the vessel results from the vapor pressure of the vessel contents), very few research was done for non-condensable gas generating systems such as the decomposition of peroxide mixture. There is still very significant work to be done to improve the methods for the measurements of the maximum gas production rate corresponding to the decomposition of a gas generating system under runaway conditions to subsequently improve the design of ERS. The existing methods have the following limitations:

- There's no consensus in the organization as per the best choice of the experimental conditions to be used with the adiabatic calorimeter for the experimental determination of the gas production rate of untempered systems.

- In closed cell configuration, gas dissolution effects can lead to the underestimation of gas production rate.
- In open cell configuration, gas temperature and mass of liquid involved in the reaction are not well defined.
- The effect of thermal inertia is corrected for temperature (classical Fisher's method [24]), time (Enhanced Fisher's method [25]), and pressure (Kossoy's proposed method [25]). However, this correction still neglects the gas dissolution effects, which can play a significant role in gas production rate (especially in closed cell test).
- The scarcity of large scale venting experiments make difficult to predict the gas production rate of untempered systems.

The objective of this thesis work is to study experimentally the decomposition of a gas generating system, Cumene Hydroperoxide (CHP) in Cumene, under runaway condition using adiabatic calorimetry and assess the maximum gas production rate corresponding to the runaway. A critical analysis of the current methodologies to interpret experimental data to assess the maximum gas production rate will be done. The effect of the experimental condition in adiabatic calorimetry (open vs closed cell; initial fill level, the initial pressure of the test) on the measured gas production rate will be investigated.

4 METHODOLOGY

A series of laboratory scale tests were conducted with Cumene Hydroperoxide (CHP) in Cumene, a gas generating system, using PHITEC II adiabatic calorimeter (HEL Ltd). The experiments were performed with the following different test cell configurations with the adiabatic calorimeter (see *Figure 17*): closed cell configuration, open cell configuration (cell directly open to the containment vessel cell) and open cell to external vessel (cell outlet connected to an external vessel). The later configuration was specially tested in this research project.

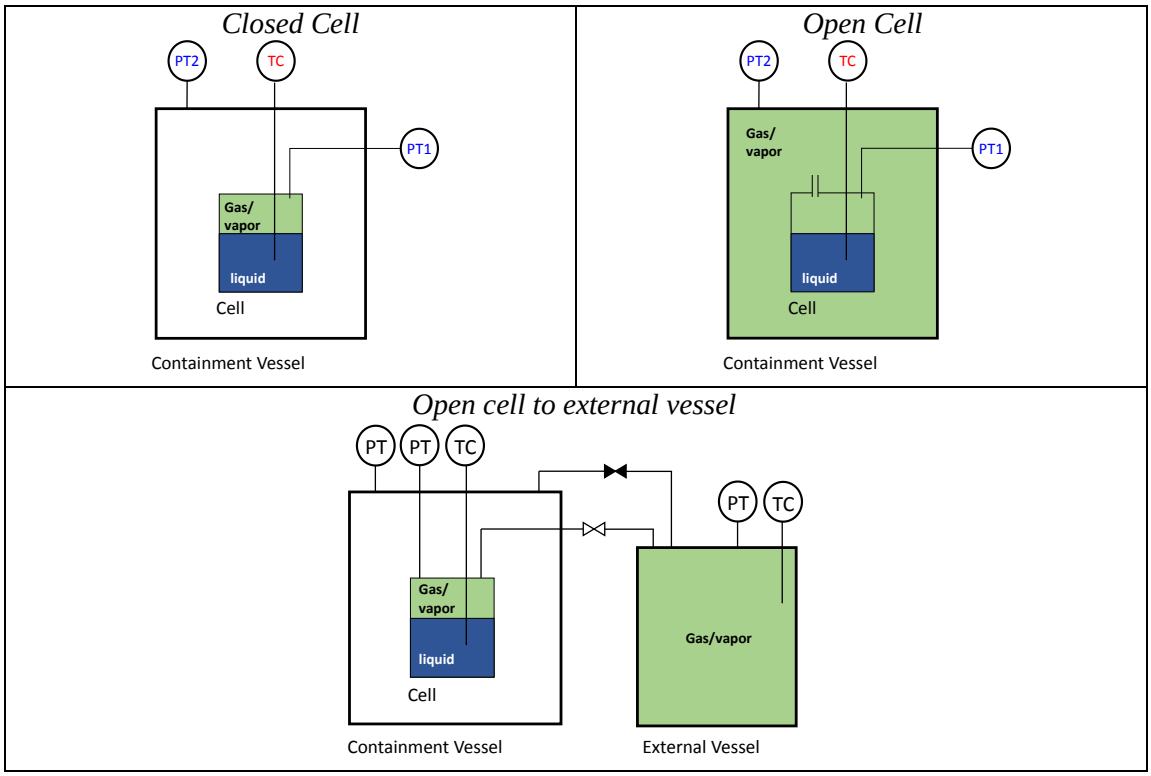

Figure 17: Schematic diagram of the configurations of the adiabatic calorimeter for the experimental work of this thesis.

The experiments were performed while varying the concentration of the peroxide solution, the initial fill level of the test cell and the initial pressure of the tests (for open cell configurations only) were varied. The raw temperature and pressure data were analyzed to assess the influence of the experimental conditions on the specific gas production rate.

The experimental temperature data obtained with the closed cell configuration were corrected for φ using the classical Fisher's method and the Enhanced Fisher's method. Kossoy's method for the correction of pressure data was also tested to correct the gas production rate for φ factor. This part of the work highlighted the importance of correcting both temperature and pressure data for φ factor, which is currently rarely done for gas generating systems because of the lack of available methodologies.

Finally, conclusions are drawn regarding the limitations, advantages and disadvantages of the current methodologies for the assessment of the maximum gas production rate for runaway of gas generating systems.

4.1 CUMENE HYDROPEROXIDE IN CUMENE CHEMICAL SYSTEM

Cumene Hydroperoxide (CHP) is a typical example of an organic peroxide that decomposes giving non condensable gasses. CHP is primarily used in the production of acetone and phenol. It is also used as a catalyst for rapid polymerization, especially in redox systems, a curing agent for unsaturated polyester resins, an initiator for polymerization of styrene and acrylic monomer, and a chemical intermediate for the cross-linking agent.

Cumene is also known as Isopropylbenzene, is a volatile, colorless liquid at room temperature with a characteristic sharp, penetrating, aromatic odor. Cumene is used in the manufacturing of polymerization catalysts and as a raw material for peroxides. We chose Cumene as a solvent for the peroxide solution in this work.

Different researchers have been working on the thermal decomposition process of CHP in Cumene from the thermal and kinetics point of view [30], [31], [32]. However, the decomposition mechanism and associated kinetics are still to be fully understood. The major discrepancy is found in the literature regarding the reaction order for the decomposition reaction of CHP in Cumene. Some researchers describes the reaction as an n^{th} order reaction (n = 0.5 [31]; n = 1 [33]) reaction while others consider an autocatalytic mechanism [34].

The reaction pathway of CHP and associated hazards over concentration are important for developing an inherently safer process where CHP is employed. In 2010, Y. Lu *et al*.[35] studied the effects of CHP concentration on runaway reactions by using adiabatic calorimeter RSST^{TM}. The runaway reaction parameters such as onset temperature, maximum temperature, maximum self-heating rate, and maximum pressure rate were observed at different CHP concentration. The results confirm that 40% (w/w) CHP is a critical concentration where the reaction mechanism begins to change.

Appendices A, B and C provide information on properties of CHP and Cumene.

4.2 EXPERIMENTAL SETUP AND DATA ANALYSIS

The experiments were run using the PHITEC II adiabatic calorimeter (manufactured by HEL Ltd). The equipment and test procedure are discussed in the following sections.

Figure 18: PHI-TEC II adiabatic calorimeter

4.2.1 PHI-TEC II adiabatic calorimeter

PHI-TEC II (*Figure 18*) is a bench scale adiabatic calorimeter that allows the experimental investigation of runaway reactions. It is a low φ calorimeter that can perform both closed and open cell test as described in sections 2.4.2 and 2.5.2. The maximum temperature and pressure that can be measured are set to 500°C and 100 bar. If the temperature and pressure of the runaway exceed these values, an automatic shutdown procedures is initiated and the test stopped.

The PHI-TEC II is composed of the following elements [36]:

Test cells:

The calorimeter uses a 110 ml thin walled stainless steel test cell in which a reactive substance of mixture can be taken to runaway in adiabatic conditions. The test cell can stand a maximum pressure of 4 bar before bursting.

Wrapped around heater:

A pre-coiled metallic wire heater wrapped around the test cell is used to provide external heat to the sample. This heater is used to bring the liquid sample to an initial test temperature (when fixed), or to search for an onset temperature until an exotherm is detected.

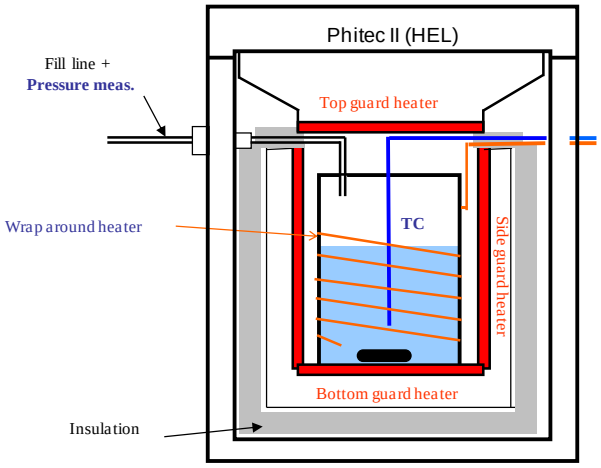

Figure 19: Schematic diagram of PHI-TEC II

Guard heaters:

The purpose to the guard heaters is to create an adiabatic environment to the sample. In the calorimeter, the test cell is surrounded by top, bottom and side guard heater heaters independently controlled by a PID control algorithm [36]. These heaters are automatically set to a temperature slightly higher than the cell temperature when in adiabatic mode to minimize the heat losses and allow the sample to react in adiabatic conditions.

Containment vessel and pressure compensation system:

The test cell and the heaters are located within a stainless-steel containment vessel rated at 200 bars (@ 100°C) [36]. The containment vessel is used to prevent the explosion of the pressurized test cell via an automatic pressure compensation system. It also provides protection for the personnel should the explosion of the cell occur.

Automatic pressure compensation system:

An automatic pressure compensation system maintains a differential pressure of less than 3 bars between the test cell and the pressure vessel. This is done automatically by injecting/removing nitrogen gas into the containment vessel.

Instrumentation and data acquisition system:

Type K thermocouples (temperature range -200 to 1250 °C [37]) are used to measure the temperatures of the test cell and the heaters. An absolute pressure transducer measures the pressure of the containment (range 0-200 bar, 0.1% accuracy of full scale). A differential pressure transducer is used to measure the pressure difference between the test cell and the containment vessel (range ± 14 bar, <±0.1% accuracy of full scale). The readings are sent to a data acquisition system linked to a computer with WinISO control software. The frequency of data storage is determined by the instantaneous self-heat rate.

External Vessel:

For experiment with open cell to external vessel, the test cell is connected to a 1 litre external stainless vessel (rated at 200 bars) by a 1/8" stainless steel tube (*Figure 20*). To allow the pressurization of the system cell plus external vessel to a given initial pressure using nitrogen gas, a by-pass line (1/8" stainless steel) is installed between the external

vessel and containment vessel. The external vessel is equipped with a Type K thermocouple, a pressure gauge (range 0-137 bar) a pressure transducer (range 0-200 bar, ± 0.1% accuracy of full scale) and a rupture disc (rating pressure 137 bar).

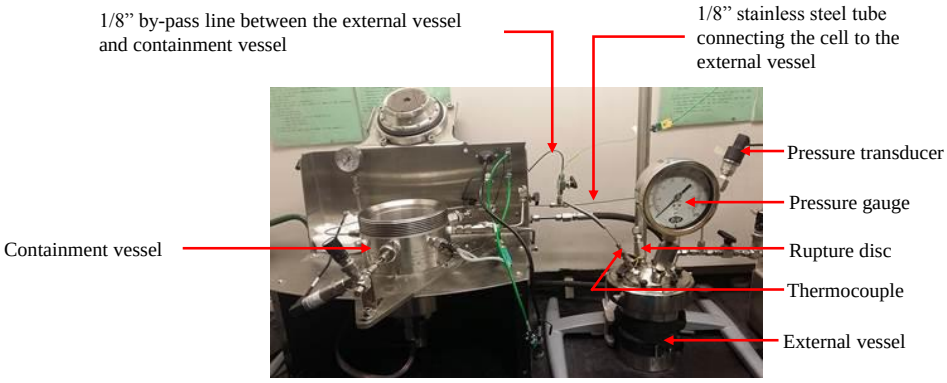

Figure 20: PHI-TEC II with external vessel

4.2.2 Test procedure

The flow chart of an experimental test with PHI-TEC II is shown in *Figure 21*.

4.2.2.1 Preparation of the sample and sample loading

The solution of CHP in Cumene is prepared under a fume hood and loaded into the test cell using a glass syringe and a feeding pipe. The cell is weighted before and after the sample loading. The cell is then inserted into the calorimeter's containment vessel following the proper configuration (closed cell, open cell or open cell to external vessel). After the containment vessel is closed and the calorimeter setup is put under 3 bars of nitrogen gas and tested for leaks using leak detection solution. This task is very time consuming and is very important to guarantee the quality of the data.

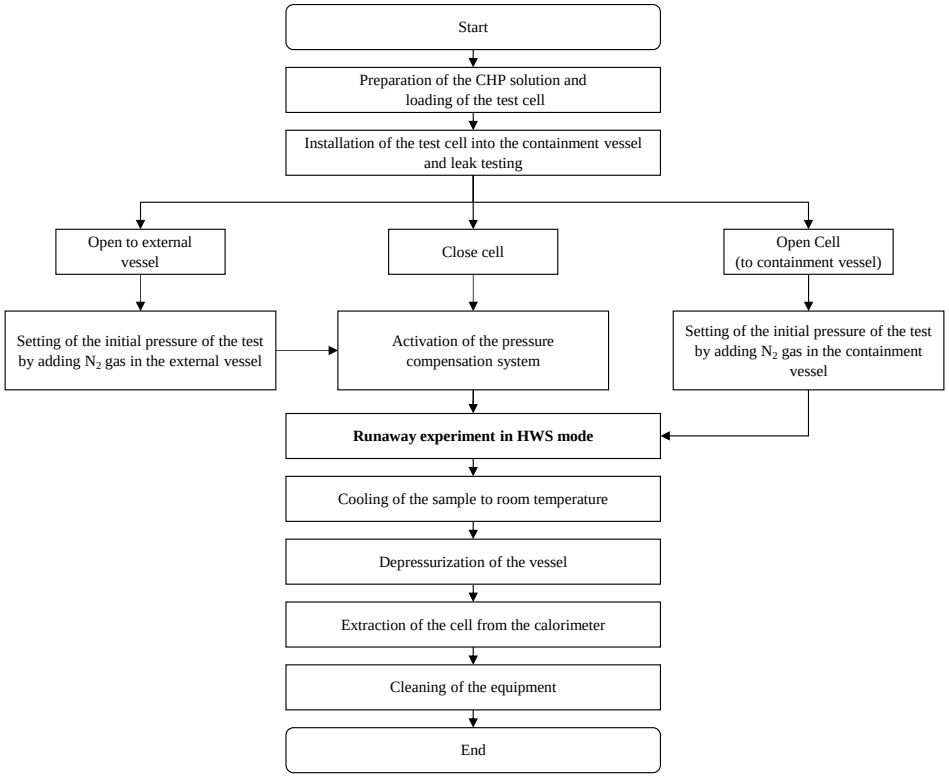

Figure 21: Flow chart of a PHI-TEC II experiment

4.2.2.2 Runaway experiment in heat wait and search (HWS) mode

All the experiments were performed by using the Heat-Wait-Search (HWS) mode. In this mode, the sample is heated up (Heat) and stabilized (Wait) to a temperature specified by the user, then maintained at this temperature in adiabatic conditions (Search) until self-heating is detected by the equipment. The sensitivity of the equipment for the detection of exotherm is 0.02 °C/min. If no exotherm is detected then the sample is taken to a higher temperature, the temperature step being set by the user. When an exotherm is detected, the equipment switches to adiabatic mode until the completion of the runaway. *Figure 22* and *Figure 23* below depict the steps of HWS mode.

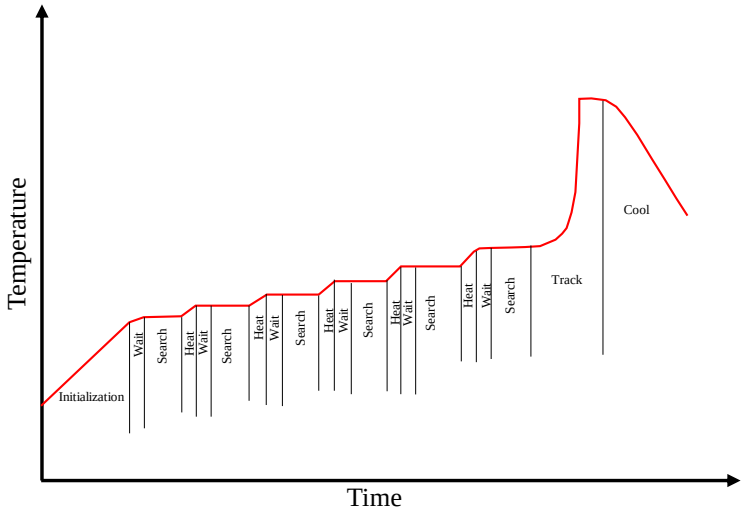

Figure 22: Temperature curve in heat wait and search (HWS) mode

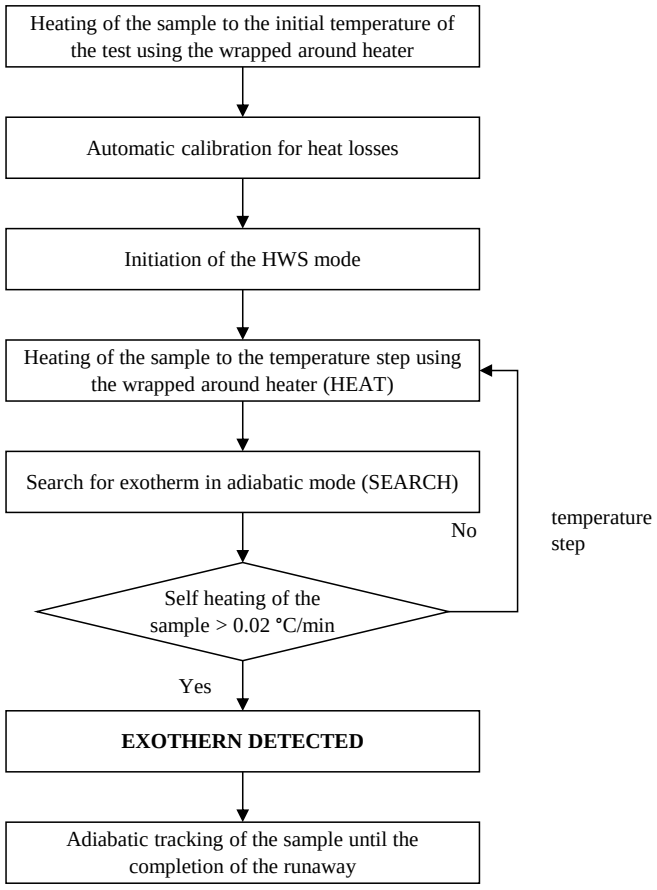

Figure 23: Heat wait and search (HWS) mode flow chart

4.2.2.3 End of the test

At the end of the run, the sample is cooled down to room temperature (natural cooling). The calorimeter is then slowly depressurized (with the assistance of the automatic pressure compensation system for closed cell and open cell to external vessel configurations) and opened to extract the test cell.

The cell containing the reacted sample is weighted. The sample mass loss is then quantified using the following mass loss ratio:

$$\frac{\Delta m}{m_0} = \frac{m_0 - m_f}{m_0} \qquad (36)$$

Where m_0 and m_f are the initial and final mass of the sample in the test cell before and after the tests respectively.

The equipment is then fully cleaned and prepared for a future experiment.

4.2.3 Maintenance of the equipment

Several maintenance and calibration tasks were performed to guarantee the best possible quality of the data. These included the calibration of the thermocouples and pressure transducers. The elements of the calorimeter containment vessel were occasionally fully dismantled and cleaned. This particular task was time-consuming (around one week).

4.2.4 Data analysis

The data analysis included the analysis of the raw data to extract the necessary information to calculate the specific maximum gas production rate for each experiment.

For closed cell experiment, the raw data were corrected for φ. Finally, the overall comparison of the results is done.

A flow chart of data analysis is shown in *Figure 24.*

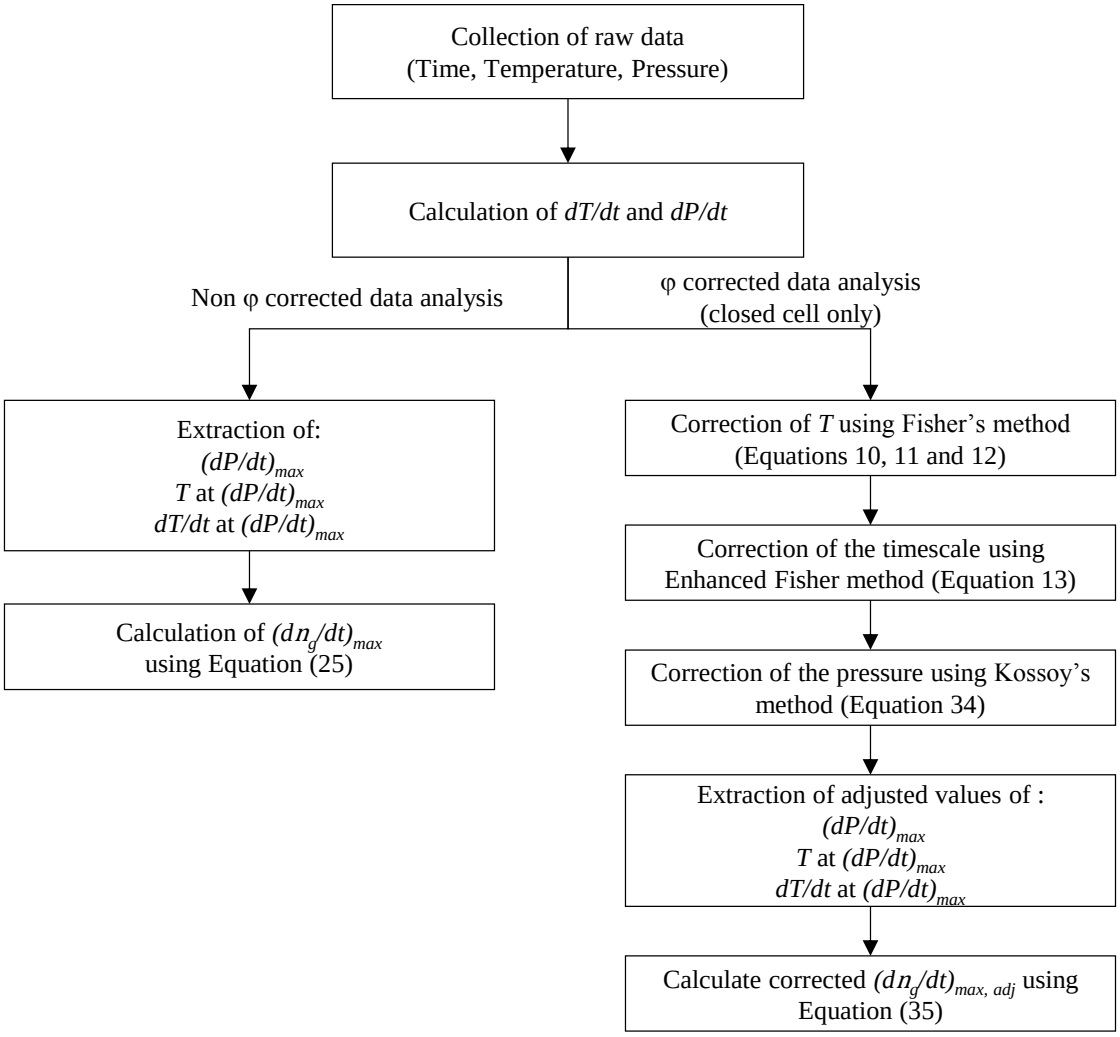

Figure 24: The flow chart of data analysis

4.2.4.1 Analysis of the raw data

The raw data file obtained from the calorimeter contain the cell temperature (liquid) and pressure, the containment vessel pressure and the external vessel temperature and pressure. The derivative of the temperature and pressure with respect to time were calculated from the raw data. Others experimental variables were also available but not used for the subsequent calculations (e.g. guard heaters temperatures, heater power, etc).

The temperature of the liquid and pressure of the gas/vapor (test cell, containment vessel or external vessel depending on the configuration) were plotted as a function of time. The following specific data were extracted from these graphs (see *Figure 25*):

- The onset temperature (T_{on});
- The maximum liquid temperature (T_{max}) and;
- The maximum pressure of the cell of the containment/external vessel (P_{max}).

The derivatives of the liquid temperature (*dT/dt* also referred to as the self heat rate SHR), gas/vapor temperature (dT_g/dt), gas/vapor pressure (dP/dt) were plotted as a function of the liquid temperature. The following specific data were extracted from these graphs (see *Figure 25*):

- The maximum pressure rise rate $(dP/dt)_{max}$;
- The liquid temperature at the maximum pressure rise rate (T at $(dP/dt)_{max}$);
- The liquid temperature rise rate at the maximum pressure rise rate (dT/dt at $(dP/dt)_{max}$).

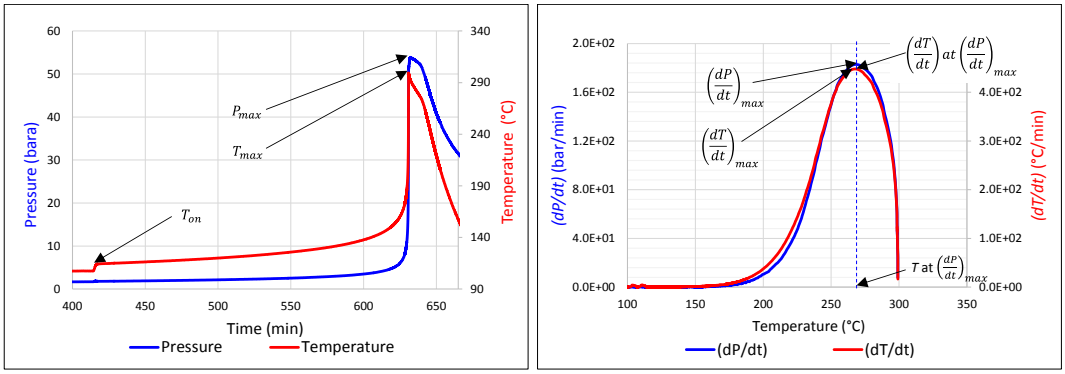

Figure 25: Temperature and pressure profiles (left), temperature and pressure rise rates (right)

The *dT/dt* = f(*T*) curve was also used to extract the value of the apparent activation energy of the reaction. Since the conversion rate at the beginning of reaction is relatively low at early stages of the reaction, the kinetic of the reaction can be considered as a zero order reaction. The activation energy can be extracted from the slope of the ln*(dT/dt)* = f(-1000/*T*) plot (see *Figure 26*). The slope of the graph gives *E*/1000*R* where R is the ideal gas constant. The activation energy is subsequently used to correct the experimental data for φ factor.

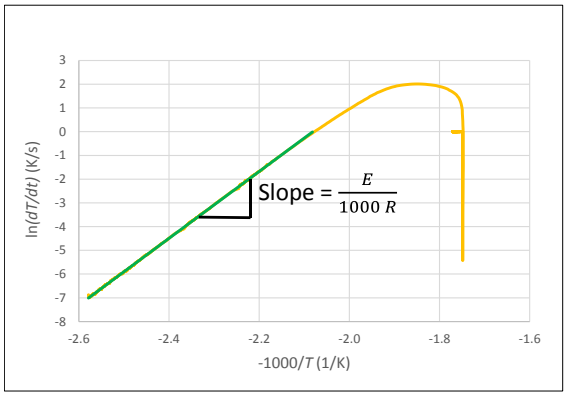

Figure 26: Activation energy calculation

4.2.4.2 Calculation of the specific gas production rate from raw data (non-corrected for φ factor)

For all the experiments, the specific gas production rate was calculated using the approach derived in Section 2.5.2.2.

4.2.4.3 φ factor correction and calculation of the specific gas production rate from φ corrected data

The adiabatic data obtained for the closed cell configuration were corrected using Fisher's method (see Section 2.4.3.1). Equations *(10)*, *(11)* and *(12)* were used to calculate the adjusted onset temperature, adjusted temperature profile and adjusted SHR respectively. The time data were corrected by using Enhanced Fisher method (see Section 2.4.3.2). The pressure data were corrected using the method recently proposed by A.A. Kossoy *et al.* (see Section 2.5.4). Equation *(34*) was used to calculate the total corrected pressure. Finally, all the corrected data were used to calculate the corrected maximum specific gas production rate using Equation *(35*).

5 EXPERIMENTAL RESULTS AND DISCUSSION

This section discusses the experimental results obtained with the PHI-TEC II adiabatic calorimeter with the runaway of Cumene Hydroperoxide (CHP) in solution in Cumene. *Table 3* summarizes the experimental conditions of the experiments. The concentration of CHP chosen for the tests were 20, 30 and 40 % (w/w). The experiments were performed with three configurations of the adiabatic calorimeter: closed cell, open cell and open cell to external vessel.

Three different experimental conditions were tested with the closed cell configuration. For these tests, the fill level was set to 55% v/v and the effect of the concentration on the runaway were studied (20%, 30% and 40% w/w).

Thirteen different experimental conditions were tested with the open cell configuration. For these tests the effect of the fill level (55 and 70 % v/v), the initial pressure of the test (1, 5 and 20 bars pressure of nitrogen gas at the beginning of the test) oxide concentration (20%, 30% and 40% w/w) on the runaway reaction were investigated.

Six different experimental conditions were tested with the open cell to external vessel configuration. For these tests the concentration of the peroxide (30% w/w) and the fill level (55 % v/v) were fixed and the effect of the initial pressure of the test (1, 3, 5, 10, 20 and 30 bars pressure of nitrogen gas at the beginning of the test) was investigated. For selected experimental condition repeatability tests were performed.

The following discusses the results from the three test cell configuration separately then makes the cross comparison of the results.

Table 3: Experimental plan of this research

Closed cell experiment		
Fill Level (v/v %)	Concentration (w/w %)	
55	20	
	30	
	40 (exploded)	
Open cell to containment vessel experiment		
Fill Level (v/v %)	Initial Pressure (bara)	Concentration (w/w %)
55	1	20
		30
		40
	5	20
		30
		40
	20	30
70	1	20
		30
		40
	5	20
		30
		40
Open cell to external vessel experiment		
Fill Level (v/v %)	Concentration (w/w %)	Initial Pressure (bara)
55	30	1
		3
		5
		10
		20
		30

5.1 CLOSED CELL EXPERIMENT

As mentioned in the previous sections, in the closed cell configuration (*Figure 12* - left), the gas/vapor produced by the runaway is pressurized the cell itself. The volume available for the gas/vapor in the cell depends on of the test cell fill level and is relatively small. A total of 4 experiments were performed in closed cell configuration at 55% (v/v) fill level with the following concentration of CHP (% w/w) in Cumene: 20%, 30% (twice for repeatability) and 40%. The experiments at 20% and 30% concentration were successfully completed. The experiment at 40% concentration was unsuccessful as the gas

production rate resulting from the decomposition of the peroxide resulted in the explosion of the test cell. Indeed, the rate of pressure compensation of the calorimeter was not fast enough to compensate for the pressure rise rate in the test cell. This confirms one of the limitation of the choice of closed test cell for gas production systems discussed in Section 2.5.2.1. The summary of the results is shown in *Table 4*.

Table 4: Summary of the results in closed cell configuration _ 55% (v/v) fill level

Properties	Unit	Concentration (w/w %)			
		20	30 (Trial-1)	30 (Trial-2)	40
Initial mass	$10^{-2} \times$ kg	5.447	5.577	5.564	5.689
φ factor	-	1.32	1.21	1.21	1.15
Final mass	$10^{-2} \times$ kg	53.72	54.59	55.50	ND
$\Delta m/m_0$	%	1.38	2.12	2.05	ND
T_{on}	°C	114.66	114.65	114.89	95.8
T_{max}	°C	236.55	299.12	295.31	ND
$(dT/dt)_{max}$	K/s	0.73	7.46	6.31	ND
P_{max}	Bara	29.55	51.52	48.73	ND
$(dP/dt)_{max}$	Bar/s	0.25	3.05	2.43	ND
T @ $(dP/dt)_{max}$	°C	214.92	268.17	269.5	ND
P @ $(dP/dt)_{max}$	Bara	20.97	38.44	37.13	ND
(dT/dt) @ $(dP/dt)_{max}$	K/s	0.73	7.46	6.26	ND
$(d\dot{n}_g/dt)_{max}$	Moles of gas /kg of liquid/s	4.95×10^{-3}	4.97×10^{-2}	3.94×10^{-2}	ND

ND: No Data (cell exploded)

Repeatability test:

The experiment of 30% (w/w) CHP in Cumene was repeated to check the uncertainty associated with the experimental results. *Table 4* shows that T_{on}, T_{max}, P_{max} and $\Delta m/m_0$ (or the percentage of initial liquid sample mass loss; see Equation (36)) of both experiments were very close with an uncertainty of less than 5%. $(dT/dt)_{max}$ and $(dP/dt)_{max}$

are associated with a level of uncertainty of 15% and 20% respectively, which remains reasonable and typical of adiabatic calorimetry tests [38]. This uncertainty will later reflect on the uncertainty associated to the maximum specific gas production rate.

5.1.1 Effect of the peroxide concentration on temperature and pressure profiles

The experiment results showed that the concentration of the peroxide, within the concentration range investigated 20-30% w/w didn't have a noticeable influence on T_{on} (see *Table 4*) which was around 115°C. T_{on} for the 40% was significantly lower by approximately 20°C. As mentioned above, excellent repeatability was obtained on T_{on} for the 30% (w/w) experiments.

As shown in *Figure 27* and as expected to increase the peroxide concentration leads to a significant change in the temperature and pressure and their derivatives. The observed change is $(dT/dt)_{max}$ and $(dP/dt)_{max}$ is one order of magnitude higher for the 30% w/w solution than the 20% w/w solution (which is much higher than the 20% uncertainty associated with the measurement of the rates rate as shown above). Indeed, a more concentrated peroxide solution tends to lead to a more violent decomposition, i.e. with a faster reaction kinetics and higher total heat of reaction. The change of thermal profile of the decomposition for higher concentration solutions may also be due (in a lesser extent) to the difference in the specific heat capacity of the solution and the resulting φ factor.

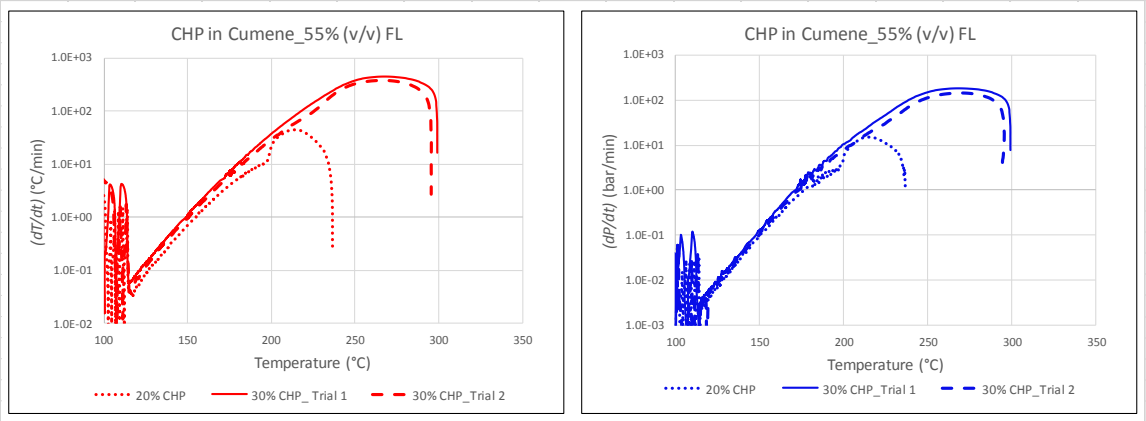

Figure 27: Temperature rise rate and pressure rise rate in closed cell experiments for 20% and 30% w/w CHP in Cumene (55% v/v initial fill level)

5.1.2 Calculation of the total mass of product gas

According to literature, the gas produced from the decomposition of CHP in Cumene is mainly methane [30], [35]. See Appendix C for the literature data on the decomposition reactions of CHP in Cumene. To estimate the total amount of gas produced in this experiment from the experimental data, we used and compared two approaches.

5.1.2.1 Approach I: Liquid mass loss assessment

In this approach, a very crude attempt to evaluate the mass of gas produced by the reaction consisted in measuring the test cell mass loss as described in Equation (36) for the calculation of $\Delta m/m_0$ .Since it is a closed cell experiment, the difference of liquid mass before and after the experiment was assumed to be representative of the amount of gas produced by the reaction. *Table 5* presents the measured masses of liquid for the experiments. The assessed specific gas production were of 1.38 and 2.08 (average) kg of gas/kg of initial solution for the 20% and 30% w/w solutions of peroxide.

Table 5: Total mass loss in closed cell experiments _ Approach I

Concentration	Initial mass of reactant	Final mass of reactant	Total mass loss during the experiment	Specific amount of gas produced
w/w%	g	g	g	kg of gas/kg of initial solution
20	53.989	53.243	0.746	1.38×10^{-2}
30 (Trial-1)	55.121	53.955	1.166	2.11×10^{-2}
30 (Trial-2)	55.461	54.323	1.138	2.05×10^{-2}

This approach is associated with a certain degree of uncertainty which is difficult to assess. Indeed, it assumes that no liquid loss occurs occur during the depressurization of the cell before the opening the containment vessel. In our case, the depressurization of the cell was done very slowly using a needle valve at the outlet of the test cell to minimize liquid carry over during the depressurization. Moreover, during the experiment some liquid may vaporize and leave the test cell either:

- Through minor leaks in the test cell that may lead to a loss of liquid because of a leak of vapor or a leak of the gas itself (in our case a leak test was performed on the equipment before and after the experiment to confirm there was no leak in the experiment);
- Through the piping directly connected to the outlet of the test cell. The vapor may condense in the cold part of the piping system (for instance in the cold chamber of the pressure transducer connected to the cell).

These experimental difficulties induce a level of uncertainty in the evaluation of the specific gas production difficult to quantify using this simple approach. This approach however provides an idea of the maximum specific gas production for the reactive solution. This value may be overestimated.

5.1.2.2 Approach II: Use of ideal gas equation

When the runaway reaction is complete, the test cell is cooled down naturally to the ambient temperature. The residual pressure in the test cell when the liquid reaches the ambient temperature can reasonably be assumed to be a result of:

- The pressure of the non-dissolved gas product (P_g);
- The pad gas pressure (P_p), i.e. the pressure of air initially present in the cell at the start of the experiment, and;
- The vapor pressure (P_v) of the liquid mixture.

In this approach, we assumed that the vapor pressure of the Cumene (solvent)[1]. P_v associated with Cumene is much less than P_g when the reaction has reached the ambient temperature and can be neglected. P_g can be assessed by simply subtracting the pad gas pressure (1.013 bar) to the total pressure and the number of moles of gas can be assessed using the ideal gas law. A sample calculation for 30 w/w% CHP in Cumene is shown in below. *Table 6* shows the mass of product gas from different experiments.

$$P_g V = \frac{m_g}{M_w} RT$$

$$m = \frac{PV\,M_w}{RT}$$

$$= \frac{17.37 \times 4.95 \times 10^{-5} \times 16}{8.314 \times 10^{-5} \times 294.43}$$

$$= 0.562 \text{ g}$$

Where, P_g = 17.37 bar

V = gas volume = 4.95 x 10^{-5} m^3

T= final temperature in the cell= 294.43 K

M_w = molecular wt. of CH_4 = 16 g/mole

R = 8.314 x 10^{-5} m^3.bar/mole/K

[1] However, there's still an uncertainty as per the P_v of the potential reaction products which are unknown.

Table 6: Mass of product gas in closed cell experiments _ Approach II

Concentration	Initial mass of reactant	Mass of produced gas	Specific amount of gas produced
w/w%	g	g	kg of gas/kg of initial solution
20	53.989	0.374	6.92×10^{-3}
30 (Trial-1)	55.121	0.562	1.02×10^{-2}
30 (Trial-2)	55.461	0.551	9.93×10^{-3}

The only source of experimental difficulties inducing uncertainties in approach II is the presence of potential minor leaks in the test cell. As mentioned in Approach I, a leak test was systematically performed on the equipment before and after the experiment to confirm there was no leak in the experiment. The major source of concern is related to the amount of gas dissolved in the liquid which can not be quantified easily. So the value of the gas production calculated with the Approach II may be underestimated. Another uncertainty is related with the nature of the gas so its molecular weight.

5.1.2.3 Comparisons of approaches I and II

Table 7 shows that the mass calculated in Approach II is around 50% lower than approach I. As discussed above these two approaches show significant drawbacks that add a significant level of uncertainty to the specific gas production. We need to make the analysis of the gas produced and study the solubility of the gas in the liquid before reaching a better conclusion.

Table 7: Comparison of product gas in Approach I and II

Concentration	Specific amount of gas produced		$\frac{\text{Approach II}}{\text{Approach I}} \times 100$
	Approach I	Approach II	
w/w%	kg of gas/kg of initial solution		%
20	1.38×10^{-2}	6.92×10^{-3}	50.08
30 (Trial 1)	2.11×10^{-2}	1.02×10^{-2}	48.19
30 (Trial 2)	2.05×10^{-2}	9.93×10^{-3}	48.42

5.1.3 Calculation of the maximum specific gas production rate from the raw data

The maximum specific gas production rate is calculated by using the raw experimental data and Equation *(25*) following the methodology derived in Section 2.5.2.2. *Figure 28* shows the value of the specific gas production rate calculated for the closed cell experiments. As expected maximum specific gas production rates was one order of magnitude higher for the 30% (w/w) CHP experiments than the 20% (w/w) CHP experiment, the runaway being more violent for a more concentrated solution (*Table 4*). The uncertainty in the repeatability test of 30% (w/w) experiments regarding $(dP/dt)_{max}$ and $(dT/dt)_{max}$ (see Section 5.1.1) are naturally propagated to the assessment of the specific gas production rate (around 25 % uncertainty). No value of specific gas production rate was assessed for the 40% w/w solution as the cell exploded. This in turn means that no vent sizing could have been performed for such solution using the PHI-TEC II in the closed cell configuration.

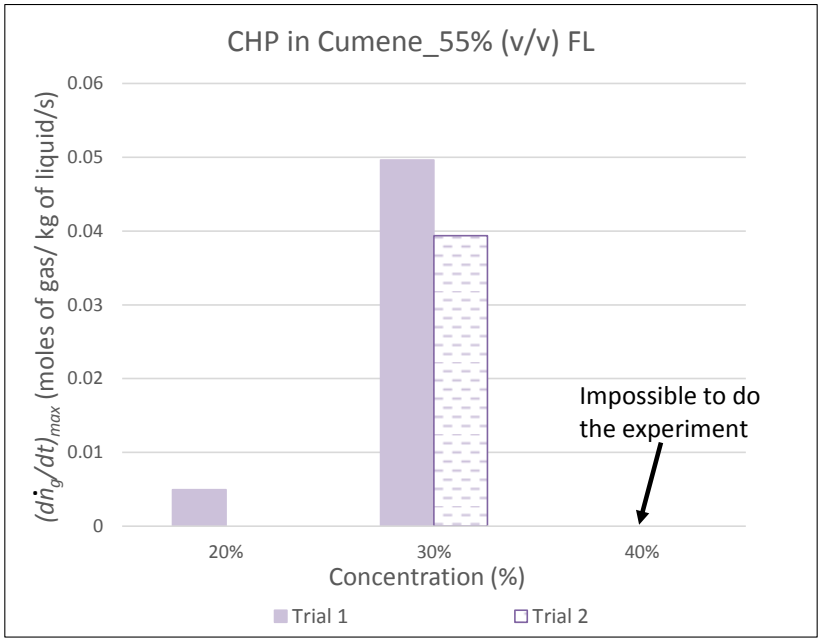

Figure 28: Maximum specific gas production rate of closed cell configuration from the raw data.

5.1.3.1 The effect of gas temperature rise rate on maximum specific gas production rate

Equation (25) for the calculation of the specific gas production rate $(d\dot{n}_g/dt)_{max}$ is composed of a pressure rate term (with $(dP/dt)_{max}$) and a temperature rate term (with $dT/dt)_{max}$). The temperature rate term translate the gas/vapor thermal expansion term that needs to be taken into account while assessing the specific gas production rate from the pressure data. The literature indicates that it is possible to neglect the *(dT/dt)* term from *Equation (25)* to calculate $(d\dot{n}_g/dt)_{max}$ for open cell configuration [3]. It is interesting to check the sensitivity of $(d\dot{n}_g/dt)_{max}$ to the *(dT/dt)* term for the closed cell configuration. *Figure 29* shows the predicted specific gas production rate with and without the (dT_g/dt) term.

It is clear that if one neglects the (dT_g/dt) term from *Equation (25)*, $(d\dot{n}_g/dt)_{max}$ can be overestimated by 21% and 14% of for the experiments at 30% w/w and 20% w/w CHP solutions respectively. This emphasies the importance of accounting for the gas/vapor thermal expansion term in the evaluation of $(d\dot{n}_g/dt)_{max}$ for closed cell experiments.

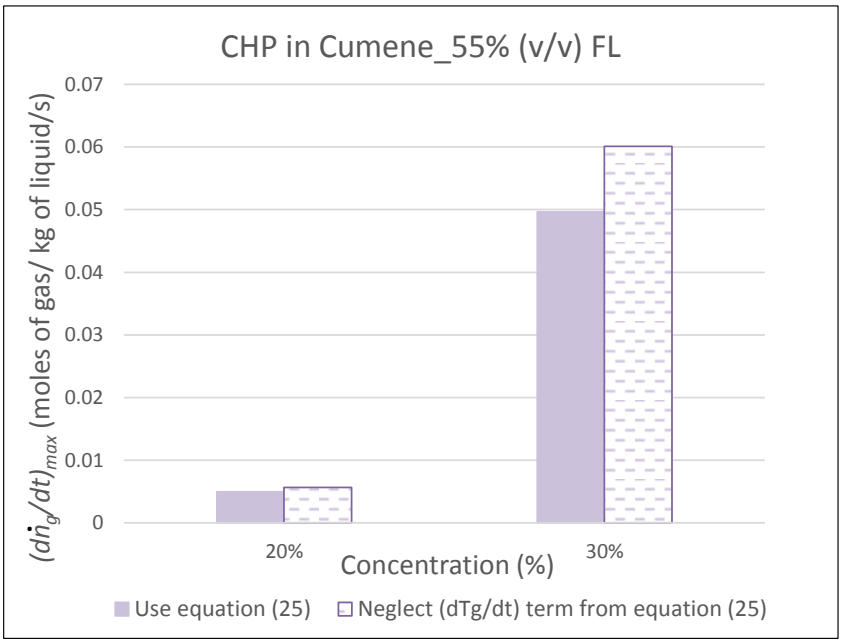

Figure 29: Maximum specific gas production rate_effect of (dT_g/dt)

5.1.3.2 Calculation of the gas production rate by considering the noncondensable gas pressure

As mentioned in Sections 5.1.2.2 and 2.5.4, the pressure in the cell is due is a result of the pressure of the non-dissolved gas product (P_g), the pad gas pressure (P_p) and the vapor pressure (P_v) of the liquid mixture. The values of $(d\dot{n}_g/dt)_{max}$ calculated by using the total pressure are therefore ignoring the fact that vapor and pad gas also contribute to the

total pressure. It is not straightforward to calculate gas production rate due to the non-condensable gases only as the calorimeter only measures a total pressure without distinction between the individual contributions of the non-condensable gas, pad gas and vapor.

In an attempt to evaluate the gas production rate by considering the non-condensable gas pressure only, we made the following assumptions:

- Only the solvent Cumene produces vapor pressure. The Antoine equation was used to evaluate P_v = f (T).
- The gas is non-soluble into the liquid.

At each time step of the experiment, P_g was assessed by simply subtracting the pad gas pressure and P_v of Cumene to the total pressure (see *Figure 30*). The number of moles of gas was then calculated from P_g using the ideal gas law for each time step and the maximum specific gas production rate was calculated using *Equation (25)*.

Table 8 and *Figure 31* show the $(d\dot{n}_g/dt)_{max}$ calculated by using the gas pressure only. The gas generation calculated from the gas pressure only are obviously less than the ones calculated with the total pressure. This shows that ignoring the contribution of the vapor pressure to the total pressure when analyzing the closed cell data may lead to an over-estimation of the non-condensable gas generation rate. On the other side the assumption that the gas is non soluble in the liquid leads to an under-estimation the non-condensable gas generation rate. This simple approach highlights here again the necessity to evaluate better the contribution of the vapor pressure to the total pressure and the gas dissolution to have a better assessment of the maximum specific gas production rate.

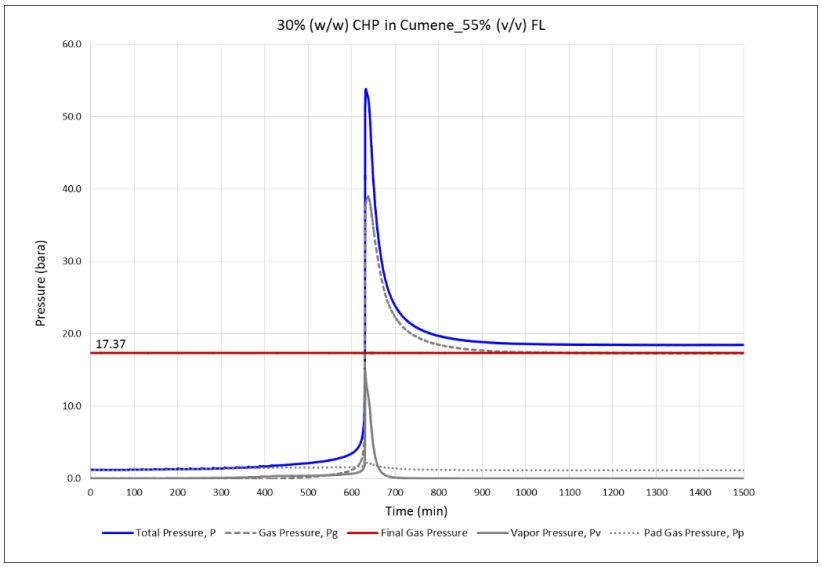

Figure 30: Pressure components of a runaway reaction (30% CHP in Cumene_55% FL)

Table 8: Data required to calculate maximum specific gas production rate

Parameter	Unit	20% (w/w)	30% (w/w)_Trial 1
$(dPg/dt)_{max}$	(bar/min)	11.66	115.25
T at $(dP_g/dt)_{max}$	(°C)	214.79	264.97
P_g at $(dP_g/dt)_{max}$	Bara	15.23	25.77
(dT/dt) at $(dP_g/dt)_{max}$	(K/s)	0.73	7.44
$(d\dot{n}_g/dt)_{max}$	moles of gas / kg of liquid/s	3.84×10^{-3}	3.104×10^{-2}

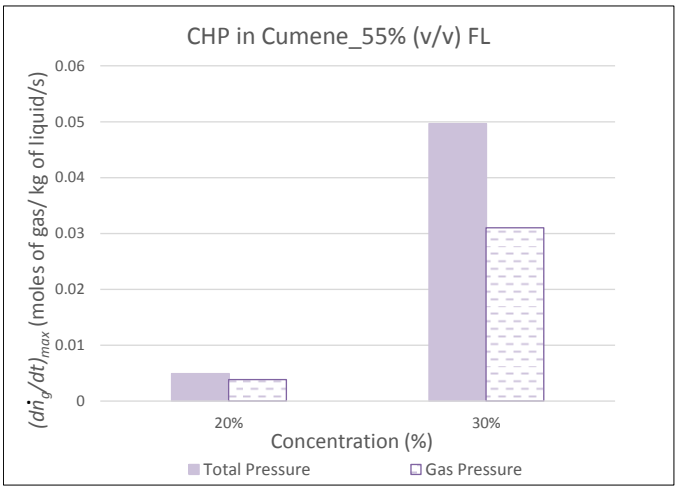

Figure 31: Maximum specific gas production rate _ ignoring vapor pressure

5.1.3.3 Calculation of the maximum gas production rate by correcting the adiabatic data for φ factor

The 30 w/w% CHP in Cumene on closed cell configuration (Trial 1) was selected to do study the effect of the φ factor of the temperature and pressure evolutions of the runaway and the corresponding maximum gas production rate. For this experiment the φ factor was evaluated at 1.21 (see *Table 4*). We followed a multi-step procedure as described in the literature section as follows:

a) Calculation of the adjusted temperature and self heat rate (SHR) using Fisher's method (see Section 2.4.3.1)
b) Correction of the timescale using the Enhanced Fisher method (see Section 2.4.3.2)
c) Correction of the pressure data using the method recently proposed by A.A. Kossoy *et al.* (see Section 2.5.4)

Finally, all the corrected data were used to calculate the corrected maximum specific gas production rate using Equation *(35).*

5.1.3.3.1 Calculation of the adjusted temperature and self heat rate (SHR)

The procedure for the correction of the temperature and SHR profiles using Fisher's method was previously described in Section 2.4.3.1.

Figure 32 shows the experimental and adjusted temperature profiles. The adjusted (for φ=1) maximum temperature is almost 36.5°C higher than the experimental value. As already mentioned the Fisher's method does not take into account the fact that at φ=1 the reaction is faster. The adjusted temperature curve therefore follows the same timescale than the experimental data.

Figure 33 shows the experimental and adjusted SHR curves. It can be seen that at the beginning of the reaction, the SHR adjusted values are close to the experimental ones. When the reaction accelerates, the adjusted SHR is much higher (by a factor 5) than the experimental value.

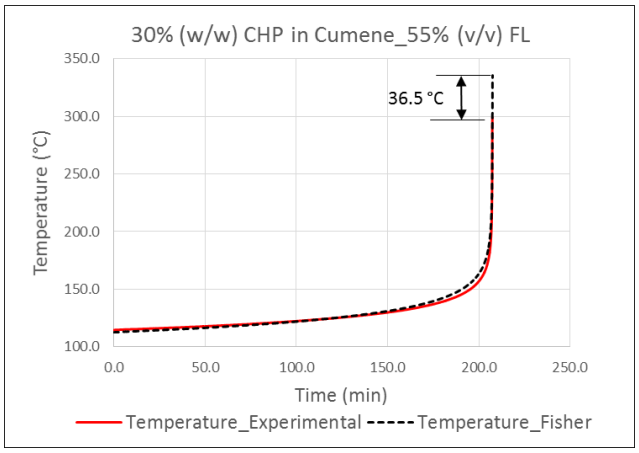

Figure 32: Temperature profiles for experimental and φ corrected data (Fisher method)

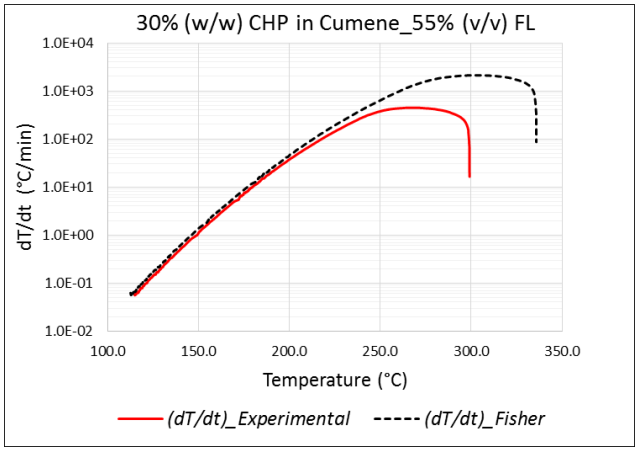

Figure 33: SHR profiles for experimental and φ corrected data (Fisher method)

5.1.3.3.2 Correction of the timescale using the Enhanced Fisher method

We reconstructed the adjusted timescale by using the Enhanced Fisher method as described in Section 2.4.3.2. The reciprocal of the SHR was used and the integration was done with respect to the corrected temperature between $T_{on\ adj}$ to $T_{max\ adj}$. *Figure 34* shows that the reconstructed timescale predicts a faster reaction time and thus a reaction completion time 15.7 minutes less than the experimental data.

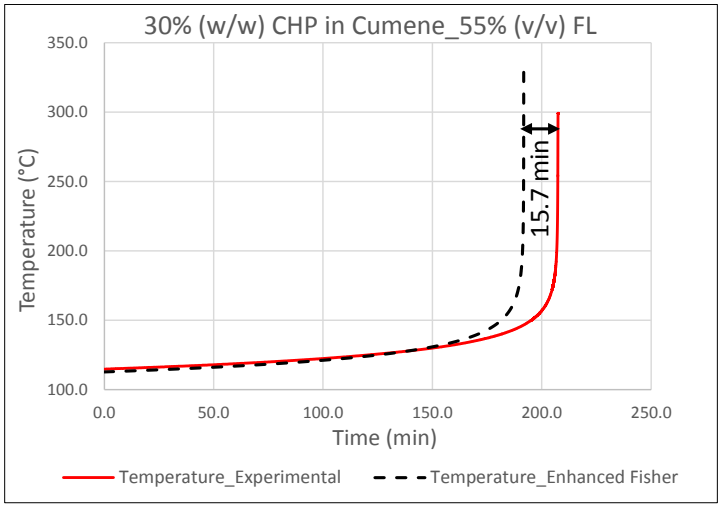

Figure 34: Temperature profiles for experimental and φ corrected data (Enhanced Fisher method)

The adjusted values of temperature and time scale were used to calculate the new adjusted Enhanced Fisher SHR. *Figure 35* compares the experimental and the Enhanced Fisher SHR. Since the corrections are only made between onset and maximum temperature, the corrected SHR ends at maximum temperature.

The maximum SHR for Enhanced Fisher method is **26.7 times** higher than experimental SHR. This indicates that the Enhanced Fisher's method predicts a much higher SHR than the classical Fisher's method.

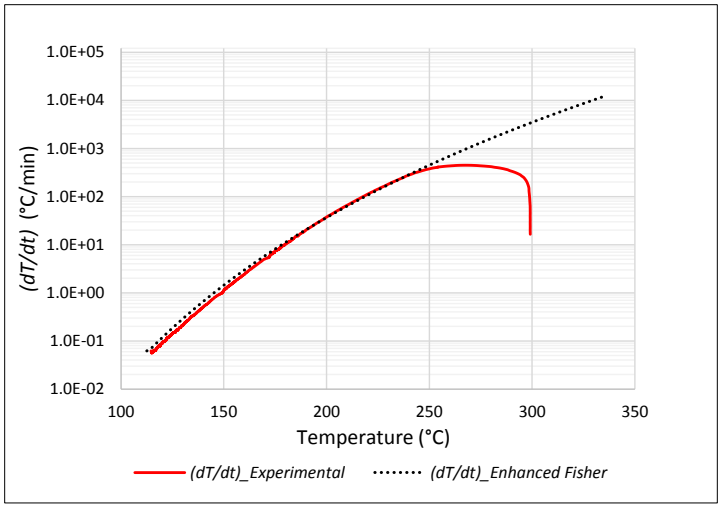

Figure 35: SHR for experimental and φ corrected data (Enhanced Fisher method)

5.1.3.3.3 Calculation of the adjusted pressure and pressure rise rate

The adjusted pressure data were calculated using the using the method recently proposed by A.A. Kossoy *et al.* (see Section 2.5.4). It is important to emphasize that this correction method neglects the **gas dissolution effects**, which can be significant with closed cell data. The reconstructed total pressure profile and pressure rise rates are shown in *Figure 36* and *Figure 37*. The maximum reconstructed total pressure was around 21% higher than the experimental value. The maximum corrected pressure rate was around **30 times** higher than the experimental value.

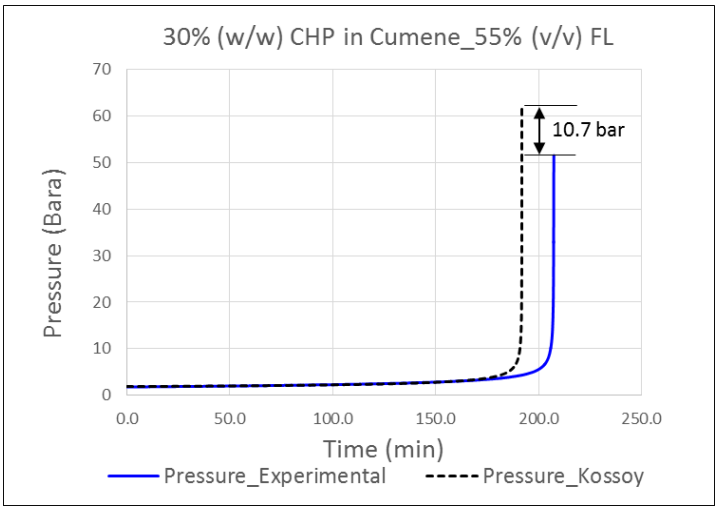

Figure 36: Pressure profiles for experimental and corrected (Kossoy method) data

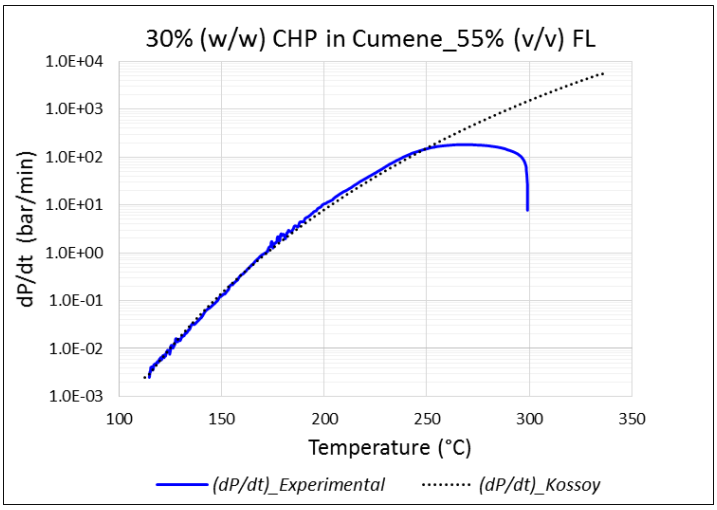

Figure 37: Pressure rise rates for experimental and corrected (Kossoy method) data

5.1.3.3.4 Calculation of the maximum specific gas production rate

Figure 38 summarizes the experimental and φ-corrected temperature and pressure data for the 30% CHP solution in Cumene and 55% v/v fill level (Trial 1). *Figure 39*

shows the comparison of the specific predicted gas production rate or $(d\dot{n}_g/dt)_{max}$ for the following cases:

- ***Case A***: $(d\dot{n}_g/dt)_{max}$ calculated using of the experimental temperature (T) and total pressure (P) data;
- ***Case B***: $(d\dot{n}_g/dt)_{max}$ calculated using of the experimental temperature (T) and evaluated gas pressure (P_g) data;
- ***Case C***: $(d\dot{n}_g/dt)_{max}$ calculated using of the φ-corrected temperature (T_{adj}) and total pressure (P_{adj}) data;
- ***Case B***: $(d\dot{n}_g/dt)_{max}$ calculated using of the φ-corrected temperature (T_{adj}) and gas pressure ($P_{g,adj}$) data;

It can be seen that if the calculation is done using total pressure (disregarding the potential contribution of vapor to the observed pressure), correcting the data for the φ factor will lead to an estimated value of the specific gas production rate almost 25 times higher than the prediction using the raw experimental data. If the calculation is done using the reconstructed pressure of gas only, the predicted value of the specific gas production rate is still almost 9 times higher than the prediction using the raw experimental data. These calculations emphasize the importance of the φ factor correction for the assessment of the gas production rate. However as mentioned in the previous sections, the methodology used for the correction of the pressure response suffer from important limitation due to the assumptions made (e.g. gas is considered non-soluble) and still required experimental validation.

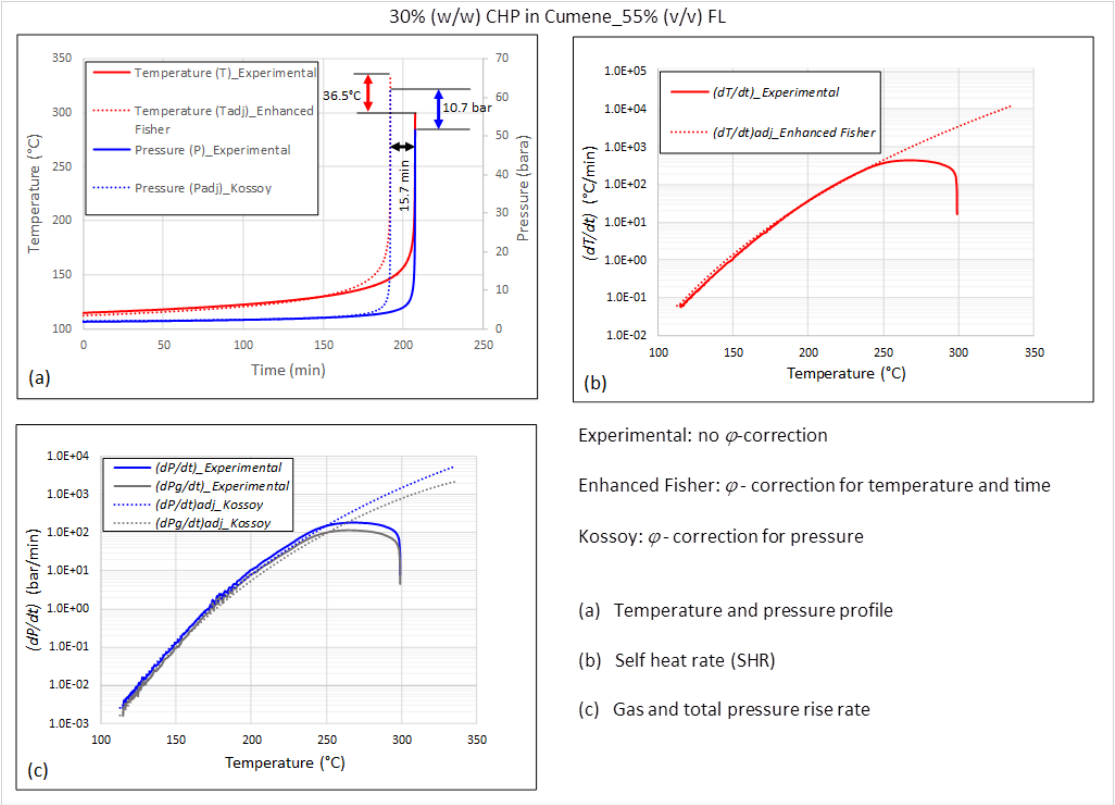

Figure 38: Experimental and corrected runaway profiles

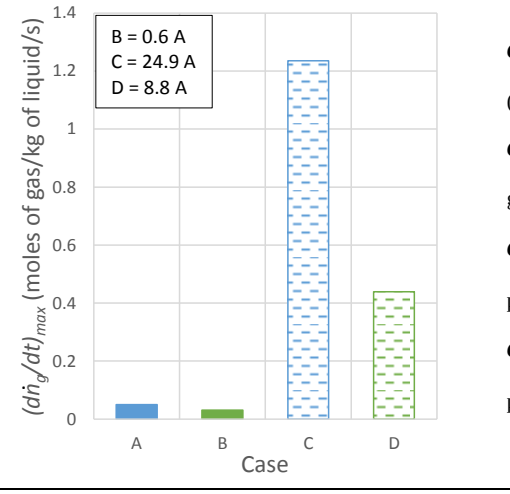

Case A: Use of the experimental temperature (T) and total pressure (P) data;

Case B: Use of the experimental temperature (T) and evaluated gas pressure (P_g) data;

Case C: Use of the ***φ*-corrected** temperature (T_{adj}) and total pressure (P_{adj}) data;

Case B: Use of the ***φ*-corrected** temperature (T_{adj}) and gas pressure ($P_{g,adj}$) data.

Figure 39: Non-corrected and corrected maximum specific gas production rate

5.1.4 Conclusion for the closed cell tests

Closed cell experiments were possible with 20% and 30% w/w CHP solutions. The experiment with the 40% CHP solution led to the explosion of the test cell, which demonstrates the limitation of the closed cell configuration for gas generating systems. For closed cell experiments, the temperature rise rate, pressure rise rate and the maximum specific gas production rate all are increasing with the increase of concentration. Although the repeatability test for 30% (w/w) concentration experiment shows that some parameters varied around 15-20%, they are still one order of magnitude higher than the 20% (w/w) concentration experiment. Very importantly the correction of the φ factor using the Enhanced Fisher method (for temperature) and the Kossoy's method (for pressure) was shown to have a great impact on the maximum specific gas production rate. Indeed the φ corrected value is one order magnitude higher than the non-corrected value. However, none of the methods take into account the gas dissolution effect which can lead to the underestimation of the gas production rate. So, to improve the assessment of the specific gas production rate from closed cell data, it is necessary to study experimentally the gas dissolution effect and extend or modify the Kossoy's method to take into consideration the gas dissolution in the correction of the pressure data for φ factor.

5.2 OPEN CELL EXPERIMENT (OPEN TO CONTAINMENT VESSEL)

In the open cell configuration (*Figure 12* - right), the test cell is opened to the containment vessel (with a hole in the upper side/lid of the test cell). The gas/vapor produced by the runaway reaction pressurizes the entire containment vessel which offers a much larger volume for the gas compared to the closed cell configuration. For open cell

test DIERS recommends to set an initial pressure in the containment vessel (using nitrogen gas) suppress potential boiling of the sample.

In this work, a total of 13 experiments were performed with the open cell configuration by varying the following experimental parameters:

- Initial fill level of the test cell (55% and 70% v/v);
- Initial pressure of the tests (1, 5 or 20 bara);
- Concentration of CHP (% w/w) in Cumene: 20%, 30% and 40%.

The summary of the experimental conditions and the corresponding results is shown in *Table 9* and *Table 10* for the 55% and 70% v/v initial fill levels respectively.

The following part will analyze the experimental result to highlight the effect of the peroxide solution concentration, the test cell initial fill level, initial pressure of the test on the following parameters:

- Temperature and pressure profiles and derivatives;
- The mass of sample lost to the containment vessel during the experiment, which is quantified using the initial mass loss ratio $\Delta m/m_0$; see equation *(36)*;
- The specific gas production rate calculated using the raw experimental data;

Table 9: Open cell tests with CHP in Cumene, 55 % v/v initial fill level, test conditions and experimental results

Property	Unit	Experimental data						
Initial Pressure	(Bara)	1			5			20
Concentration	(% w/w)	20	30	40	20	30	40	30
Initial mass	10^{-2} x Kg	5.45	5.56	5.69	5.45	5.56	5.69	5.56
Final mass	10^{-2} x Kg	1.83	1.66	0.64	4.76	3.77	1.89	5.17
$\Delta m/m_0$	%	66.49	70.14	88.77	12.66	32.26	66.86	7.05
T_{on}	°C	115.67	111.09	104.81	118.01	114.03	109.33	106.78
T_{max}	°C	190.74	225.19	248.78	219.99	258.80	287.97	284.71
$(dT/dt)_{max}$	K/s	0.0229	0.1303	0.9718	0.3652	1.7633	5.7408	2.7650
P_{max}	Bara	2.17	2.80	3.32	7.24	7.75	9.58	25.92
$(dP/dt)_{max}$	Bar/s	0.0007	0.0035	0.0252	0.0063	0.0385	0.2375	0.0847
T @ $(dP/dt)_{max}$	°C	175.01	210.88	248.42	210.18	241.26	261.44	267.77
$(d\dot{n}_g/dt)_{max}$	moles of gas / kg of liquid/s	0.00079	0.00356	0.02422	0.0066	0.0381	0.2243	0.0813

Table 10: Open cell tests with CHP in Cumene, 70 % v/v initial fill level, test conditions and experimental results

Property	Unit	Experimental data					
Initial Pressure	(Bara)	1			5		
Conc.	(% w/w)	20	30	40	20	30	40
Initial mass	10^{-2} x Kg	6.93	7.1	7.24	6.93	7.08	7.25
Final mass	10^{-2} x Kg	3.75	2.11	1.07	6.16	4.72	1.99
Mass loss	%	45.95	70.20	85.20	11.16	33.34	72.61
T_{on}	°C	122.88	115.75	104.83	116.12	113.96	103.07
T_{max}	°C	196.64	235.66	259.53	231.47	264.63	293.27
$(dT/dt)_{max}$	K/s	0.0332	0.2200	1.2442	0.3220	1.4360	6.8522
P_{max}	Bara	2.46	3.58	4.24	7.81	8.55	10.15
$(dP/dt)_{max}$	Bar/s	0.0009	0.0076	0.0389	0.0095	0.0410	0.3195
T @ $(dP/dt)_{max}$	°C	185.10	212.50	238.98	216.50	248.87	254.84
$(d\dot{n}_g/dt)_{max}$	moles of gas / kg of liquid/s	0.0007	0.0062	0.0297	0.0077	0.0316	0.2387

5.2.1 Effect of the experimental parameters on the temperature and pressure data

Figure 40 and *Figure 41* respectively show the temperature and pressure rise rates for the open cell experiments.

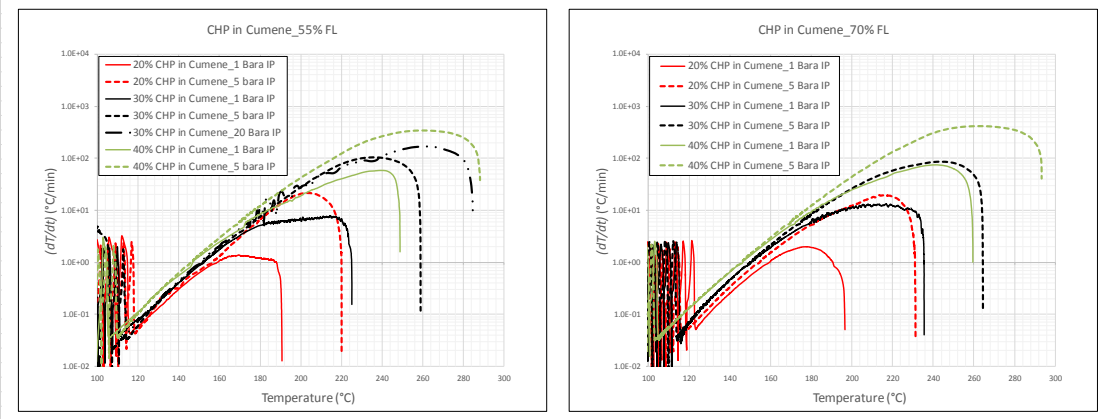

Figure 40: Open cell experiments with CHP in Cumene; effect of the experimental parameters on the SHR

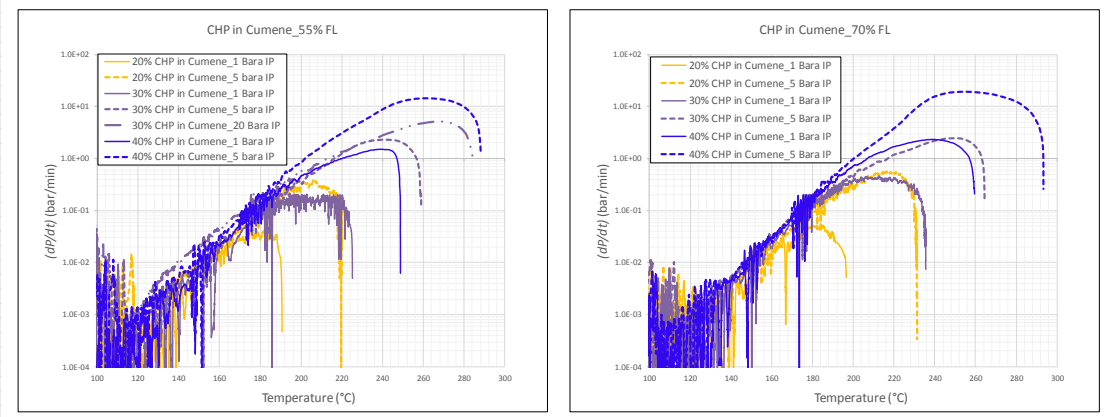

Figure 41: Open cell experiments with CHP in Cumene; effect of the experimental parameters on the pressure rise rates

Figure 42 clearly shows that T_{on} decreases when the peroxide concentration increases. This effect was not observed with 20 and 30% w/w CHP, 55% fill level in the closed cell configuration. T_{on} also increases with the initial pressure of the open cell test. However, no clear trend on the sensitivity of T_{on} to the test cell fill level was observed.

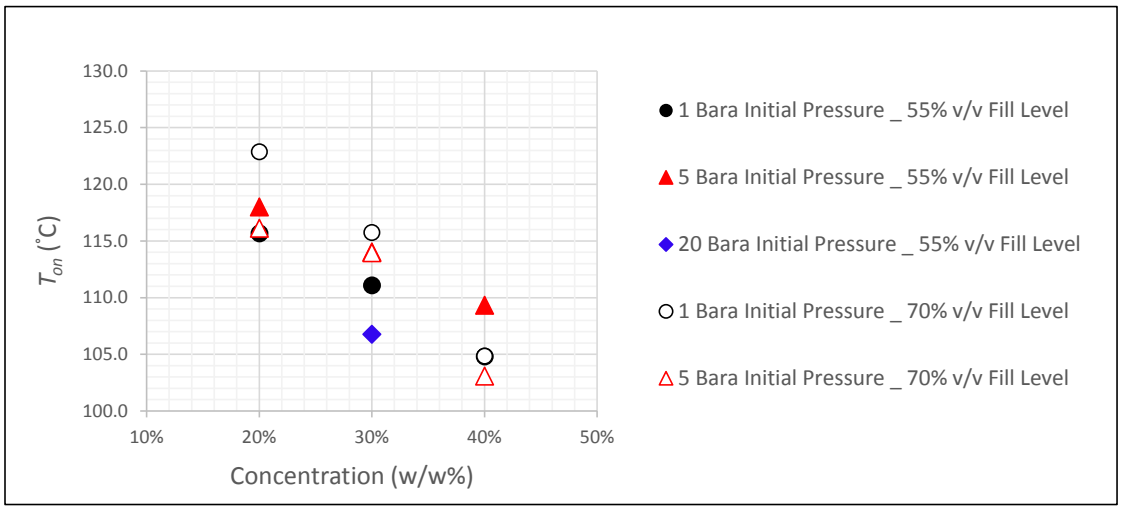

Figure 42: Open cell experiments with CHP in Cumene; effect of the experimental parameters on T_{on}

Figure 43 and *Figure 44* show how T_{max} (that translate the heat of reaction used to heat up the liquid) and $(dT/dt)_{max}$ (that translate the reaction rate) are sensitive to the experimental parameters. T_{max} and $(dT/dt)_{max}$ increase with the concentration which is not surprising. Indeed, an increase of concentration corresponds to a higher heat of reaction and also a higher reaction kinetics, which explains these observations.

T_{max} and $(dT/dt)_{max}$ increase when increasing the initial pressure of the test. This was less foreseeable. This translate the effect of the vaporizable component on the thermal

balance of the chemical system. At low initial pressure, boiling or preferential boiling of the component mixture may act as a heat sink for the reactive mixture such slowing down the reaction. This show that our system is hybrid and not purely gassy.

At low concentration (20 % w/w) the effect of the fill level on $(dT/dt)_{max}$ is not obvious. This is more obvious when the concentration increases. In general, even if the impact is moderate, we can see that the increase of the fill level tends to lead to slightly higher T_{max} and $(dT/dt)_{max}$. This observation may explain by the fact that an increase in the fill level leads to a decrease of the φ factor, which in turns play a role in the overall thermal balance of the reactive system.

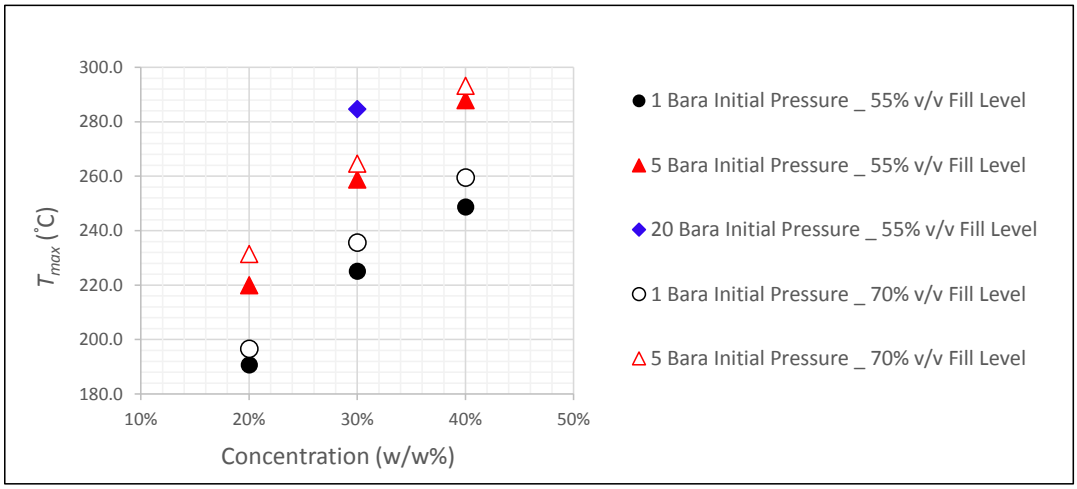

Figure 43: Open cell experiments with CHP in Cumene; effect of the experimental parameters on T_{max}.

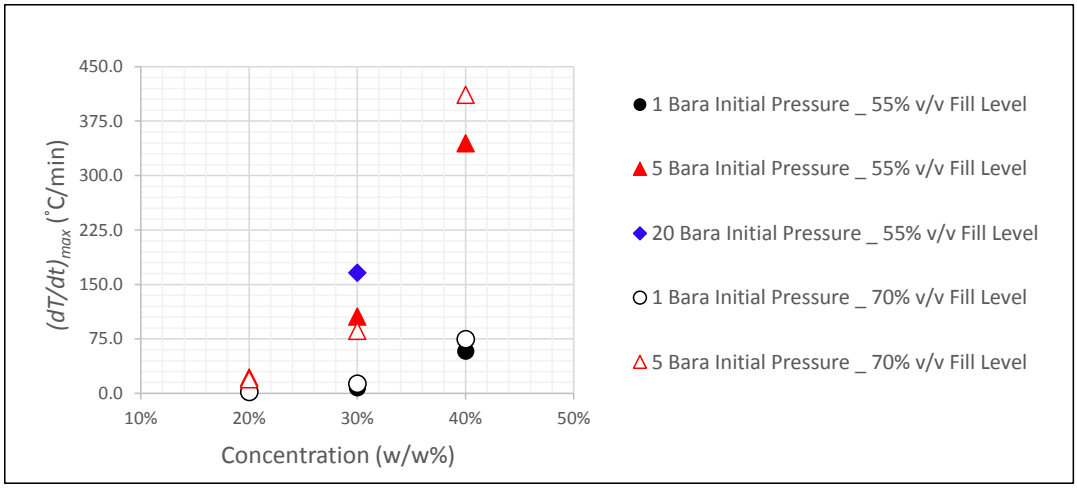

Figure 44: Open cell experiments with CHP in Cumene; effect of the experimental parameters on $(dT/dt)_{max}$

The experiments being performed at different initial pressure, instead of plotting only P_{max} to observe the effects of the experimental conditions on the pressure increase, we plotted the pressure increase relative to the initial pressure: $P_{max} - P_{in}$ *Figure 45* & *Figure 46* show that $(P_{max} - P_{in})$ and $(dP/dt)_{max}$ follow the trends of T_{max} and $(dT/dt)_{max}$ respectively. The higher the concentration of the solution, the higher the quantity of decomposition gasses produced and thus the pressure build up.

The effect of initial pressure and fill level on the $(P_{max} - P_{in})$ and $(dP/dt)_{max}$ can be explained in same ways the trends of T_{max} and $(dT/dt)_{max}$ were explained above.

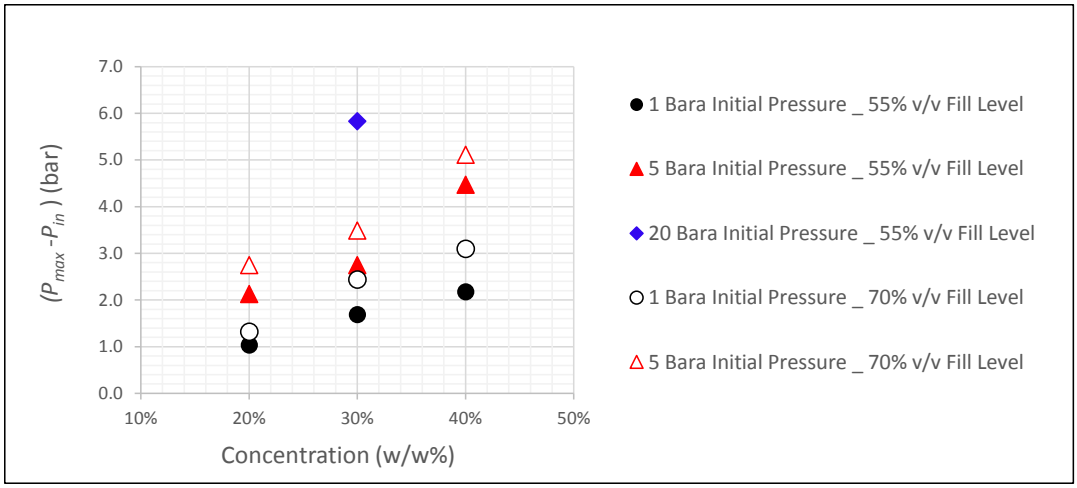

Figure 45: Open cell experiments with CHP in Cumene; effect of the experimental parameters on P_{max} - P_{in}

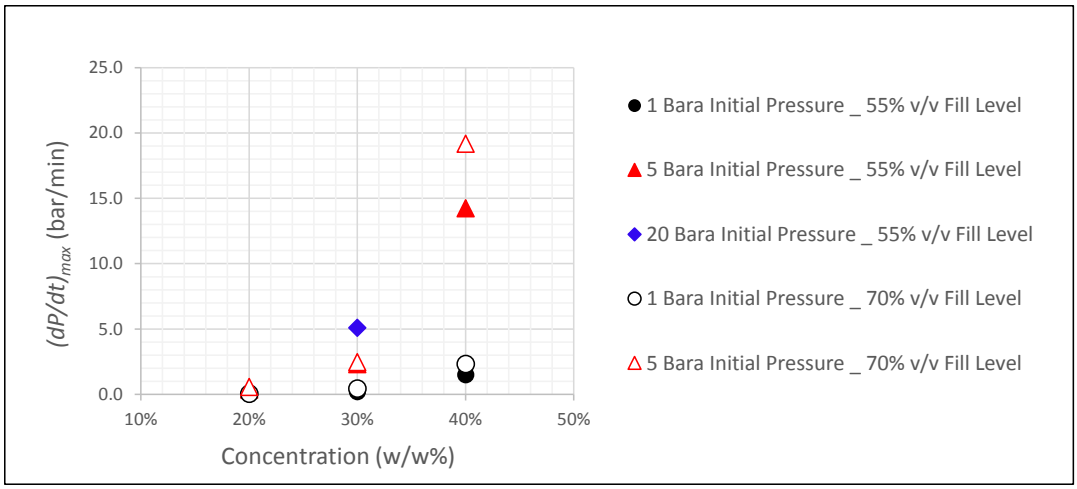

Figure 46: Open cell experiments with CHP in Cumene; effect of the experimental parameters on $(dP/dt)_{max}$

Figure 47 shows the *T* at $(dP/dt)_{max}$ increases with the increase of initial pressure and peroxide concentration. However, the effect of fill level on this parameter does not follow any trend (increase or decrease).

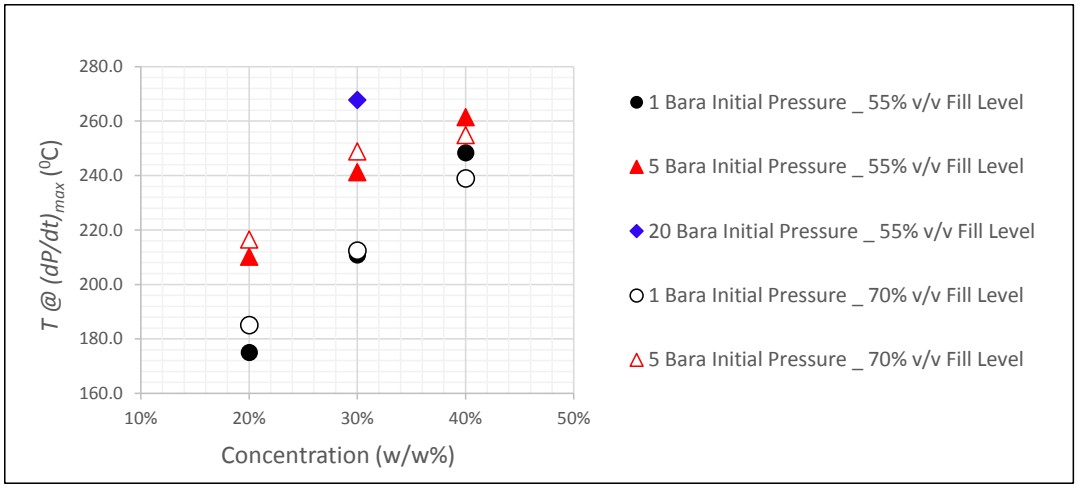

Figure 47: Open cell experiments with CHP in Cumene; effect of the experimental parameters on T @ $(dP/dt)_{max}$

5.2.2 Effect of the experimental parameters on the initial mass loss ratio $\Delta m/m_0$

Figure 48 shows the effect of experimental parameters on the initial mass loss ratio. The more concentrated the peroxide, the higher the mass loss. These results may be related to the fact that the increase of concentration leads to a more vigorous reaction. This may increase the level swell effects during the runaway, i.e. the bubbles of gas or vapor generated within the liquid tend to swell the liquid in the cell, eventually leading to the venting of a two-phase reactive mixture out of the test cell into the containment vessel. The initial reactant mass is then partially lost into the containment vessel and no longer reacts in adiabatic conditions.

Figure 48 shows the initial mass loss ratio decreases significantly when increasing the initial pressure of the test. Indeed, the increase in initial pressure has two effects:

- It suppresses boiling phenomenon, so less production of bubbles of vapor in the liquid;

- It may increase the density of the gas that will work against the level swell phenomenon [3].

However, the initial mass loss ratio does not follow any trend with the change in fill level.

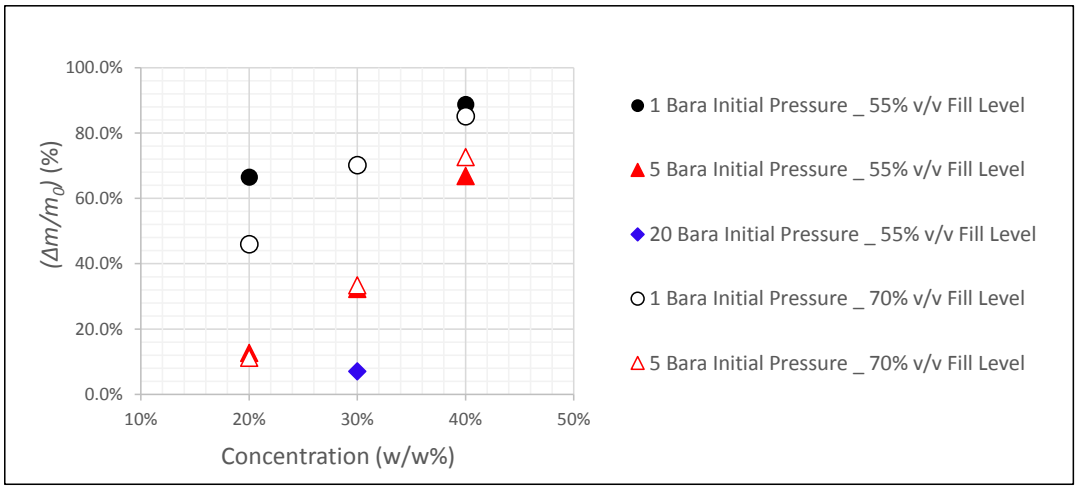

Figure 48: Open cell experiments with CHP in Cumene; effect of the experimental parameters on the mass loss

5.2.3 Effect of the experimental parameters on specific gas production and maximum specific gas production rate

The parameters measured above were used to calculate the specific gas production and the maximum specific gas production rate.

The specific gas production was calculated using the ideal gas law using the pressure build up taken at the end of the experiment when the calorimeter has cooled down (P_{end} - P_{ini}) and the initial mass of sample. *Figure 49* shows that the specific gas production

tends to increase with the increase of concentration. The initial pressure and the fill level do not seem to affect significantly the specific gas production for the 1 bar (70% fill level only), 5 bara and 20 bara initial pressure experiments. However, the 1 bara initial pressure 55% fill level show much lower values of specific gas production compared to the other tests. This result is unexpected and needs to be repeated for confirmation.

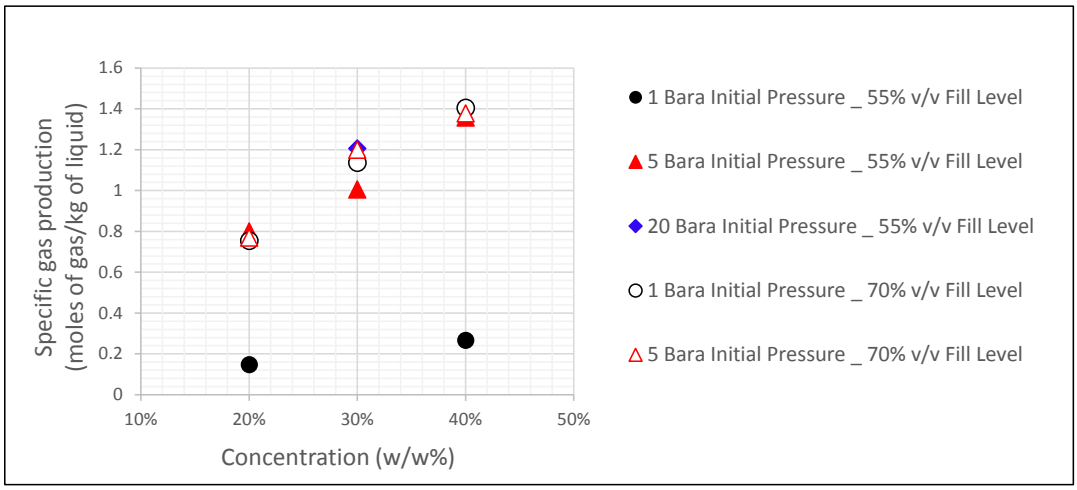

Figure 49: Open cell experiments with CHP in Cumene; effect of the experimental parameters on the specific gas production (relative to the initial sample mass)

For the calculation of the maximum specific gas production rate, we neglected the term (dT_g/dt) from Equation *(25)* following the recommendations of the DIERS for open cell experiments[2]. Since these are open cell experiments; there is always an uncertainty regarding the mass of liquid involved in the reaction when the runaway reaches its maximum rate (when $(dP/dt)_{max}$, used for the calculation of the gas generation rate is

[2] We will discuss the importance of (dT_g/dt) for an open cell to external vessel experiment (see Section 5.3.3.3.1).

measured). Indeed, we know exactly both the initial and final mass of the sample, but there is no way to measure the mass of sample effectively in the test cell during the runaway. Therefore, for experiments where initial mass loss ratio is high (e.g. experiment at low initial pressure and/or at high concentration), a significant uncertainty is related to the mass of sample to be used to estimate the specific gas production rate[3]. Consequently, we used both initial and final mass of the sample to calculate the specific gas production rate and we compared the results. The difference was considered as an uncertainty related to the specific gas production rate.

Figure 51 shows that the maximum specific gas production rate increases while increasing the peroxide concentration as expected. Very importantly, it shows that for the open cell experiment, the initial pressure can have a very strong influence on the specific gas production rate. This is well highlighted for the 30% w/w concentration experiments at 55% v/v initial fill level (*Figure 50*). Increasing the initial pressure of the test from 1 to 20 bara leads to an increase of the specific gas production rate by an order of magnitude. It can be recommended that to have a better assessment of the specific gas production rate in the open cell configuration, one should perform experiments with increasing values of the initial pressure until the value of the specific gas production rate stops increasing (plateau is reached).

[3] The same comment apply to the specific gas production calculated above. However this is more critical when it comes to the evaluation of the specific gas production rate, as it will directly impact the evaluation of the size of the vent.

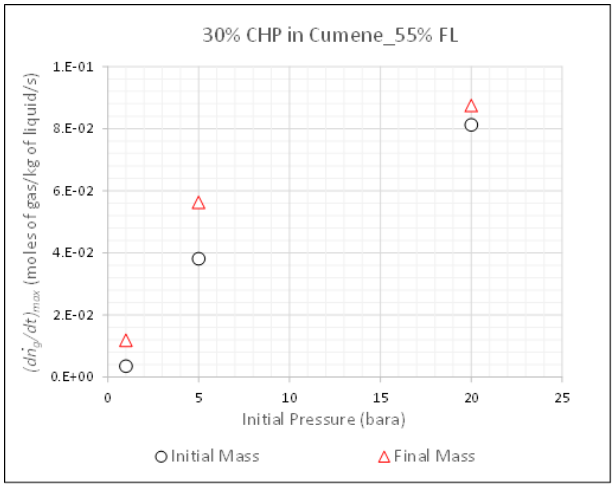

Figure 50: Open cell experiments with 30% CHP in Cumene, 55% fill level; effect of the initial pressure on the maximum specific gas production rate

In addition, since the initial mass loss ratio is lower is minimum at high pressure and low concentration, the uncertainty in the specific gas production rate associated with the mass of the sample used for the calculation is lower.

Finally, for given concentration and initial pressure, the maximum specific gas production does not seem to be sensitive to the fill level (see *Figure 51*). This is because the fill level has a very negligible or moderate effect on temperature and pressure which are discussed in see section 5.2.1.

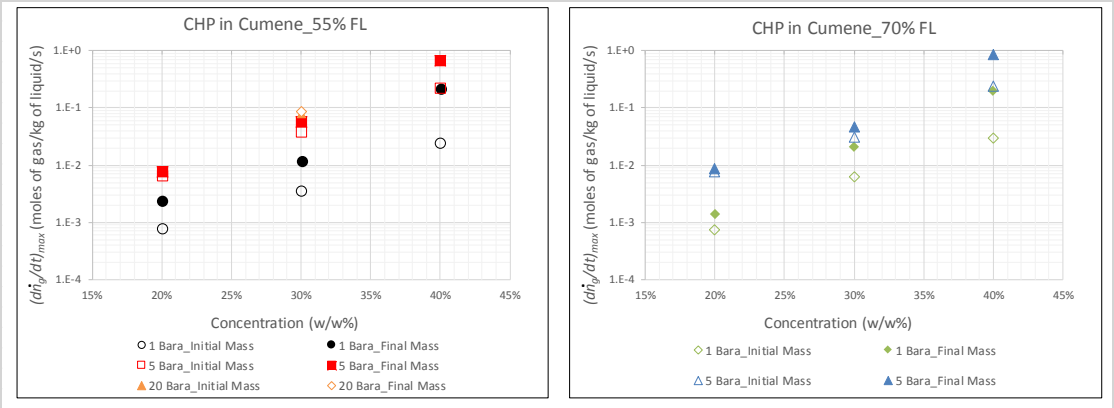

Figure 51: Open cell experiments with CHP in Cumene; effect of the experimental parameters on the maximum specific gas production rate

5.3 OPEN CELL EXPERIMENT (OPEN CELL TO EXTERNAL VESSEL)

The test in open cell configuration (open to containment vessel), while relatively convenient to perform, suffer from some technical limitations:

- The temperature of the gas is not measured in the original PHI-TEC II setup (as provided by the manufacturer). This issue can be solved by upgrading the calorimeter.
- The open cell tests are dirty. Indeed the fact that the cell is open to the containment vessel leads to the contamination on the insulation within the calorimeter (leaving a smelly calorimeter) with the chemical vapor/gases. The instrumentation within the containment vessel also degrades pretty quickly because of their exposure to the chemicals.

To overcome these limitations we tried to open the test cell to an external vessel. In the open cell to external vessel configuration (see *Figure 17* – bottom), a 1 litre external vessel was connected to the test cell by a 1/8" stainless steel tube. This expanded available

space for the gas/vapor produced by the runaway reaction. Pressure transducers were connected directly to the test cell and to the external vessel. The external vessel was equipped with a Type K thermocouple to measure the temperature of the gas phase (in the external vessel).

A total of 8 experiments (including 2 repeatability experiments) were performed in this configuration by varying the initial pressure of the tests (1, 3, 5, 10, 20 or 30 bara). The concentration of CHP and the fill level (FL) for these experiments were chosen as 30% (w/w) and 55% (v/v) respectively. The summary of the experimental conditions and results is shown in *Table 11*.

The following part will analyze experimental result to highlight the effect of the initial pressure of the test on the following parameters:

- Temperature and pressure profiles and their rise rates;
- The initial mass loss ratio $\Delta m/m_0$;
- The specific gas production rate calculated using the raw experimental data.

Table 11: Summary of the results of open cell (open to external vessel) experiment

Properties		Unit	Initial Pressure (Bara)							
			1	3	5*	5**	10*	10**	20	30
Initial mass		10^{-2}xkg	5.56	5.56	5.57	5.56	5.56	5.54	5.56	5.56
Final mass		10^{-2}xkg	1.46	2.89	3.79	3.80	4.42	4.37	5.19	5.23
Initial mass loss ratio, $\Delta m/m_0$		%	73.7	48.0	31.9	31.7	20.6	21.2	6.6	6.0
Liquid properties	T_{on}	°C	114.28	117.17	113.45	114.70	116.53	114.59	112.66	109.72
	T_{max}	°C	222.98	250.93	263.88	267.11	280.74	273.91	283.30	289.52
	$(dT/dt)_{max}$	K/s	0.10	1.98	5.83	5.51	4.90	5.39	3.96	7.63
	P_{max}	Bara	2.37	6.40	9.73	10.64	13.28	14.09	22.35	34.00
	$(dP/dt)_{max}$	Bar/s	0.003	0.17	0.48	0.52	0.25	0.37	0.08	0.30
	T @ $(dP/dt)_{max}$	°C	210.40	233.28	232.72	233.85	250.50	239.91	252.55	243.43
	P @ $(dP/dt)_{max}$	Bara	2.22	5.56	7.71	8.59	12.32	13.67	21.88	32.84
	(dT/dt) @ $(dP/dt)_{max}$	K/s	0.09	1.85	5.50	5.18	4.75	5.14	3.86	6.90
	$P_{max} - P_{in}$	Bar	1.27	3.33	4.65	5.48	3.18	3.91	2.26	4.01
Gas properties	T_{max}	°C	23.00	62.01	36.18	45.69	29.56	46.57	23.10	23.13
	$(dT_g/dt)_{max}$	K/s	0.004	0.079	0.046	0.062	0.026	0.079	0.010	0.009
	P_{max}	Bara	2.36	4.70	7.02	7.01	12.09	12.33	22.16	32.64
	$(dP/dt)_{max}$	Bar/s	0.00	0.01	0.01	0.01	0.01	0.01	0.01	0.01
	T @ $(dP/dt)_{max}$	°C	22.87	22.93	22.18	21.63	21.27	21.17	21.04	20.94
	P @ $(dP/dt)_{max}$	Bara	1.90	3.80	5.87	5.87	10.80	10.82	20.99	31.03
	(dT_g/dt) @ $(dP/dt)_{max}$	K/s	0.002	0.061	0.043	0.050	0.020	0.072	0.008	0.007
	Cell P_{max} – EV P_{max}	Bar	0.01	1.70	2.71	3.63	1.19	2.76	0.19	1.36
Maximum specific gas production rate $(d\dot{n}_g/dt)_{max}$		moles of gas/kg of liquid/s	0.0013	0.0038	0.0052	0.0051	0.0065	0.0064	0.0064	0.0074

* Trial 1 ** Trial 2

Repeatability test:

The experiments of 5 and 10 bara initial pressure were done twice to check the uncertainty associated with the experimental results. *Table 11* shows that all the parameters in the external vessel (i.e. gas temperature, pressure and their rise rate) were within an uncertainty of less than 10%. All the parameters in the cell (i.e. $T_{on,}$ $T_{max,}$ $\Delta m/m_0$ etc.) were also within an uncertainty of less than 10% except $(dP/dt)_{max}$. The uncertainty of $(dP/dt)_{max}$ was around 30%. Although the uncertainty of pressure rise rate in the cell was significant, it did not affect the maximum specific gas production calculation as we used maximum pressure rise rate in the external vessel (representing the gas pressure rise rate) which was in within the repeatability range for the calculation. As a result, the maximum specific gas production rate was also within range of 2% uncertainty.

5.3.1 Effect of initial pressure on temperature and pressure data

Figure 52 shows the temperature and pressure rise rates for open to external vessel experiments. There was no clear trend of T_{on} for experiments performed under 1 to 10 bars initial pressure as shown in *Figure 53*. T_{on} seems to decrease when increasing the initial pressure for initial pressure above 10 bars.

Figure 54 shows that T_{max} of the open to external vessel experiments increased with the initial pressure which was expected for the same reasons given in section 5.2.1.

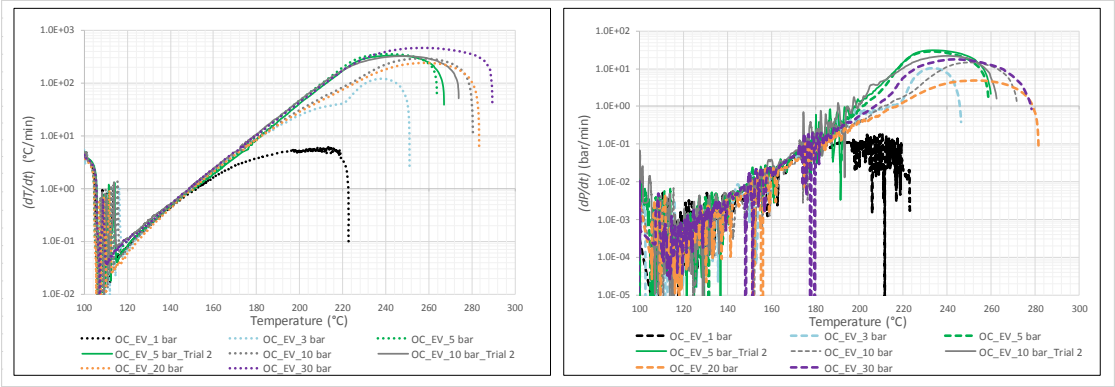

Figure 52: Open cell to external vessel experiments with CHP in Cumene; effect of initial pressure on temperature and pressure rate profiles

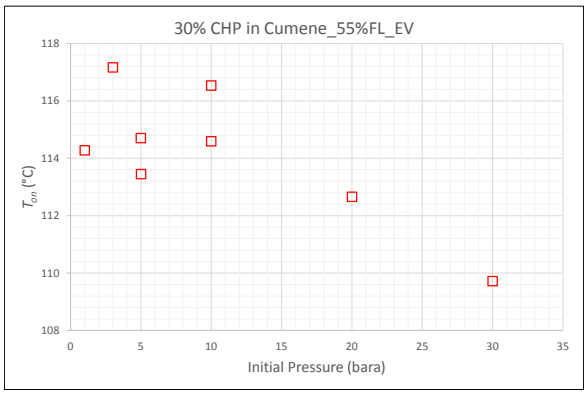

Figure 53: Open cell to external vessel experiments with CHP in Cumene; effect of initial pressure on the onset temperature

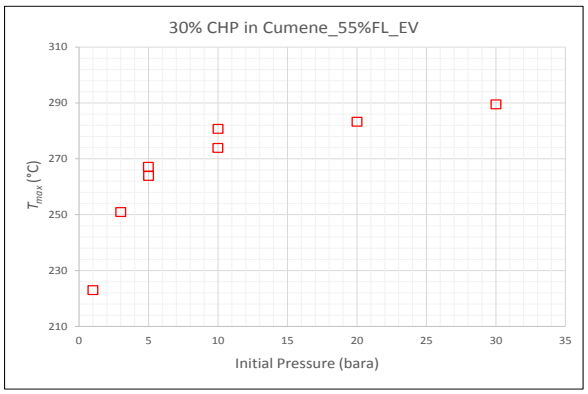

Figure 54: Open cell to external vessel experiments with CHP in Cumene; effect of initial pressure on T_{max}

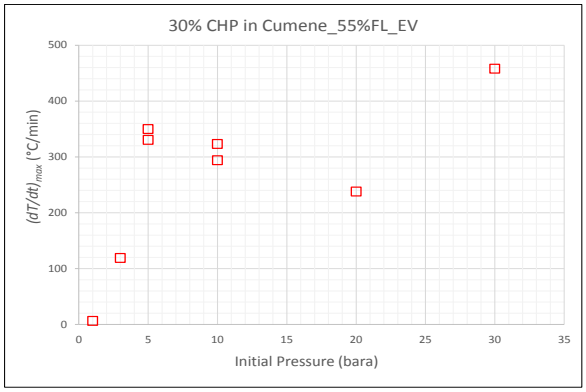

Figure 55: Open cell to external vessel experiments with CHP in Cumene; effect of initial pressure on $(dT/dt)_{max}$

It is very interesting to note that $(dT/dt)_{max}$ as a function of the initial pressure does not follow a constantly increasing trend as we observed with the experiments with the open to containment vessel configuration. As shown in *Figure 55*, $(dT/dt)_{max}$ seems to increase between 1 and 5 bars, decrease between 5 and 20 bars and finally increase between 20 and 30 bars. This behavior indicates an influence of the experimental setup and the initial pressure on the reaction kinetics.

To further understand this behavior it is worth having a closer look at the pressure profiles in the test cell and the external vessel. The whole idea behind the addition of an external vessel was to use the pressure increase in the external vessel to assess the maximum gas production rate. This implicitly assumes that the pressure increases in a relatively homogeneous way in the space available to the gas, i.e. the free volume of the test cell plus the pipe between the cell and the external vessel and the external vessel itself. *Figure 56* plots the pressure profiles in the test cell and the external vessel (zoomed version). For the 1 bar initial pressure experiment, the pressure in the test cell and the

external vessel are the same, and so are the *dP/dt*. This is not the case of the other experiments! It is very clear that the maximum pressure at the cell and the external vessel were different and the maximum value reached at different time (see *Figure 56*). This is due to the fact that the 1/8" tube between the cell and the external vessel restricts the flow of gas or two-phase mixture creating a pressure difference between the cell and the external vessel. We have also previously shown that the pressure at which the test is performed has a direct effect on the reaction kinetics. Equally, in this particular set of experiment the resistance to the flow that permits a pressure buildup in the test cell, also influences the reaction kinetics. This explains why the $(dT/dt)_{max}$ as a function of the initial pressure does not follow a constantly increasing trend. The difference between the maximum pressures in the cell and the external vessel indicates the same trend as $(dT/dt)_{max}$ except for the 30 bara experiment. It is also very interesting to note that the pressure difference tends to decrease as the initial pressure of the test increases between 5 and 20 bars. This indicates that the flow between the cell and the external vessel encounter less resistance when the test is performed under a higher pressure. This may be explained by the fact that an increased pressure decreases the level swell phenomena which in turn plays a role in the nature and composition of the flow being vented from the test cell to the external vessel.

It is important to stress that for all the experiments in this configuration (except for the test at 1 bar), the pressure was increasing faster (at least by one order of magnitude) in the cell compared to the external vessel. The time at which the maximum pressure rise rate occurred was also different.

We can therefore rightfully say that the reading of the pressure in the external vessel is in no way is a good indicator of the gas production rate!

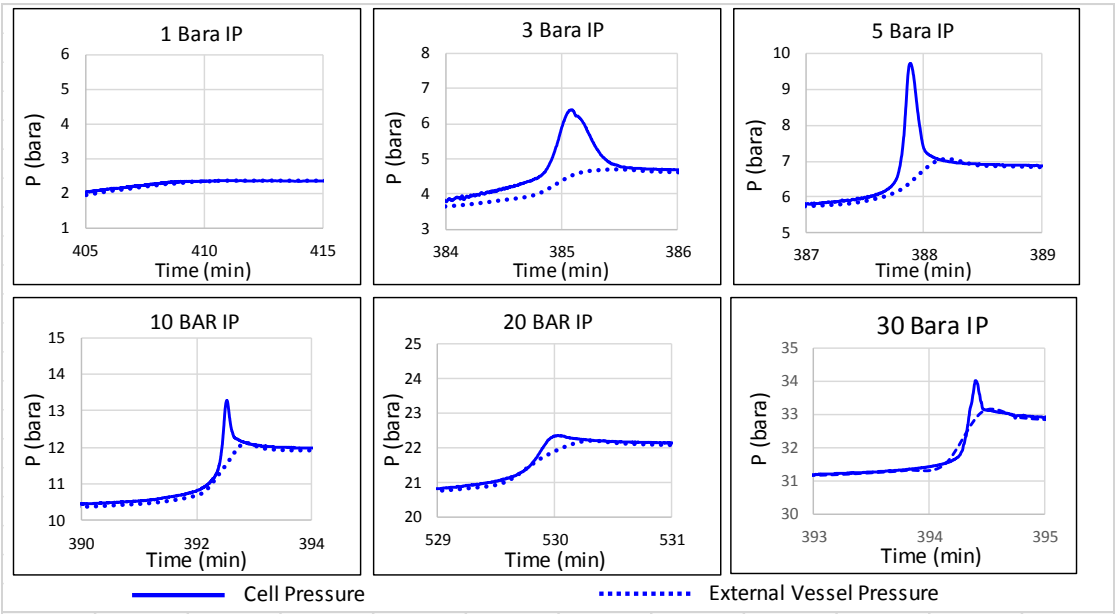

Figure 56: Open cell to external vessel experiments with CHP in Cumene; pressure profiles in the test cell and the external vessel

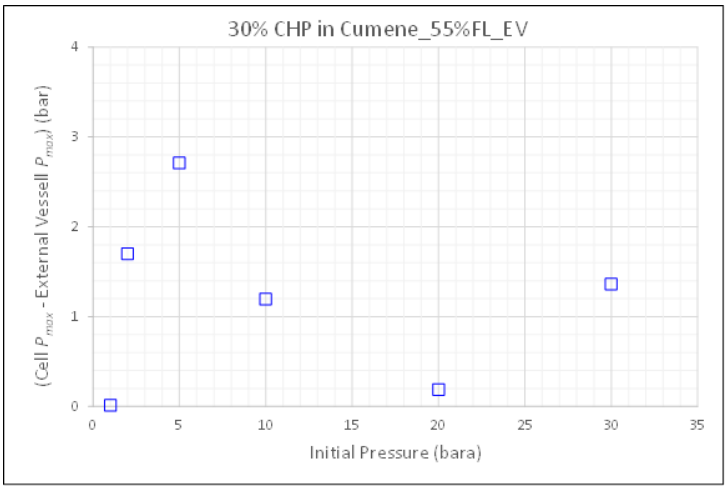

Figure 57: *Open cell to external vessel experiments with CHP in Cumene; difference of maximum pressure in the cell and external vessel;*

Table 12: Difference of pressure rates in the cell and the external vessel

Initial Pressure	$(dP/dt)_{max}$ in the cell	$(dP/dt)_{max}$ in the external vessel	Ratio (cell/external vessel)
(bara)	(bar/s)	(bar/s)	-
1	0.0030	0.0017	1.75
3	0.1715	0.0050	34.14
5 (Trial-1)	0.4791	0.0068	70.25
5 (Trial-2)	0.5164	0.0067	77.35
10 (Trial-1)	0.2474	0.0085	29.23
10 (Trial-2)	0.3657	0.0082	44.42
20	0.0835	0.0083	10.08
30	0.2953	0.0096	30.73

We measured the temperature rise rate of the gas in the external vessel, as it is needed for the calculation of the gas generation rate. The experimental results show that temperature in the external vessel (gas temperature) was much lower than the temperature in the cell (mainly liquid temperature) at the time the maximum pressure rise rate is reached in the external vessel (*Table 12*). For all experiments, the temperature in the external vessel remains almost constant (22±1°C). *Table 13* shows the temperature rise rates in the cell (liquid temperature) and in the external vessel (gas temperature) at the time the maximum pressure rise rate is reached in the external vessel.

Table 13: Temperature rise rates in the cell and in the external vessel at $(dP/dt)_{max}$ in the external vessel

Initial Pressure	$(dT/dt)_{max}$ at $(dP/dt)_{max}$ in the external vessel	
	Cell (liquid)	External vessel (gas)
(bara)	(K/s)	(K/s)
1	0.0907	0.0018
3	1.8452	0.0608
5 (Trial-1)	5.5039	0.0433
5 (Trial-2)	5.1754	0.0499
10 (Trial-1)	4.7499	0.0205
10 (Trial-2)	5.1417	0.0719
20	3.8569	0.0080
30	6.8987	0.0073

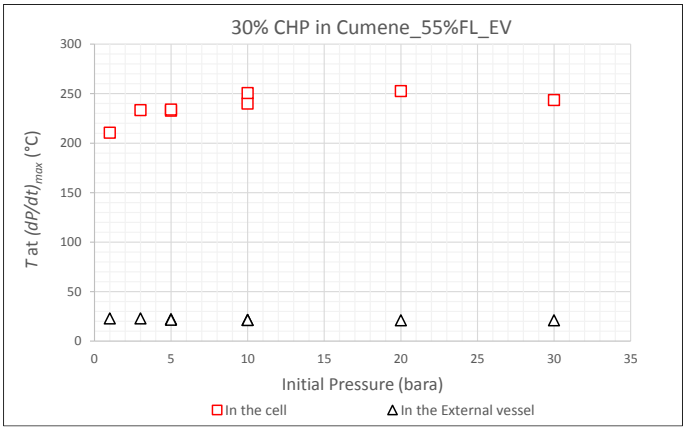

Figure 58: Temperature in the cell and the external vessel at maximum pressure rate

5.3.2 Effect of initial pressure on initial mass loss ratio $\Delta m/m_0$

Figure 59 shows that the initial mass loss ratio decreases with the increase of pressure and the trend is similar to the open to containment vessel experiments. The behavior shows the effect of the initial pressure on the level swell phenomena as explained in Section 5.2.2.

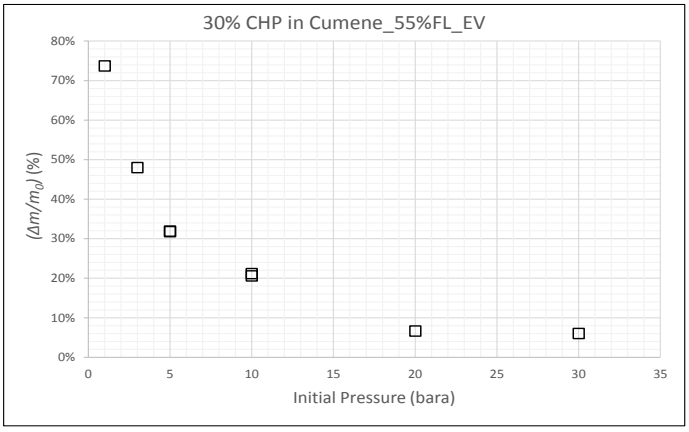

Figure 59: Effect of initial pressure on initial mass loss ratio

5.3.3 Effect of the initial pressure on the specific gas production and maximum specific gas production rate

In the following part, we will voluntarily use $(dP/dt)_{max}$ in the external vessel to calculate the maximum specific gas production and production rate even if we have already demonstrated that this approach is non-correct (see Section 5.2.3). We will later be able to quantify the impact of such approach the evaluation the specific gas production and gas production rate compared to the closed cell and open cell to containment vessel experiments.

The procedure for the calculation of the specific gas production was discussed in Section 5.2.3. As a reminder, we have calculated the specific gas production using the initial mass of liquid, the pressure of the external vessel after cooling to the ambient temperature and the ideal gas law. The calculated specific gas production are shown in *Figure 60*. As the concentration and the fill level remain the same for all experiments, the same specific gas production can be expected. However, it is clear that the assessed specific gas production is sensitive to the initial pressure of the test. This behavior seems to indicate the different amount to reactant were involved in the production of the total amount of gas. This may be due to the effect of the initial pressure on the level swell and the venting of the reactant material into the external vessel. Once vented into the relatively cold external vessel, the reactive material may be quenched and the reaction seriously slowed down. For experiments with a high initial mass loss ratio, we have indeed observed in the external vessel a clear solution (probably unreacted) at the end of the experiment.

Gas dissolution can play a role in the specific gas production, particularly at high pressure. More analysis is necessary to explain our observations.

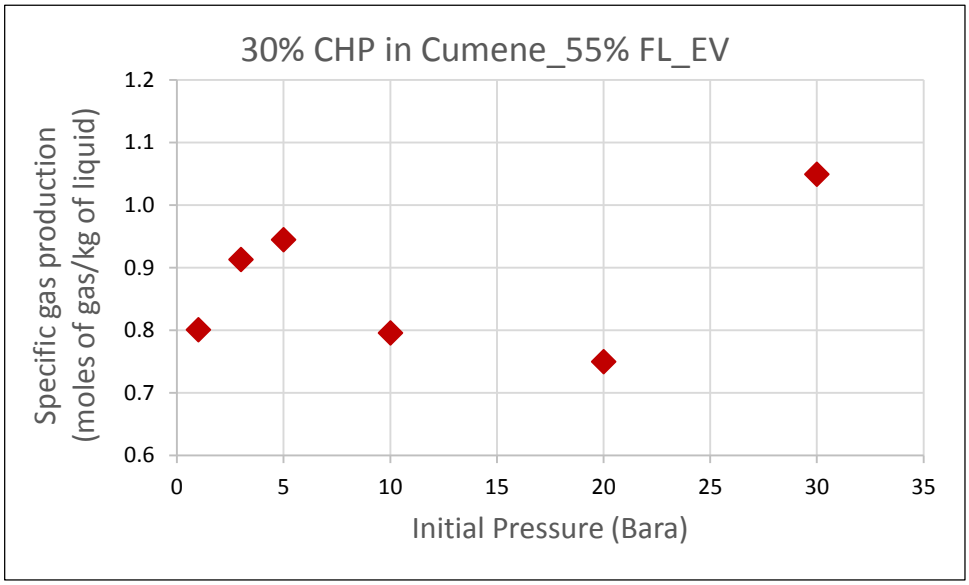

Figure 60: Effect of initial pressure on specific gas production

The parameters (temperature and pressure) measured in the external vessel (discussed in section 5.3.1) were used to calculate the maximum specific gas production rate. *Figure 61* shows the calculate the maximum specific gas production rate using equation *(25)* with and without the thermal expansion term (dT_g/dt) and using the initial mass of the sample. First of all, we can see that the initial pressure of the test has a strong influence on the maximum specific gas production rate. Indeed, the specific gas production rate increases with the initial pressure. Secondly, although the literature [3] says that it is possible to neglect the (dT_g/dt) for open cell experiments, our results show

that neglecting this term can lead to an overestimation of the gas production rate by around 7-15% depending on the initial pressure of the test.

Figure 62 shows the maximum specific production rate by considering initial and final mass of the liquid. At low pressure, the difference of $(d\dot{n}_g/dt)_{max}$ is much higher because the mass loss is highest at low pressure. This difference decreases with the increase of initial pressure, but the uncertainty associated with the choice of the mass of the sample to evaluate the specific gas production rate still plays a significant role.

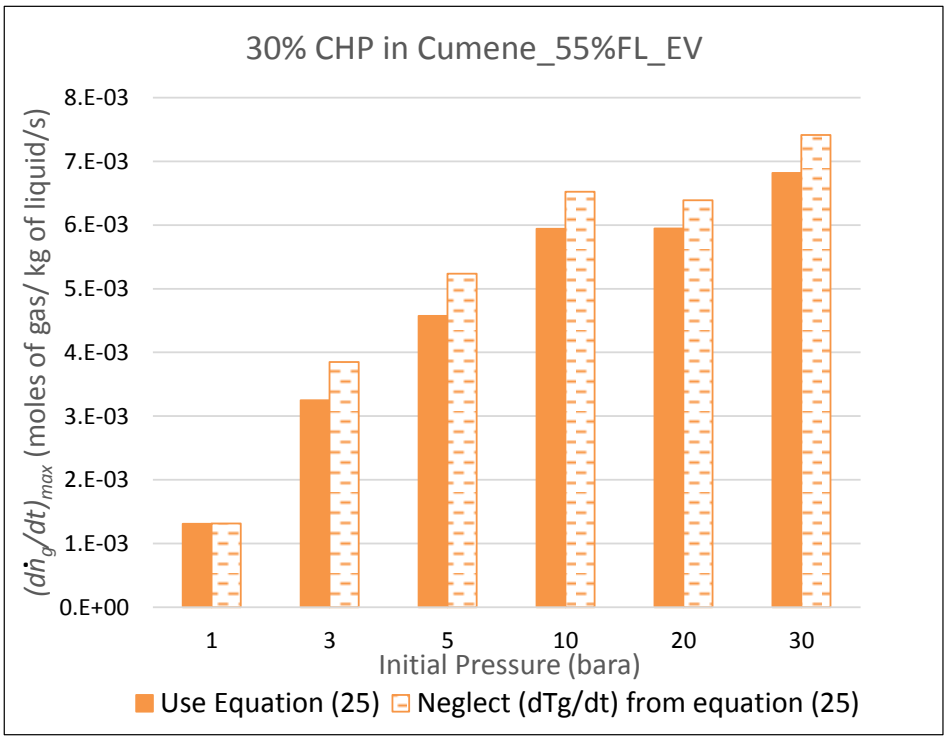

Figure 61: Effect of gas temperature change (dT_g/dt) on maximum specific gas production rate

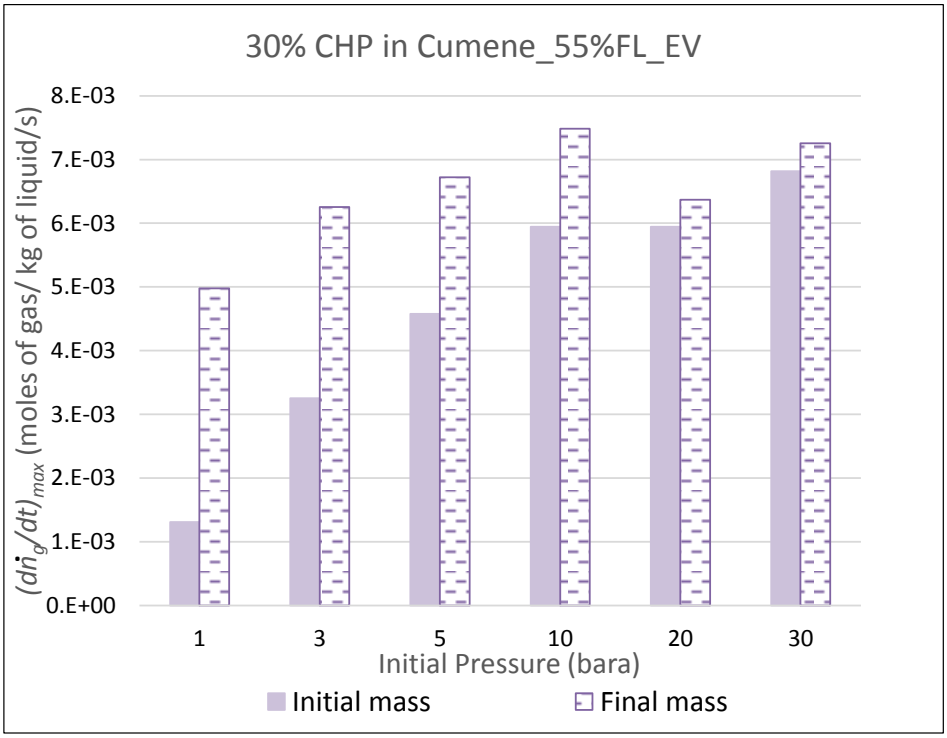

Figure 62: Effect of liquid mass on maximum specific gas production rate

5.4 COMPARISON OF THE GAS PRODUCTION RATE OBTAINED WITH THE DIFFERENT TEST CONFIGURATIONS

The experiments with 30% w/w CHP in Cumene at 55% v/v fill level with different initial pressure (1, 5 or 20 bara) were used for the comparison of the specific gas production and specific gas production rate between the 3 different configurations: closed cell, open cell to containment vessel and open cell to external vessel.

5.4.1 Specific gas production

The calculation procedure of specific gas production is discussed in the Section 5.1.2.2 and 5.2.3. *Figure 63* shows the specific gas g production from a particular chemical

system (30% w/w CHP in Cumene, 55% fill level) in different test configurations (closed/open cells). Since same chemical systems were used for all experiments, it was expected to get the same amount of gas at the end of the reactions. The specific gas production in the closed cell was lower than open cell to containment vessel and open cell to external vessel experiments. In the open cell experiments, there was uncertainty on the mass of liquid involved in the reaction that might change the specific gas production. Although there is no issue related to the liquid mass in closed cell experiment, at high-pressure gas dissolution might decrease the specific gas production.

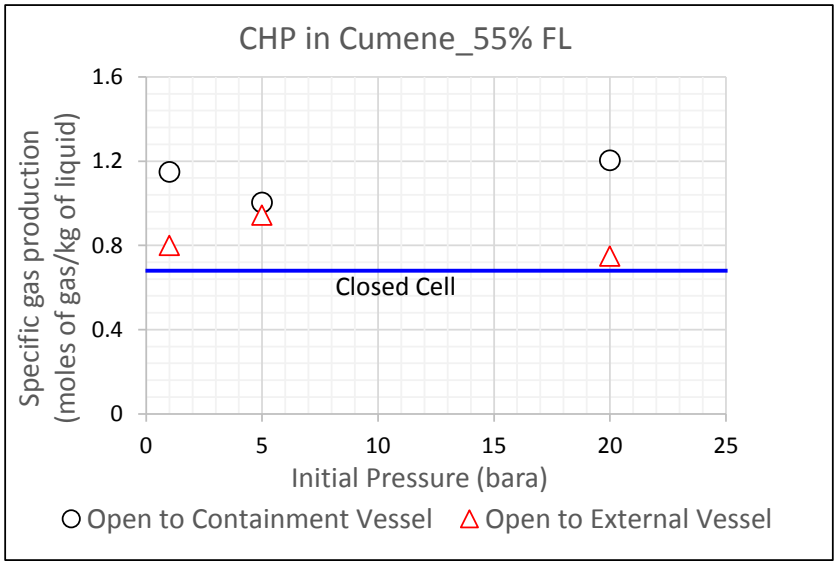

Figure 63: Specific gas production in closed cell and open cell configurations

5.4.2 Maximum specific gas production rate

The maximum specific gas production rate for different configurations is shown in *Figure 64*. The maximum specific gas production rate in open to containment vessel is

lower at the low initial pressure experiment and it increases with the increase of initial pressure. However for the open to external vessel experiment, the increment of the rate with the increase of pressure is insignificant and the rates are much less than the open to containment vessel tests. This happens because, the maximum pressure rise rate in the external vessel was around an order of magnitude less than to the containment vessel.

The solid portion of each bar represents the uncertainty related to the initial mass loss ratio. This uncertainty is around 70%, 32% and 7% for 1, 5, and 20 bara initial pressure experiment respectively for both open cell configurations. The maximum specific gas production rate in closed cell experiment is less than the open to containment vessel experiment at 20 bara initial pressure. On the other hand, the corrected (φ factor) specific gas production rate for closed cell experiment is at least one order of magnitude higher than all other results. However, the φ factor corrections were not possible for the open cell tests because of the uncertainty on the mass of reactive mixture in the cell at the maximum pressure rise rate and the lack of methodology on the correction of gas temperature.

This comparison shows the very high sensitivity of the specific gas production rate to the experimental conditions and the huge discrepancies in the current approaches.

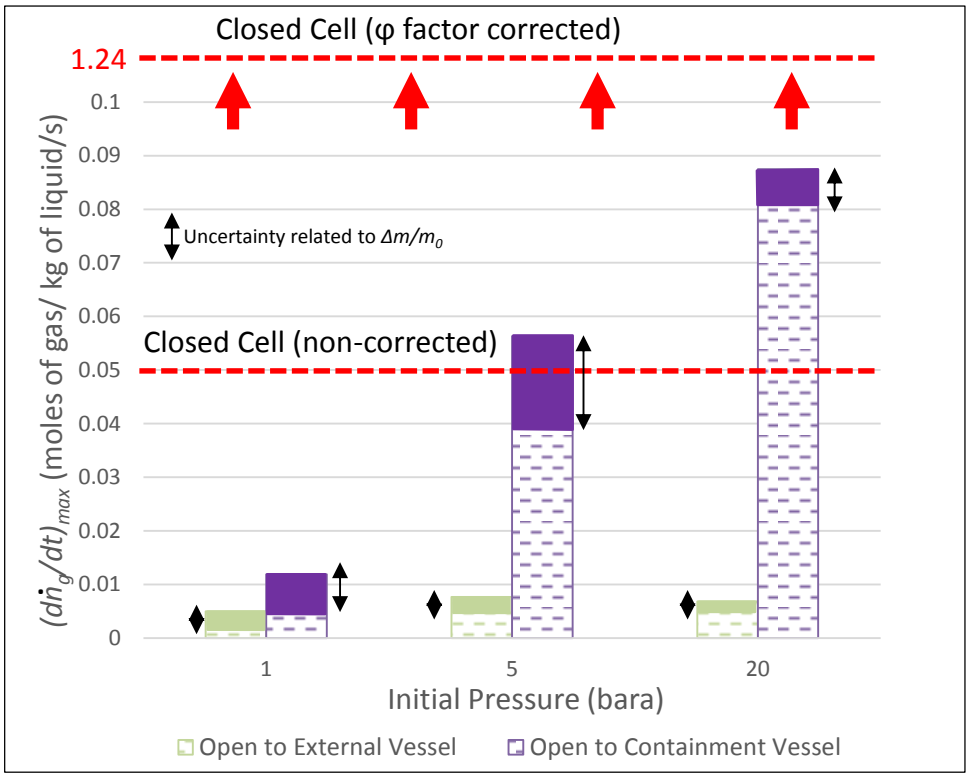

Figure 64: Maximum specific gas production rate in closed cell and open cell configurations

.

6 SIMULATION OF A CLOSED CELL EXPERIMENT

In the latest stages of this thesis, the simulation of the runaway reaction of a gas generating chemical system was performed using a model recently developed by Kanes *et al.* [39]. This is a comprehensive computer model that describes the behavior of a vessel containing a reactive system under runaway conditions before and after the opening of a pressure relief system (during the depressurization phase). The model is sophisticated as it uses a rigorous thermodynamic evaluation of component and mixtures properties coupled with the kinetic model. **The model is also able to predict the gas dissolution effects in a liquid mixture!** The model rigorously calculates the change of liquid and gas phase composition at each time step of the runaway, before and after venting (gas phase venting only).

To help us in performing the critical analysis of our experimental observation in closed cell configuration, the simulation of the decomposition of Di-tert-butyl Peroxide (DTBP) in Toluene in a closed vessel was performed using the model. This system is similar to the CHP in Cumene investigated in the experimental work of this thesis.

The input data for the simulation were as follows:

- Chemical system: 20% (w/w) DTBP in Toluene
- Decomposition of DTBP: DTBP $\rightarrow$ 2 Acetone + Ethane
- Volume of the closed vessel: 10L
- Fill level: 60%
- Initial pressure: 3 bara

- Initial Temperature: 115°C
- φ = 1
- List of the species in the vessel: DTBP, toluene, acetone, ethane and nitrogen.
- Toluene is just a solvent and does not participate to the reaction.

The temperature and pressure profiles predicted by the simulation are shown in *Figure 65*. As mentioned above, the model is able to rigorously evaluate the composition of the liquid and gas phase at each time step of the runaway. *Figure 66* & *Figure 67* show the mass fraction of the liquid and gas phase respectively. The number of moles of all components in the liquid phase increase as the runaway proceeds except DTBP, which is consumed by the decomposition reaction to produce acetone and ethane. The number of moles of acetone, ethane and toluene in the gas phase increase as the runaway occurs. However, at the maximum reaction rate (max *dT/dt* and *dP/dt*), the moles number of acetone, ethane, and toluene in gas phase start to decrease. This is because at high pressure, toluene and acetone tend to condensate. At the same time, some amount of ethane dissolved into the liquid.

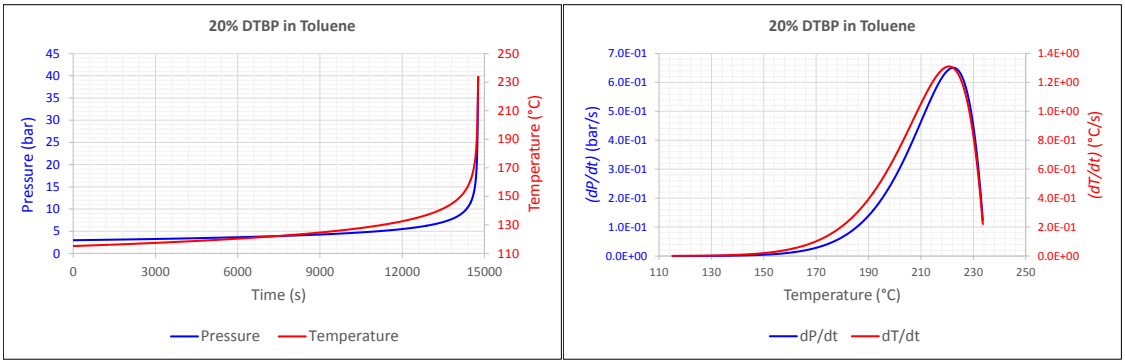

Figure 65: Simulated temperature and pressure profiles

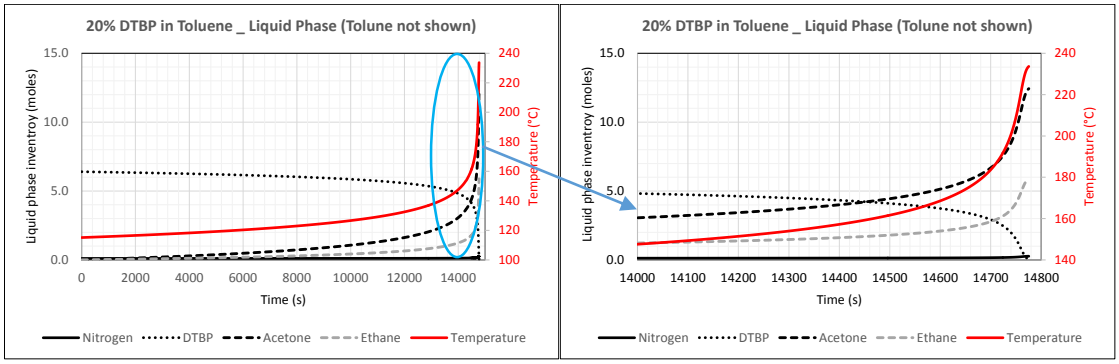

Figure 66: Simulation of DTBP in toluene; number of moles in liquid phase

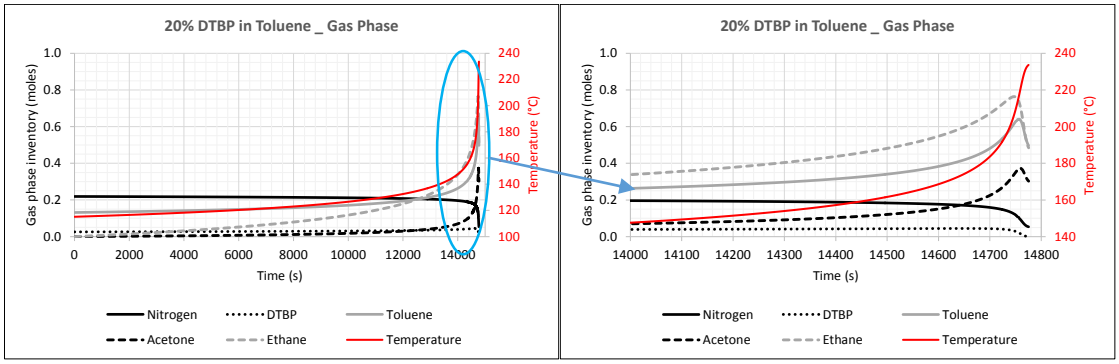

Figure 67: Simulation of DTBP in toluene; number of moles in gas phase

Figure 68 represents the simulated total gas generation rate in the gas phase. This total gas generation rate is the derivative of the total number of moles in the gas phase as calculated rigorously by the model. It can be seen that the total gas generation rate in the closed vessel is negative when the temperature rise rate reaches its maximum value. This was an unexpected observation, as the general approach when analyzing calorimetric data assumes that the maximum gas generation rate occurs at the maximum temperature or pressure rise rate. This is in disagreement with the prediction of the rigorous model.

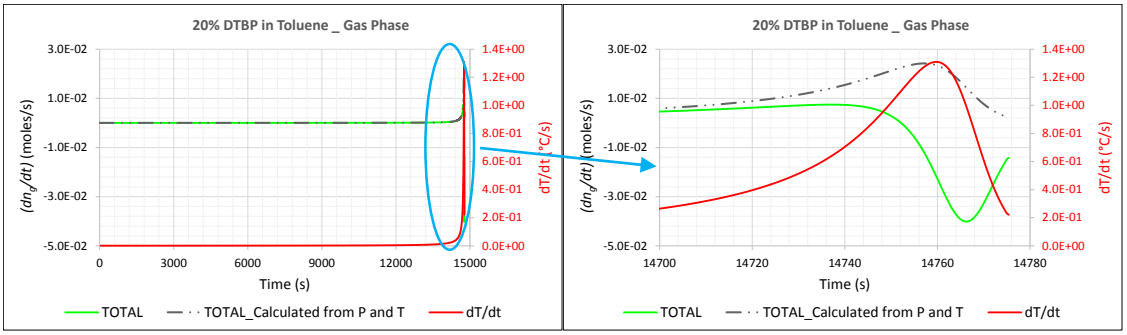

Figure 68: Simulated and calculated gas production rate

We used the simulated temperature and pressure data as if they were experimental data to evaluate the gas generation rate using the ideal gas law. This is using an approach identical to the way we have analyzed all our calorimetric data in the work. *Figure 68* shows that the maximum gas generation rate calculated using this approach is 2.4×10^{-2} moles/s and it occurs at t = 14757 s. The simulated total gas generation rate in the gas phase by the rigorous model shows that the maximum generation rate is 0.8×10^{-2} moles/s and it occurs at t = 14737 s. **Therefore, the simple use of the temperature and pressure data along with the ideal gas law to calculate the gas generation rate can not reflect the actual gas generation rate in a closed vessel.**

The general approach used for the interpretation of calorimetric data assumes that the pressure of a test cell is a good reading of the evolution of the number of moles of the gas phase. This is wrong. The pressure reading is a consequence of different phenomenon that includes: gas dissolution, the amount of production of gas, the amount of production of vapor, condensation of vapor and expansion of gasses. However, none of the existing methods considered the above phenomenon (i.e. gas dissolution, vapor condensation etc.) to conduct the maximum gas generation rate. In experimentally, when we measured the

maximum gas generation rate, it is not really the maximum generation rate. The maximum gas generation occurs well before. Moreover, the time at which we measured the maximum gas generation rate at that time it already under the maximum rate.

7 CONCLUSION AND FUTURE WORK

The objective of this thesis work was to study experimentally the decomposition of a gas generating chemical system, Cumene Hydroperoxide (CHP) in Cumene, under runaway condition using adiabatic calorimetry. A critical analysis of the current methodologies for the assessment of the maximum gas production rate was done. The effect of the experimental condition in adiabatic calorimetry (open vs closed cell, initial fill level, the initial pressure of the test) on the measured gas generation rate was investigated.

Closed cell experiments were possible with 20% and 30% w/w CHP solutions. The experiment with the 40% CHP solution led to the explosion of the test cell, which demonstrates the limitation of the closed cell configuration for gas generating systems. For closed cell experiments, the temperature rise rate, pressure rise rate and the maximum specific gas production rate all are increasing with the increase of concentration. Very importantly, the correction of the φ factor using the Enhanced Fisher method (for temperature and timescale correction) and the Kossoy's method (for pressure correction) was shown to have a great impact on the maximum specific gas production rate. Indeed, the φ corrected value of maximum specific gas production rate is one order magnitude higher than the non-corrected value. However, these results are inherently suffering from the limitations of the Kossoy's method which ignored the gas dissolution effect.

Open cell (open to containment vessel) experiments were conducted with different fill level, initial pressure and the concentration of the peroxide. As expected, the specific

gas production rate increased with the increase of peroxide concentration. No significant influence of the fill level on specific gas production rate was found. However, we could see a very strong influence of the initial pressure on the estimated gas generation rate. The initial pressure was showed to have an influence on the thermal balance of the reaction (because of the vapor production) and therefore the reaction kinetics. Consequently, the higher the initial pressure of the tests, the higher the specific gas generation rate. One of the most important drawbacks of the open cell experiment is the influence of the initial pressure on the quantity of sample vented from the test cell to the containment vessel during the runaway. The lower the initial pressure of the test the higher the mass loss. This sample mass loss induces an uncertainty on the specific gas production rate, the actual sample mass involved in the reaction during the maximum reaction rate being unknown.

A number of experiments were performed in open to external vessel configuration with different initial pressure. An unexpected behavior of the temperature and pressure rise rates were observed in the experiments. This behavior was explained by the difference of pressure generated between the cell and the external vessel due to the flow restriction caused by the 1/8" tube. This flow restriction leading to the influence of pressure buildup in the test cell and also influence in the reaction kinetics. **Therefore, we can rightfully say that the reading of the pressure in the external vessel is in no way is a good indicator of the gas production rate!**

The comparison of three configurations for 30% w/w CHP 55% v/v fill level showed that very high sensitivity of the specific gas production rate to the experimental conditions and in the current approaches. Indeed, the lowest values of specific gas

generation rate were obtained from the open to external vessel tests (this is not surprising as it was demonstrated that the pressure in the external vessel should not be used for this purpose). The specific gas generation rate calculated from the closed cell experiment (non φ corrected) was lower than the value calculated with open cell experiment under an initial pressure of 20 bars (non φ corrected). This shows that closed cell experiment tends to underestimate the gas generation rate because of the strong gas dissolution effect. On the other hand, the open cell experiment under an initial pressure of 1 bars (non φ corrected) was lower than the value calculated with the closed cell experiment (non φ corrected). This shows the tendency of open cell experiment at low initial pressure to underestimate the gas generation rate because of the sample mass loss and the effect of the low pressure on the thermal balance and the reaction kinetics.

In addition, the simulation of the runaway reaction of a gas generating chemical system, DTBP in toluene (similar to CHP in Cumene), was performed using a model recently developed by Kanes *et al*. The model was rigorously calculating the change of liquid and gas phase composition at each time step of the runaway, before and after venting (gas phase venting only). The simulation result demonstrated that, use of the temperature and pressure data along with the ideal gas law to calculate the gas generation rate cannot reflect the actual gas generation rate in a closed vessel. This put into question our current usage of calorimetric data and their interpretation for the estimation of the gas generation rate.

Major efforts are still needed to improve the gas generation rate calculation from adiabatic calorimetry data.

Currently, there is no experimentally validated method to calculate the maximum specific gas production rate of a gas generating system from calorimetric data. The development of such methods require a much better understanding of the phenomena involved in the runaway when performed in the adiabatic calorimeter. This work has generated a large amount of experimental data that if, coupled with a rigorous runaway reaction model, would allow such development.

Our recommendation is to perform an in-depth study of the kinetics of decomposition of CHP in Cumene. For this purpose, a Thermogravimetric Analyzer (TGA) can be used to characterize the reaction products, estimate the nature of the generated gas. A Differential Scanning Calorimeter (DSC) can also be used to characterize the thermal behavior of the system and proposed a kinetic model. This kinetic needs to be incorporated it into the rigorous thermodynamic model developed by Kanes *et al.* to help in the better interpretation of the calorimetric data.

In a longer run, the improvement of the vent sizing methodology for gas generating systems requires the development of descriptive model coupling the reaction kinetics, the hydrodynamic of the reactive mixture in the vessel (level swell) and through the vent (two-phase flow) and the thermodynamic of the mixture. Such model needs to be validated against medium to large scale experiments.

REFERENCES

[1] D. A. Crowl and J. F. Louvar, Chemical Process Safety: Fundamentals with Applications, Third Edit. 2011.

[2] US Chemical Safety and Hazard Investigation Board CSB, "Reactive Chemical Incidents," 2003. [Online]. Available: http://www.csb.gov.

[3] J. Etchells and J. Wilday, Workbook for Chemical Reactor Relief System Sizing. HSE,Health & Safety Executive, 1998.

[4] L. Véchot, J.-P. Bigot, D. Testa, M. Kazmierczak, and P. Vicot, "Runaway reaction of non-tempered chemical systems: Development of a similarity vent-sizing tool at laboratory scale," J. Loss Prevention in the Process Industries, vol. 21, no. 4, pp. 359–366, Jul. 2008.

[5] J. Barton and R. Rogers, Chemical Reaction Hazards, 2nd ed. Wiltshire: Gulf Professional Publishing, 1997.

[6] M. Papadaki, E. Marqués-Domingo, J. Gao, and T. Mahmud, "Catalytic decomposition of hydrogen peroxide in the presence of alkylpyridines: Runaway scenarios studies," J. loss Prev., vol. 18, no. 4–6, pp. 384–391, Jul. 2005.

[7] M. S. Mannan, H. H. West, K. Krishna, A. Aldeeb, N. Keren, S. R. Saraf, Y.S. Liu, and M. Gentile, "The legacy of Bhopal: The impact over the last 20 years and future direction," J. Loss Prevention in the Process Industries, vol. 18, no. 4–6, pp. 218–224, Jul. 2005.

[8] S. Sriramachari, “Bhopal gas tragedy: scientific challenges and lessons for future,” J. Loss Prevention in the Process Industries, vol. 18, no. 4–6, pp. 264–267, Jul. 2005.

[9] S. Saraf and M. Karanjikar, “Literary and economic impact of the Bhopal gas tragedy,” J. Loss Prevention in the Process Industries, vol. 18, no. 4–6, pp. 274–282, Jul. 2005.

[10] R. Varma, “The Bhopal Disaster of 1984,” Bull. Sci. Technol. Soc., vol. 25, no. 1, pp. 37–45, Feb. 2005.

[11] R. Ball, “Oscillatory thermal instability and the Bhopal disaster,” Process Safety and Environmental Protection, vol. 89, no. 5, pp. 317–322, Sep. 2011.

[12] P. a Bertazzi, “Long-term effects of chemical disasters. Lessons and results from Seveso.,” Science of the Total Environment., vol. 106, no. 1–2, pp. 5–20, Jul. 1991.

[13] U.S. Chemical Safety and Hazard Investigation Board, “Investigation report - T2 Laboratories, Inc. Runaway Reaction (4 killed, 32 injured) - Report No. 2008-3-I-FL,” 2009.

[14] D. Crowl and J. Louvar, Chemical process safety: fundamentals with applications, Third Edit. Paul Boger, 2001.

[15] B. F. Gray, “Critical behaviour in chemically reacting systems: I-Difficulties with the Semenov theory,” Combust. Flame, vol. 20, no. 3, pp. 313–316, 1973.

[16] O. Regimes, M. Massot, V. A. Volpert, and A. Mathematics, “Interaction of thermal Explosion and natural convection : critical conditions and new oscillating regimes,”

vol. 63, no. 1, pp. 351–372, 2016.

[17] P. F. F. Beever, “Self-heating and spontaneous combustion,” in SFPE Handbook of Fire Protection Engineering, 2nd ed., P. J. Dinenno, Ed. Quincy, Boston, Mass.: National Fire Protection Association ; Society of Fire Protection Engineers, 1995, pp. 180–189.

[18] J.-M. Hsu, M.-S. Su, C.Y. Huang, and Y.S. Duh, “Calorimetric studies and lessons on fires and explosions of a chemical plant producing CHP and DCPO,” J. Hazard. Mater., vol. 217–218, pp. 19–28, May 2012.

[19] I. Di Somma, R. Marotta, R. Andreozzi, and V. Caprio, “Kinetic and chemical characterization of thermal decomposition of dicumylperoxide in cumene.,” J. Hazard. Mater., vol. 187, no. 1–3, pp. 157–63, Mar. 2011.

[20] S.J. Shen, S.H. Wu, J.H. Chi, Y.W. Wang, and C.M. Shu, “Thermal explosion simulation and incompatible reaction of dicumyl peroxide by calorimetric technique,” J. Therm. Anal. Calorim., vol. 102, no. 2, pp. 569–577, Jun. 2010.

[21] H. K. Fauske, “Revisiting DIERS’ two-phase methodology for reactive systems twenty years later,” Process Safety. Progress., vol. 25, no. 3, pp. 180–188, 2006.

[22] Center for Chemical Process Safety (CCPS), Guidelines for Pressure Relief and Effluent Handling Systems. John Wiley & Sons, 1998.

[23] J. Barton and R. Rogers, Chemical Reaction Hazards: A Guide to Safety, Second edi. Gulf Professional Publishing, 1997.

[24] H. G. Fisher, H. S. Forrest, S. S. Grossel, J. E. Huff, A. R. Muller, J. A. Noronha,

D. A. Shaw, and B. J. Tilley, Emergency Relief System Design Using DIERS Technology: The Design Institute for Emergency Relief Systems (DIERS) Project Manual. Design Institute for Physical Property Data/AIChE, 1992.

[25] A. A. Kossoy, J. Singh, and E. Y. Koludarova, "Mathematical methods for application of experimental adiabatic data – an update and extension," J. Loss Prevention in the Process Industries, vol. 33, pp. 88–100, 2015.

[26] J. C. Leung and H. K. Fauske, "Runaway system characterization and vent sizing based on diers methodology," Plant/Operations Prog., vol. 6, no. 2, pp. 77–83, Apr. 1987.

[27] J. Singh, "Vent sizing for gas-generating runaway reactions," J. Loss Prevention in the Process Industries, vol. 7, no. 6, pp. 481–491, Nov. 1994.

[28] L. Friedel and S. Korfmann, "Predictive accuracy of simplified vent area sizing methods for the case of thermal runaway reactions," J. Loss Prevention in the Process Industries, vol. 13, no. 2, pp. 125–152, Mar. 2000.

[29] L. Véchot, J. Kay, and J. Wilday, "Round robin vent sizing exercise on a gassy system: 40% dicumyl peroxide in butyrate solvent," in proceeding of the Hazards XXII Conference, IChemE Symposium Series 156, 2011, no. 156, pp. 278–286.

[30] I. Di Somma, R. Marotta, R. Andreozzi, and V. Caprio, "Detailed thermal and kinetic modeling of cumene hydroperoxide decomposition in cumene," Process Safety and Environmental Protection, no.91, pp. 262–268, July 2013.

[31] Y. Y. Duh, C. C. Kao, H. H. Hwang, and W. W. Lee, "Thermal decomposition

kinetics of cumene hydroperoxide," Process Saf. Environ, vol. 76, no. November, 1998.

[32] I. Di Somma, R. Andreozzi, M. Canterino, V. Caprio, "Thermal decomposition of cumene hydroperoxide : chemical and kinetic characterization," AIChE J., vol. 54, no. 6, pp. 1579–1584, 2008.

[33] K. Hattori, Y. Tanaka, and H. Suzuki, "Kinetics of liquid phase oxidation of cumene in bubble column," J. Chem. Eng. Japan, vol. 3, no. 1, pp. 72–78, 1970.

[34] H.Y. Hou, C.M. Shu, and Y.S. Duh, "Exothermic decomposition of cumene hydroperoxide at low temperature conditions," AIChE J., vol. 47, no. 8, pp. 1893–1896, Aug. 2001.

[35] Y. Lu, D. Ng, L. Miao, and M. S. Mannan, "Key observations of cumene hydroperoxide concentration on runaway reaction parameters," Thermochim. Acta, vol. 501, no. 1–2, pp. 65–71, Mar. 2010.

[36] HEL, "PHI-TEC Operating manual volume 1 hardware details," Herts, 2007.

[37] HEL GROUP, "PHI-TEC Operating manual volume 2 WinISO data acquisition and control software," vol. 2, no. 0, 2002.

[38] HEL, "PHI-TEC Operating manual volume 3: Verification of equipment performance and examples of data," vol. 3, no. September. pp. 1–15, 2004.

[39] R. Kanes, A. Basha, L. N. Véchot, and M. Castier, "Simulation of venting and leaks from pressure vessels," J. Loss Prevention in the Process Industries, vol. 40, pp. 563–577, 2016.

[40] M. S. Kharasch, A. Fono, and W. Nudenberg, “The chemistry of hydroperoxides. VI. The thermal decomposition fo α-cumyl hydroperoxide,” J. Org. Chem., vol. 16, pp. 113–127, 1951.

APPENDIX A

PROPERTIES OF CUMENE HYDROPEROXIDE

The major physical-chemical properties of CHP are listed in *Table 14*.

Table 14: Physical and chemical properties of CHP

Property	Information
Physical State	Colorless to pale yellow liquid
Odor	Sharp, aromatic
Melting point	-9 °C
Boiling point	100-101 °C @ 8 mm Hg
Density	1.03 g/mL @ 25 °C
Vapor pressure	0.4 mm Hg @ 55 °C
Specific gravity	1.05
Flashpoint	79 °C
Flammability	0.9 – 6.5 %
Heat of combustion	-7400 cal/g
Heat of decomposition	-475 cal/g
Solubility in water	13.9 g/L @ 25 °C

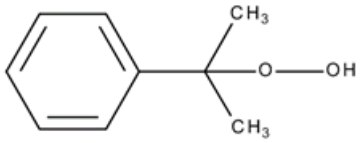

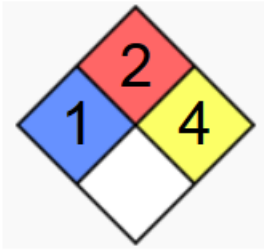

Figure 69: Molecular structure (left) and NFPA diamond (right) of CHP

APPENDIX B

PROPERTIES OF CUMENE

The major physical-chemical properties of cumene are listed in *Table 15*.

Table 15: Physical and chemical properties of Cumene

Property	Information
Physical State	Colorless liquid
Odor	Sharp, gasoline like
Melting point	-96 °C
Boiling point	152-154 °C
Density	0.864 g/mL @ 25 °C
Vapor pressure	8 mmHg @ 20 °C
Flashpoint	31 °C
Auto-ignition temperature	425 °C
Solubility in water	0.06 g/l @ 25 °C

Figure 70: Molecular Structure (left) and NFPA diamond (right) of Cumene

APPENDIX C

REACTION PATHWAYS OF CHP DECOMPOSITION

The reaction mechanism of CHP decomposition has been studied in the presence of various solvent. However, because of the instability of intermediates in the decomposition reaction, it was difficult to investigate the reaction mechanism in detail. With the help of computational quantum chemistry method, it is possible to study the intermediates involved in the decomposition reaction and the elementary reactions [30], [40]. The reaction pathways of CHP are shown in *Figure 71*.

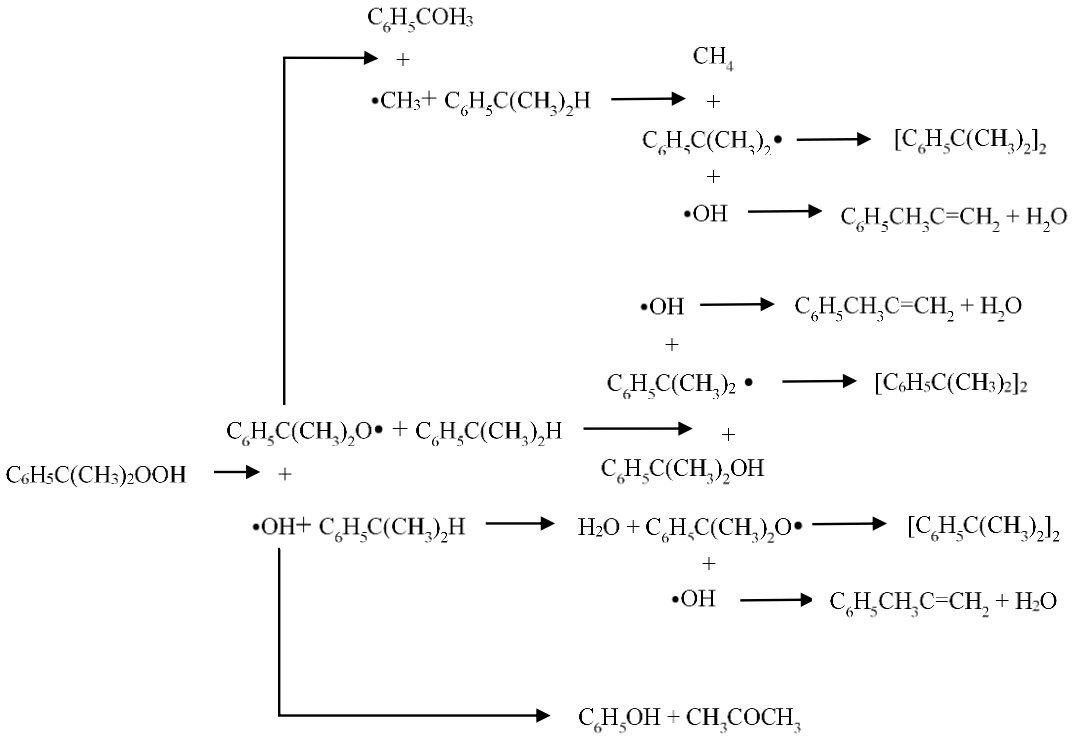

Figure 71: Reaction pathways of CHP decomposition